BIASED PROPORTIONAL NAVIGATION GUIDANCE FOR IMPACT ANGLE CONTROL WITH EXTENSION TO THREE-DIMENSIONAL ENGAGEMENTS

A THESIS SUBMITTED TO
THE GRADUATE SCHOOL OF NATURAL AND APPLIED SCIENCES
OF
MIDDLE EAST TECHNICAL UNIVERSITY

BY

KORAY SAVAŞ ERER

IN PARTIAL FULFILLMENT OF THE REQUIREMENTS
FOR
THE DEGREE OF DOCTOR OF PHILOSOPHY
IN
MECHANICAL ENGINEERING

FEBRUARY 2015

Approval of the thesis:

BIASED PROPORTIONAL NAVIGATION GUIDANCE FOR IMPACT ANGLE CONTROL WITH EXTENSION TO THREE-DIMENSIONAL ENGAGEMENTS

submitted by **KORAY SAVAŞ ERER** in partial fulfillment of the requirements for the degree of **Doctor of Philosophy in Mechanical Engineering Department, Middle East Technical University** by,

Prof. Dr. Gülbin Dural Ünver _____
Dean, Graduate School of **Natural and Applied Sciences**

Prof. Dr. R. Tuna Balkan _____
Head of Department, **Mechanical Engineering**

Prof. Dr. M. Kemal Özgören _____
Supervisor, **Mechanical Engineering Dept., METU**

Dr. Osman Merttopçuoğlu _____
Co-Supervisor, **TMS-GCD Dept., Roketsan Missiles Inc.**

Examining Committee Members:

Prof. Dr. Bülent E. Platin _____
Mechanical Engineering Dept., METU

Prof. Dr. M. Kemal Özgören _____
Mechanical Engineering Dept., METU

Prof. Dr. Ozan Tekinalp _____
Aerospace Engineering Dept., METU

Prof. Dr. Kemal Leblebicioğlu _____
Electrical and Electronics Engineering Dept., METU

Prof. Dr. Yücel Ercan _____
Mechanical Engineering Dept., TOBB ETÜ

Date: 10.02.2015

I hereby declare that all information in this document has been obtained and presented in accordance with academic rules and ethical conduct. I also declare that, as required by these rules and conduct, I have fully cited and referenced all material results that are not original to this work.

Name, Last Name: Koray Savaş Erer

Signature:

ABSTRACT

BIASED PROPORTIONAL NAVIGATION GUIDANCE
FOR IMPACT ANGLE CONTROL
WITH EXTENSION TO THREE-DIMENSIONAL ENGAGEMENTS

Koray Savaş Erer
Ph.D., Department of Mechanical Engineering
Supervisor: Prof. Dr. M. Kemal Özgören
Co-Supervisor: Dr. Osman Merttopçuoğlu

February 2015, 174 pages

This work shows that the impact angle can be controlled by means of bias addition to pure proportional navigation guidance commands. After obtaining the closed-form solution of the nonlinear differential equations governing the engagement kinematics between a pursuer and a stationary target, it is shown that the proposed strategy corresponds to the optimal solution in the linear domain. Three alternative guidance laws that do not require the time to go are proposed. The first law constitutes a two-phased approach, where the bias is removed after obtaining proper pursuit conditions. The second law, which makes use of the range-to-go information, and the third law, which leads to an exponentially decaying error profile, are single-phased approaches that do not suffer from the open-loop nature of the first one in its second phase. The framework of this study allows the treatment of both the look angle and the acceleration constraints in such a way that the impact angle capacity corresponding to any engagement geometry can be analyzed. In addition to a complete but impractical formulation, a feasible constrained guidance solution is presented. A single-gain range observer that addresses the observability issue in a convenient manner is formulated to supplement the trajectory shaping effort. The

case of moving targets is dealt with by means of constructing the collision triangle. Two different schemes are considered based on the rotations of the absolute and relative velocity vectors. The plane-pursuit midcourse guidance method proposed to confine a general engagement scenario to a single plane facilitates the extension to three-dimensional engagements.

Keywords: Impact Angle, Proportional Navigation, Bias, Constrained Guidance, Three-Dimensional Engagement

ÖZ

EK TERİMLİ ORANSAL SEYRÜSEFER GÜDÜM İLE
ÇARPMA AÇISI KONTROLÜ
VE ÜÇ BOYUTLU EŞLEŞMELERE UYARLANMASI

Koray Savaş Erer
Doktora, Makina Mühendisliği Bölümü
Tez Yöneticisi: Prof. Dr. M. Kemal Özgören
Ortak Tez Yöneticisi: Dr. Osman Merttopçuoğlu

Şubat 2015, 174 sayfa

Bu çalışma, çarpma açısının, saf oransal seyrüsefer güdüm komutlarına ek terim eklenmesiyle kontrol edilebileceğini göstermektedir. Takipçi ve sabit bir hedef arasındaki eşleşme kinematiğini yöneten doğrusal olmayan diferansiyel denklemlerin çözümünün elde edilmesinden sonra, önerilen yöntemin doğrusal ortamdaki en uygun çözüme karşılık geldiği gösterilmektedir. Kalan süreye ihtiyaç duymayan üç adet alternatif güdüm kanunu önerilmektedir. Birinci kanun, ek terimin uygun takip koşullarının elde edilmesiyle kaldırıldığı iki fazlı bir yaklaşımdır. Kalan mesafe bilgisini kullanan ikinci kanun ve hatanın üstel şekilde eritilmesini sağlayan üçüncü kanun, tek fazlı yaklaşımlardır ve birincinin ikinci fazdaki açık döngü doğasının benzerine maruz kalmazlar. Bu çalışmanın çatısı, bakış açısı ve ivme kısıtlarının değerlendirmeye alınmasına izin vermektedir; herhangi bir eşleşme geometrisine ait çarpma açısı kapasitesi analiz edilebilir. Eksiksiz fakat elverişsiz bir formülasyonun yanı sıra, uygulanabilirliği olan bir kısıt altında güdüm çözümü sunulmaktadır. Gözlemlenebilirlik sorununu uygun şekilde ele alan tek kazançlı bir menzil gözlemcisi, yörünge şekillendirmeyi desteklemek adına kurgulanmıştır. Hareketli hedeflere ilişkin durum, çarpışma üçgeninin kurulmasıyla çözülmektedir. Mutlak ve

bağıl hız vektörlerinin dönüşlerine dayanan iki farklı yöntem değerlendirilmektedir. Genel bir eşleşme senaryosunu tek bir düzleme hapsederek üç boyuta uyarlamayı sağlaması için düzlem takip adı verilen bir arafaz güdüm yöntemi önerilmektedir.

Anahtar Kelimeler: Çarpma Açısı, Oransal Seyrüsefer, Ek Terim, Kısıt Altında Güdüm, Üç Boyutlu Eşleşme

to

my father

and to

my dearest one

ACKNOWLEDGEMENTS

I would like to thank

my supervisor Prof. Dr. M. Kemal Özgören firstly for providing a free thinking environment, then for his many useful suggestions and finally for bearing with my not-so-very-systematic way of studying;

my co-supervisor Dr. Osman Merttopçuoğlu who took the trouble to answer my petty questions without letting go of his unique sense of humor;

Raziye Tekin for her invaluable technical insight she generously shared with me and for her selfless support throughout the whole process;

Paul Zarchan for the encouragement he provided;

Prof. Dr. M. Kemal Özgören once more and Prof. Dr. Bülent E. Platin for teaching me “Advanced Dynamics” and “Dynamics of Nonlinear Systems”, the graduate courses on which the foundations of this dissertation rest;

Roketsan for giving me the opportunity to combine my professional activities with my academic interests;

my mother and brother for simply being there.

TABLE OF CONTENTS

LIST OF TABLES

TABLES

LIST OF FIGURES

FIGURES

LIST OF SYMBOLS

P : Pursuer

T : Target

r : Range

v : Speed

γ : Path angle

ε : Look angle

λ : LOS angle

a : Control acceleration

$\gamma_{f,d}$: Desired impact angle

N : Navigation gain

b : Bias

ρ : Nondimensional range

τ : Nondimensional time

β : Bias-to-speed ratio

σ : Bias sign

c : Integration constant

E : Total control effort

$\hat{J}$: Jacobian matrix

t_{go} : Time to go

V : Constant speed

B : Bias integral

Γ : Potential impact angle function

L : Total engagement time

Δt : Bias duration

N_M : Midcourse navigation gain

N_T : Terminal navigation gain

n : Range-driven guidance gain

ψ : Impact angle error

m : Error-based guidance gain

τ_a : First-order pursuer lag

g : Gravity

ε^* : Look angle constraint

a^* : Acceleration constraint

C_L : Lift coefficient

κ : Aerodynamic proportionality agent

$\tilde{t}_{go}$: Time-to-go estimate

μ : Pseudo range measurement

$\tilde{r}$: Range estimate

K : Range observer gain

$\vec{\omega}$: LOS angular velocity vector

υ : Pursuer-to-target speed ratio

e_a : Angular distance to the pursued plane

$\vec{u}_{f,d}$: Desired impact vector

T_{go} : Time to go of the frozen system

k : Plane-pursuit gain

e_t : Translational distance to the pursued plane

$\vec{p}$: Position vector

H : Hamiltonian

α : Costate

LIST OF ABBREVIATIONS

LOS	: Line of Sight
PN	: Proportional Navigation
TPN	: True Proportional Navigation
PPN	: Pure Proportional Navigation
IPN	: Ideal Proportional Navigation
BPPN	: Biased Pure Proportional Navigation
INS	: Inertial Navigation System
BIPN	: Biased Ideal Proportional Navigation
BPN	: Biased Proportional Navigation
IMU	: Inertial Measurement Unit
3-D	: Three-Dimensional

CHAPTER 1

INTRODUCTION

The primary requirement of the terminal guidance process is that it must lead the pursuer to the target. In addition to this, the application of interest might necessitate other objectives. For example, the secondary objective could be approaching the target from a specific direction. Depending on the application, being able to control the shape of the trajectory and consequently the impact geometry might mean one or a combination of the following: exploiting the weak points of the target, increasing the warhead effectiveness, avoiding directional defense mechanisms, adjusting the time of arrival, or reducing the collateral damage, etc.

The rule of parallel navigation can be considered to deal with the primary requirement. This rule states that two objects will eventually meet if the line of sight (LOS) connecting them does not rotate with respect to an inertial frame of reference [1]. Hence, a pursuer that successfully implements this geometric rule must capture its target.

Proportional navigation (PN) is a guidance law that implements the parallel navigation rule [1]. It has been the most frequently utilized guidance law in guided missiles owing to its simple nature, effectiveness and ease of implementation [2]. There are several kinds of PN classified according to the direction of the applied acceleration [3]. Two well-known forms are named as true PN (TPN) [4] and pure PN (PPN) [5]. In TPN, the acceleration vector is normal to the LOS. In PPN, it is normal to the velocity vector of the pursuer. This is a distinct advantage for endoatmospheric vehicles since no change of speed is required [6]. The PPN logic is simple: The inertial rotation rate of the pursuer velocity vector is required to be equal to the inertial rotation rate of the LOS multiplied by a navigation gain. It is known that PPN can capture a nonmaneuvering target for almost all initial conditions [5]

and the closed-form solution of such an engagement is in the form of a uniformly convergent infinite product [7]. Another form of PN is ideal PN (IPN) [8], where the acceleration vector is defined to be normal to the relative velocity vector.

Under the action of PPN guidance, the impact angle, i.e. the final value of the path angle corresponding to the velocity vector of the pursuer, is determined by the initial conditions [5]. This implies that it is possible to obtain a desired impact angle by constructing the required initial geometry. However, being possible does not mean being feasible. In fact, there will be limited authority on initial conditions in a realistic situation, if any at all. A viable alternative to adjusting the initial conditions is what is called "trajectory shaping" [2]. This phrase refers to the control action performed by the pursuer in order to modify its otherwise direct course towards the target.

This is where the subject of this dissertation becomes relevant. In this work, trajectory shaping is accomplished by means of bias addition to the PPN guidance law. The idea that the impact angle can be controlled via such a biased PPN (BPPN) approach originates from the observation that the existence of gravity, which is usually compensated by biasing the guidance command, has a dramatic effect on the shape of the trajectory.

Before moving on, the reader should note that this is an application-oriented writing. The purpose is to provide practically implementable solutions to the problem of impact angle control. This statement should not be misinterpreted. For some systems, it might be the case that none of the methods presented here will be applicable at all. Nevertheless, judging from his personal experience, the author hopes that the practical contributions of this work will be more than insignificant to the guidance community.

1.1. Definition of the Basic Problem

Figure 1.1 depicts the planar engagement between a stationary target *T* and its pursuer *P*, where *r* is the range. The speed of the pursuer is *v*, γ being the path angle. The angle between the velocity vector and the LOS is the look angle ε whereas λ denotes the LOS angle. The angles are positive in counter-clockwise direction. The inertial coordinates are represented by *x* and *y*.

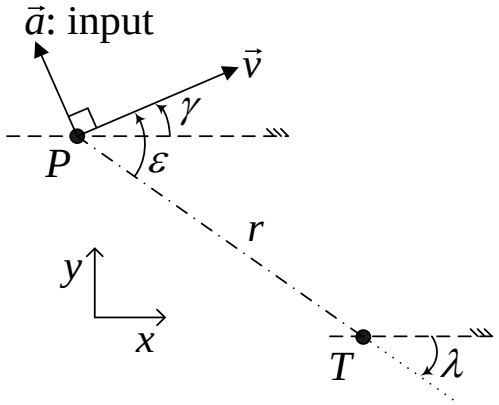

Figure 1.1 Planar engagement between a stationary target and its pursuer

The guidance objective is to finally capture the target; $r_f = 0$, with a desired value of the path angle, i.e. with a desired impact angle; $\gamma_f = \gamma_{f,d}$. Subscript f and subscript d denote the final and desired values, respectively. The control action is enabled by *a*, which is the acceleration component of *T* operating in a direction perpendicular to the velocity vector. The speed is free to vary under the action of several factors such as gravity and drag, but not with the control input.

At this point, one might be tempted to think that the guidance objectives stated above can be accomplished through trajectory planning since the target is stationary. There are, however, two potential problems with this point of view. Firstly, the position of the target may not be available. Secondly, the target might decide to move. The solution to these problems is to use a seeker head that, as an essential component of a

tactical missile, supplies information about the engagement geometry. For example, a gimballed imaging infrared seeker that provides the LOS angle and its rate would especially suit to the methods described in this writing.

1.2. Literature Review

A considerable number of works focusing on impact angle guidance found in the literature have their foundations within the framework of the optimal control theory. This group is typically characterized with a running cost involving the square of the control input that needs to be minimized. Usually, the resulting guidance laws are functions of the problematic variable termed time to go, which is in general not available. In an early example called "perfect rendezvous" [9], the aim was to intercept the target with no vertical velocity component, which may correspond to tail-chase or head-on type of engagements. In another early study [10], where it was demonstrated how the optimal control approach made it possible to compensate for pursuer dynamics in a systematic manner and the issue of control saturation was also investigated. The lift and drag characteristics were taken into account in deriving the κ-guidance law presented in [11], where the analytical forms of the time-varying guidance gains followed from the nature of the performance index penalizing low terminal velocities. In [12], where the final time was a part of the cost function, the nonlinear impact angle control problem was solved with the assumption of available target trajectory. The unknown parameters in the analytically derived guidance law were obtained from a numerical solution. A minimum-time control solution was presented in [13], where the optimal trajectory in the lag-free case turned out to be a straight line in between circular paths, which were traversed with maximum acceleration. The problem was formulated for a missile decelerating according to a specific equation in [14]. Optimal impact angle control laws were generalized for arbitrary system order and the problem of time-to-go estimation based on closed form trajectory solutions was addressed in [15]. The integrand of the cost function proposed in [16] was inversely proportional to some power of the time to go, which provided additional degree of freedom in trajectory shaping. The same performance index was considered in [17] to derive guidance laws to be used by lag-free and first-

order systems, respectively, along with a time-to-go estimation method corresponding to the former law. The impact time and angle guidance law derived in [18] had the interesting property that jerk commands were issued instead of the usual acceleration commands. In [19], a different point of view was adopted in that the body angle of the missile instead of its path angle was used as the control variable by taking the angle-of-attack dynamics into account. The state-dependent Riccati-equation-based control law given in [20] was obtained as a function of both the range to go and the time to go. In one of the few examples of directly considering the seeker field-of-view limit in the design of an impact angle control law [21], the solution dictated switching action so as to keep the look angle constant in between phases of unconstrained optimal guidance. The integrand of the running cost in [22] was formulated as the square of the ratio of the control input to the time-varying acceleration constraint, the expected profile of which was calculated using an iterative process. The boundary value problem with final time specified was numerically solved in [23]. The method proposed in [24] transformed a dynamic optimization problem to a static optimization problem, which was then solved in an iterative manner. References [9], [10], [13], [15–19], [21] and [22] used linear formulations for derivation.

There are also other forms of impact angle guidance laws which do not claim optimality. Some of these might readily be identified as a variant of the PN guidance law. There are others which are, for example, based on the sliding-mode control methodology and yet others that make use of geometrical concepts. The first attempt in this direction seems to be the scheme proposed in [25], which attempted to enhance the PN law with the addition of a bias term as a function of the range to go, which is yet another problematic variable. In another noteworthy contribution [26], the pursuer, whose aerodynamic behavior was taken into account, was guided toward the stationary target by means of PN applied in two orthogonal planes with adaptive usage of the navigation gains. In [27], the guidance law sought convergence to a circular path by utilizing the PN law with a specific value of the navigation gain. Two-phased guidance schemes were proposed in [28] and [29], where the objective of the first phase was to provide proper initial angular conditions for the second phase governed by PN. The difference between these two studies is the way the first

phases were handled: The former employed PN whereas a polynomial trajectory was followed in the latter. In [30], the idea in [28] was extended to deal with target movement by considering the fact that the pursuer and target velocity components normal to the LOS must be equal at the final instant. Another two-phased structure was presented in [31] and [32], where the PN law was enhanced with bias addition during the first phase to be able to shape the trajectory. A sliding-mode separated guidance and control approach was formulated in [33], where the guidance command had two components respectively for reaching and remaining on the sliding surface. The study in [34] established a purely geometric guidance law for lateral impact without the need for the LOS rate, a usually indispensable signal in guidance design. The law proposed in [35] was structured as a polynomial function of the time to go, where it was advised that the guidance gains be selected based on the worst case scenario so that the acceleration and body referenced look angle limits were not violated. In [36], the idea in [31] and [32] was extended to moving targets with the help of the expected collision triangle concept. The formulation in [37] derived an optimal solution by setting out with a bias-enhanced PN command and arriving at a full biasing tactic with continuous feedback. A bias shaping method compatible with [31] and [32] was introduced in [38] to be able to cope with the look angle and acceleration limits. In [39], inspired by the form of the linear optimal control, a guidance law was heuristically developed and extended to three dimensions. The guidance law in [40] was realized with path angle commands instead of the conventional method of using acceleration commands. Accordingly, the LOS angle instead of its rate was utilized in the formulation; yet, the LOS rate may also be included to account for the autopilot lag. A range-dependent guidance law was proposed in [41], where a time-to-go estimation procedure was also proposed. In [42], a geometrical three-point guidance method was proposed, where the logic was based upon maintaining a specified value of the inscribed angle without the need for the LOS rate signal. The switched-gain PN scheme developed in [43] solved the problem under the look angle and acceleration constraints. A comparison of unbiased and biased formulations of PN was made in [44], where the look angle constraint was considered directly. Only references [35] and [37] used linear formulations for derivation.

The foundations of this work can be found in [29], where the concept of PPN impact angle was presented, and in [31], where it was shown that the impact angle could be controlled by biasing the PPN law. The studies in [32], [36] and [44] have been follow-ups to these initial efforts.

1.3. Detailed Outline

Chapter 2 is where the analytical background of the BPPN guidance law is explored. In the first section, the nonlinear differential equation set governing the engagement kinematics between a BPPN-guided pursuer and its stationary target is obtained, where the states happen to be the nondimensional range and the look angle. This set is firstly brought to a nondimensional form and then solved by sacrificing the time information. The analytical expressions for several important variables are derived. A stability criterion is developed based on the behavior of the state plane trajectories. In the next section, the reference ground-to-ground engagement geometry, which is to be used in most of the example scenarios, is defined. After defining the performance index referred to as the total control effort, the results of simulation runs demonstrating the main characteristics of the BPPN law are presented. Also, the optimal solution for the reference engagement geometry, which will serve as the benchmark scenario in the rest of the text, is compared with the lowest-cost BPPN solution. The last section departs from the nonlinear domain to provide some linear insight. As a first item, the picture of the state plane in the neighborhood of the equilibrium point of the nonlinear system is presented. Then, the interest is shifted to the ever-popular issue of optimality. Adopting the total control effort as the cost function, the open-loop control corresponding to the two-point boundary value problem is solved. It is then shown that the linearized form of BPPN is equivalent to the optimal control. The chapter is concluded by revealing that the bias is actually a form of disturbance acting on the PN guidance loop.

Chapter 3 introduces the BPPN-based guidance laws for impact angle control. The formulations for the BPPN impact angle and the potential impact angle function are developed in the first section. The second section introduces three different impact

angle guidance laws based on BPPN. The first method involves switching from BPPN to PPN when proper angular conditions are obtained. This discontinuous structure renders the second phase open loop as far as the impact angle control process is concerned. In the second method, the amount of bias is determined according to the range to go, which may be supplied by a range estimator. In the third method, the bias is applied in such a way that PPN impact angle error diminishes as a first-order system. Engagement scenarios driven by these guidance laws are simulated here under ideal conditions. The third section, on the other hand, focuses on performance evaluation under several realistic forms of disturbance.

Chapter 4 investigates the problem of constrained impact angle control. In this problem, the look angle and the acceleration limitations of the pursuer are directly taken into account. It is shown that in the case where the speed is not constant, the concept of constant maximum lift coefficient may be summoned to handle the acceleration constraint properly. The important outcome of the first section is an algebraic equation that relates the BPPN navigation gain to the physical limits. After numerically solving this equation, which is obtained using the available analytical basis, the guidance parameters that lead to the full utilization of the resources can be calculated. It is then possible to compute the impact angle this fully-utilized guidance process will lead to. As an example, the impact angle contours corresponding to the reference engagement geometry are presented. In the next section, the discontinuous BPPN structure is considered instead of the continuous one. The formulation for the physically constrained impact angle problem is derived but not solved due to its uncooperative nature. The absence of a proper solution is compensated in the last section. It is shown that the constrained guidance problem may be relaxed by not considering both constraints simultaneously. The proposed approach involves dealing firstly with the look angle constraint and then checking whether the acceleration constraint gets violated while trying to reach the desired impact angle.

Chapter 5 discusses a single-gain range observer that is formulated to estimate the range to a stationary target based on seeker and angular inertial navigation system (INS) data. This tool finds its direct application in one of the guidance laws presented

in the Chapter 3. The structure of the range observer is presented in the first section and its performance is tested under various factors in the second section.

Chapter 6 is an extension of the subject to briefly cover the moving targets. With the assumption of known target velocity vector, the collision triangle concept introduced in the first section proves useful in this case. Unlike the previously reported cases, the impact angle control loop may be regarded as open because the target information is not updated during the engagement. Two alternative implementations are presented in the second and third sections. The first one is adapted from the BPPN-based solution and hence, it does not comply with the analytical guidelines exploited hitherto since the target is not stationary anymore. The second one, on the other hand, is made to comply by adopting another methodology based on IPN. The biased IPN (BIPN) logic is implemented through a PPN-like guidance law. In the last section, ideal and disturbed scenarios are simulated to demonstrate the effectiveness of the proposed solutions.

Chapter 7 is devoted to a midcourse guidance method called plane pursuit, which is useful in extending the proposed impact angle control scheme to three-dimensional (3-D) space. Since BPPN has planar implementation logic, the engagement must be made planar before attempting to control the impact angle. In the first section, the target is stationary and a guidance strategy based on the lag-compensation methodology is proposed. The results of nonlinear simulation runs governed by the linear controller are presented. Also, the details of how a desired 3-D impact direction can be achieved are presented. The exemplified impact angle guidance law is the discontinuous one; hence, the total number of phases amounts to three along with the plane-pursuit guidance. In the second section, the target is not stationary and a guidance strategy based on the lead-compensation methodology is proposed. Nonlinear simulation runs are performed with the linear controller.

1.4. Contributions

The contributions of this thesis study may be summarized as follows:

- The BPPN impact angle control methodology does not rely on the concept of linearization as many other studies do; it is a nonlinear guidance technique.
- Unlike the widespread optimal guidance methods, the BPPN approach does not rely on the time-to-go information to control the impact angle; only the rate of the LOS angle is sufficient.
- All of the three BPPN-based guidance schemes devised to control the impact angle against a stationary target can be implemented in a real system.
- Both the look angle constraint and the acceleration constraint are treated properly.
- The range observer formulated as a supplementary tool is a simple and efficient way to estimate the range to a stationary target.
- The PPN-like guidance law that implements the IPN-based solution introduced to cover the moving targets is, to the author's knowledge, a novel formulation.
- The plane-pursuit approach developed to confine the 3-D engagement geometry to a plane in space may be used in conjunction with any other 2-D guidance law.

CHAPTER 2

BIASED PURE PROPORTIONAL NAVIGATION FOR TRAJECTORY SHAPING

This chapter aspires to familiarize the reader with the basics of the BPPN guidance law, which constitutes an efficient basis for impact angle control.

2.1. Analytical Background

Since there are two degrees of freedom associated with the movement of a point in the plane, two differential equations are required to initiate the mathematical manipulation. A visual inspection of Figure 1.1 suggests that a polar representation with r and λ could be suitable. Accordingly, the first differential equation is directly written as

$$\dot{r} = -v\cos(\gamma - \lambda) \tag{2.1}$$

where the dot operator represents derivative with respect to time, i.e. $\mathrm{d}/\mathrm{d}t$. This differential equation is self-explanatory. The second one, however, might not be so and it will thus be derived below. One can start with the LOS angle:

$$\lambda = \tan^{-1}\left(\frac{r_y}{r_x}\right) \tag{2.2}$$

where r_x and r_y are respectively the x and y components of vector $\vec{r}$ that is directed from P to T. Noting that $\dot{r}_x = -v_x$ and $\dot{r}_y = -v_y$ due to the stationary target, where v_x

and v_y are respectively the *x* and *y* components of $\vec{v}$, the LOS angle rate can be obtained by differentiating Eq. (2.2) as

$$\dot{\lambda} = -\frac{r_x v_y - r_y v_x}{r^2} \tag{2.3}$$

On the other hand, the look angle is

$$\varepsilon = \gamma - \lambda \tag{2.4}$$

Application of the sine function to both sides yields

$$\sin\varepsilon = \sin\gamma\cos\lambda - \cos\gamma\sin\lambda \tag{2.5}$$

Referring to Figure 1.1, the equation above can be rewritten as

$$\sin\varepsilon = \frac{r_x v_y - r_y v_x}{r^2}\frac{r}{v} \tag{2.6}$$

A comparison with Eq. (2.3) will reveal the second differential equation. So, the nonlinear differential equation set governing the engagement geometry is written as

$$\dot{r} = -v\cos\varepsilon \tag{2.7}$$

$$r\dot{\lambda} = -v\sin\varepsilon \tag{2.8}$$

where the first equation directly follows from the combination of Eq. (2.1) and Eq. (2.4).

The PPN guidance law is expressed as [5]

$$\dot{\gamma} = N\dot{\lambda} \tag{2.9}$$

where N is referred to as the navigation gain. The BPPN guidance law, upon which this piece of writing is founded, can be obtained by adding a bias term:

$$\dot{\gamma} = N\dot{\lambda} + b \tag{2.10}$$

where b denotes the bias value.

Before proceeding, the following should be noted:

$$a = v\dot{\gamma} \tag{2.11}$$

This basic relationship can be derived by considering the infinitesimal amount of rotation caused by an acceleration vector acting perpendicular to the velocity vector of a point for an infinitesimal amount of time.

Moving on; the time derivative of Eq. (2.4) is

$$\dot{\varepsilon} = \dot{\gamma} - \dot{\lambda} \tag{2.12}$$

The combination of this equation and Eq. (2.10) modifies Eq. (2.7) and Eq. (2.8) as

$$\dot{r} = -v\cos\varepsilon \tag{2.13}$$

$$\dot{\varepsilon} = -\left(N-1\right)v\frac{\sin\varepsilon}{r} + b \tag{2.14}$$

It may be appreciated that a nondimensional differential equation set would facilitate a more general understanding of BPPN kinematics. Therefore, two new variables, the nondimensional range and time, are introduced as

$$\rho = |\beta| r \tag{2.15}$$

$$\mathrm{d}\tau = |b| \mathrm{d}t \tag{2.16}$$

Here, it is important to note that ρ is a positive quantity and that the following is so defined that it is constant:

$$\beta = \frac{b}{v} \tag{2.17}$$

Now, after the change of variables defined in Eq. (2.15) and Eq. (2.16), Eq. (2.13) and Eq. (2.14) can be expressed as

$$\rho' = -\cos\varepsilon \tag{2.18}$$

$$\varepsilon' = -(N-1)\frac{\sin\varepsilon}{\rho} + \sigma \tag{2.19}$$

where the prime operator represents derivative with respect to the nondimensional time, i.e. $\mathrm{d}/\mathrm{d}\tau$. σ denotes the sign of *b* and is therefore constant even though *b* may be varying. The equilibrium points of this system are readily seen to be

$$\rho_{\mathrm{e}} = \pm\frac{N-1}{\sigma} \tag{2.20}$$

$$\varepsilon_{\mathrm{e}} = k\frac{\pi}{2} \tag{2.21}$$

where $k = \pm 1, \pm 3, \pm 5 \ldots$

The differential equation set in Eq. (2.18) and Eq. (2.19) need to be integrated to obtain information on how the state variables ε and ρ change as the engagement progresses. To circumvent the unfavorable integration process in the time domain, Eq. (2.19) is divided to Eq. (2.18) to yield

$$\frac{\mathrm{d}}{\mathrm{d}\rho}\sin\varepsilon = \left(N-1\right)\frac{\sin\varepsilon}{\rho} - \sigma \tag{2.22}$$

The solution of this differential equation can be shown to assume the following form

$$\sin\varepsilon = c\rho^{N-1} + \frac{\sigma}{N-2}\rho \tag{2.23}$$

Here, c is an integration constant that defines the family of state plane trajectories. This solution is obviously invalid for $N = 2$, in which case it becomes

$$\sin\varepsilon = \rho\left(-\sigma\ln\rho + c\right) \tag{2.24}$$

Moreover, the transformation in Eq. (2.15) modifies Eq. (2.10) as

$$\gamma' = N\lambda' + \sigma \tag{2.25}$$

and Eq. (2.4) leads to

$$\varepsilon' = \gamma' - \lambda' \tag{2.26}$$

The combination of Eq. (2.25) and Eq. (2.26) yields

$$\gamma' = \frac{N\varepsilon' - \sigma}{N-1} \tag{2.27}$$

Combination of this equation with Eq. (2.19) gives

$$\gamma' = -N\frac{\sin\varepsilon}{\rho} + \sigma \tag{2.28}$$

For $N \neq 2$, substituting the sine term from Eq. (2.23) gives

$$\gamma' = -cN\rho^{N-2} - \frac{2\sigma}{N-2} \tag{2.29}$$

Here, the path angle rate is with respect to the nondimensional time; the dimensional form, which is the scaled form of the acceleration, can be obtained via Eq. (2.16). It is important to note that the equations indicate nonzero acceleration at the final instant if the bias is still present. The derivative of Eq. (2.29) with respect to the nondimensional range can be written as

$$\frac{\mathrm{d}}{\mathrm{d}\rho}\gamma' = -cN\left(N-2\right)\rho^{N-3} \tag{2.30}$$

This last equation may be considered to be some form of jerk, i.e. the derivative of the acceleration, and its behavior towards the end of the engagement might have important implications. The limit of Eq. (2.30) as ρ goes to zero is

$$\lim_{\rho\to 0}\frac{\mathrm{d}}{\mathrm{d}\rho}\gamma' = \begin{cases} 0 & \text{if } N \geq 3 \\ \pm\infty & \text{if } N < 3 \end{cases} \tag{2.31}$$

As seen, the limit goes to infinity when the navigation gain is smaller than 3. This could constitute a potential problem for pursuers with slow command following dynamics: The miss distance will increase in response to increasing lag. The designer should be aware of this phenomenon.

As a last item, the path angle at any nondimensional range may be obtained via the following integral obtained by combining Eq. (2.29) with Eq. (2.23) and Eq. (2.18):

$$\gamma = \gamma_{\mathrm{i}} + \int_{\rho_{\mathrm{i}}}^{\rho} \frac{cN\theta^{N-2} + \dfrac{2\sigma}{N-2}}{\sqrt{1-\left(c\theta^{N-1} + \dfrac{\sigma}{N-2}\theta\right)^2}}\,\mathrm{d}\theta \tag{2.32}$$

where subscript i denotes the initial value and θ is a dummy variable. Unfortunately, it seems that no general analytical solution exists. One needs to resort to numerical means to obtain the solution.

2.1.1. State Plane Trajectories

The original motivation of this study is the need to increase the impact angle in ground-to-ground engagements. In such scenarios, the pursuer would benefit from increasing its altitude as much as possible, which can be done with positive biasing, i.e. $\sigma = 1$.

Notice: From this point on, $\sigma = 1$ will be utilized without notification.

State plane trajectories for several navigation gain and integration constant values are plotted in Figure 2.1. The plot does not have the sense of time because it passes on the information obtained from Eq. (2.23) and Eq. (2.24). It is interesting to note that one can travel on a variety of open and closed curves, each having a period of 2π along the vertical axis, depending on the *c* value or, equivalently, on initial conditions. An important observation is the intersection of some of the trajectories at the origin: In the general case where both objects are moving, the final relative velocity vector must lie on the LOS for a successful capture. On the other hand in this specific case of stationary target, the relative velocity vector is the absolute velocity vector of the pursuer. This implies that when the pursuer reaches the target, if it does so at all, it must have its look angle zero. Although the origin is not an equilibrium point in the mathematical sense, trajectories eventually arriving at it may be classified as stable because they practically terminate with capture.

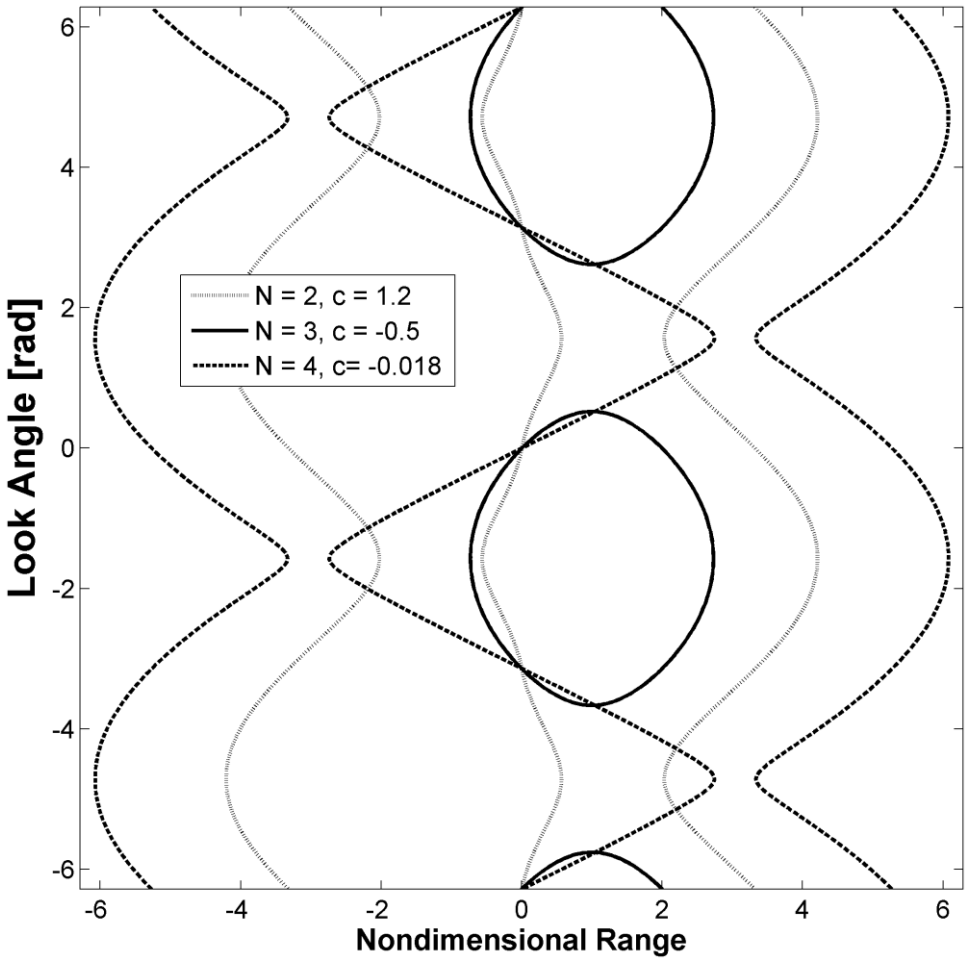

Figure 2.1 BPPN state plane trajectories for different parameters

Realistic trajectories, where $\rho > 0$ and $-\pi < \varepsilon < \pi$, are plotted in Figure 2.2, Figure 2.3 and Figure 2.4 respectively for $N = 2$, $N = 3$ and $N = 4$ utilizing the "pplane" software [45] based on Eq. (2.18) and Eq. (2.19). The arrows superimposed indicate the direction in which the pursuer travels with increasing time. The corresponding *c* values are indicated on some of the curves. It is seen that the same general principle applies to each figure: There is an equilibrium point somewhere on the upper half-plane. The trajectories roughly above the imaginary line connecting the upper left corner and this equilibrium point are seen to diverge from the origin whereas those roughly below the same line converge to it. The locations of the singular points for different *N* values can be verified to be compatible with Eq. (2.20).

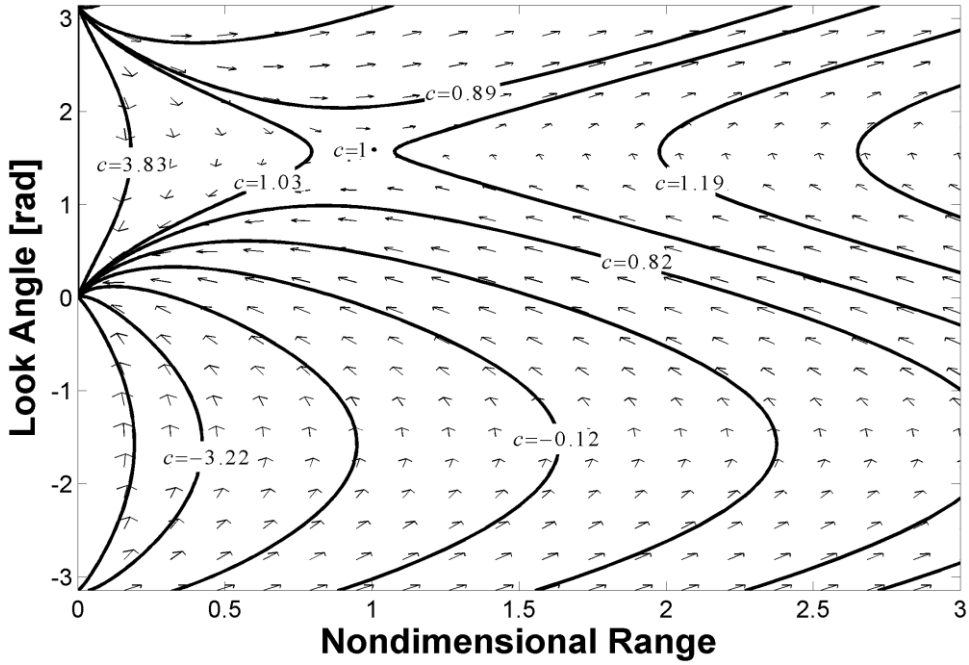

Figure 2.2 BPPN state plane trajectories for $N = 2$

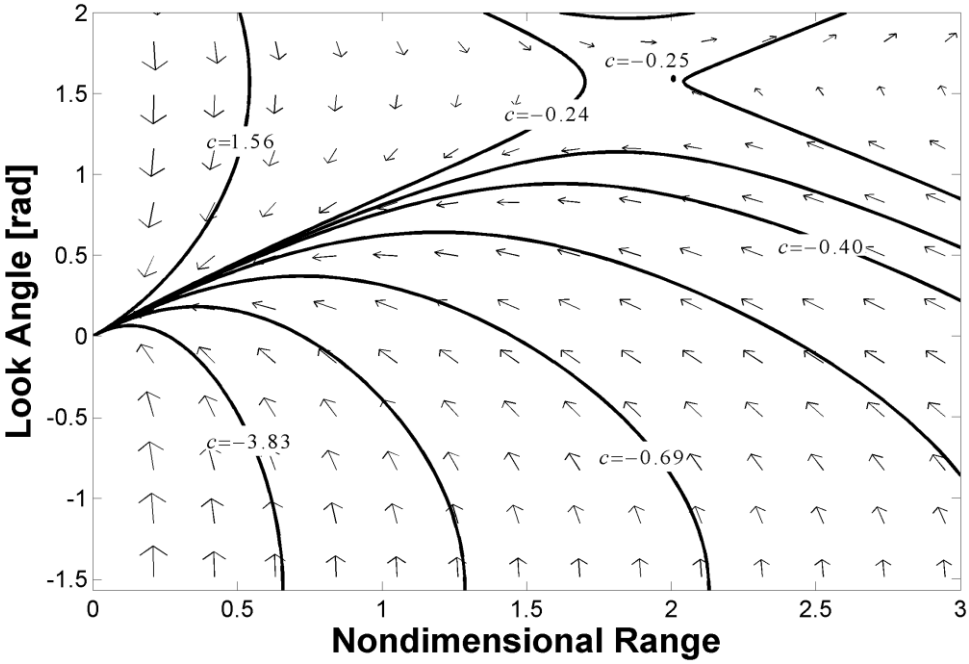

Figure 2.3 BPPN state plane trajectories for $N = 3$

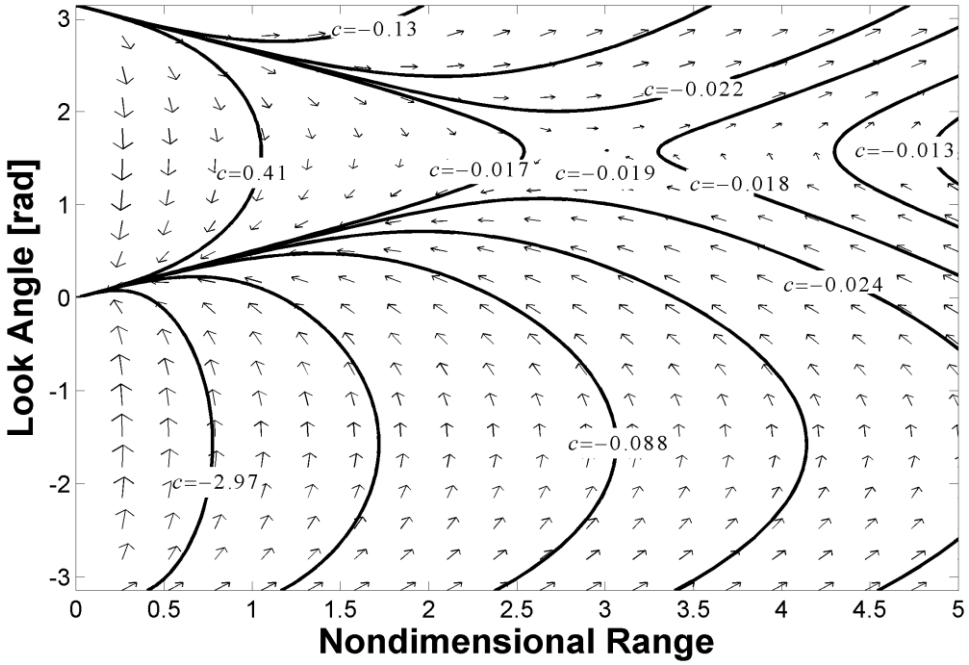

Figure 2.4 BPPN state plane trajectories for $N = 4$

2.1.2. Stability

To determine if a particular engagement will lead to capture, a stability criterion for the BPPN guidance law can be developed by making use of the integration constant of the equilibrium point. For $N \neq 2$, Eq. (2.23) can be utilized to obtain

$$c_{\mathrm{e}} = \frac{1}{\rho_{\mathrm{e}}^{N-1}}\left(\sin\varepsilon_{\mathrm{e}} - \frac{\rho_{\mathrm{e}}}{N-2}\right) \tag{2.33}$$

With $\varepsilon_{\mathrm{e}} = \pi/2$, it follows that

$$c_{\mathrm{e}} = -\frac{1}{(N-1)^{N-1}(N-2)} \tag{2.34}$$

As for $N = 2$, Eq. (2.24) can be used to get $c_{\mathrm{e}} = 1$.

Figure 2.2, Figure 2.3 and Figure 2.4 show that convergence does not depend solely on c since the same value may result in both divergent and convergent trajectories. By inspection, it can be concluded that the pursuer travels on a convergent trajectory if

$$\left\{c \geq c_{\mathrm{e}} \ \wedge \ \rho < \rho_{\mathrm{e}}\right\} \ \vee \ \left\{c \leq c_{\mathrm{e}} \ \wedge \ \varepsilon < \pi/2\right\} \tag{2.35}$$

where $\wedge$ is the AND operator and $\vee$ is the OR operator. The definition of ρ would be useful for physical interpretation of this criterion. For the same range, a small nondimensional range implies low bias (and/or high speed). The limiting case of low bias is having no bias at all. The guidance law in such a case becomes PPN, which always captures a stationary target unless $\varepsilon = -\pi$. It is thus reasonable that BPPN approaches to instability as ρ increases. Also, the criterion tells that BPPN may fail for high look angle values. This result is compatible with Eq. (2.13), which yields positive range rate for $\varepsilon > \pi/2$.

To determine whether a given bias value will lead to stability or instability, Eq. (2.15) and Eq. (2.34) can be used in Eq. (2.23) to yield

$$\sin\varepsilon_{\mathrm{i}} = -\frac{1}{(N-1)^{N-1}(N-2)}\left(\frac{b_{\mathrm{lim}} r_{\mathrm{i}}}{v}\right)^{N-1} + \frac{b_{\mathrm{lim}} r_{\mathrm{i}}}{(N-2)v} \tag{2.36}$$

or in Eq. (2.24) to yield

$$\sin\varepsilon_{\mathrm{i}} = \frac{b_{\mathrm{lim}} r_{\mathrm{i}}}{v}\left(\ln\frac{v}{b_{\mathrm{lim}} r_{\mathrm{i}}} + 1\right) \tag{2.37}$$

Here, b_{lim} is the limiting bias value above which the guidance loop goes unstable, which can be found by solving, possibly with numerical means, the preceding equations.

2.2. Examples of Continuous Bias Application

The reference engagement geometry considered throughout this thesis is as follows: A pursuer with an initial speed of 250 m/s is launched from the ground to capture a stationary ground target 5 km away. The initial path angle is 15° and this is also the initial look angle since the initial LOS angle is zero. The desired impact angle is $\gamma_{\mathrm{f,d}} = -90^{\circ}$. The simulations are terminated when the range goes below 1 m. In the examples below, the speed of the pursuer, which follows the guidance commands without lag, is constant. Such a basic approach is adopted in this preliminary section because it will make the interpretation of the results more straightforward.

There are two ways of finding the continuous bias corresponding to a specific value of the navigation gain that will lead to a desired impact condition. Unfortunately, both ways involve iteration, which is why the BPPN law as it is, i.e. the continuous bias application, is not promoted in this dissertation as a feasible guidance solution. The user may either repeatedly run simulations or solve Eq. (2.32) with different bias values until the desired impact angle is achieved. The number of simulations or solution attempts would depend on the how smart the iteration algorithm is.

For any engagement geometry, there are infinitely many combinations of the navigation gain and the bias that will result in a desired impact angle. This is why an impartial metric would be extremely useful for comparison. The total control effort, which is the time integral of the acceleration squared, can be used for this purpose [9]. The mathematical representation of this cost function is

$$E = \frac{1}{2}\int_{0}^{t_{\mathrm{f}}} a^{2}\,\mathrm{d}t \tag{2.38}$$

where t_{f} is the final time.

Figure 2.5 displays the variation of control effort values as a function of the navigation gain for the reference engagement geometry. It happens that the lowest

cost can be obtained with a gain of about 3.8. This minimizing value would change for other engagement geometries. This result might seem to be in contradiction with what will be presented in Section 2.3.2.3 about the optimality with $N = 3$ in the linear domain. The discrepancy is due to the fact that the environment is nonlinear. If the impact angle were to be gradually decreased so that the simulation environment approaches linearity, one would at a certain point start to see that the total control effort with $N = 3$ cannot be outperformed.

The bias values corresponding to the gain values of 2, 3, 3.8 and 4 turn out to be 3.37 °/s, 6.94 °/s, 9.64 °/s and 10.30 °/s, respectively. It is logical to have the bias increasing with the navigation gain because more bias is needed to oppose the LOS angle rate multiplied with a higher gain.

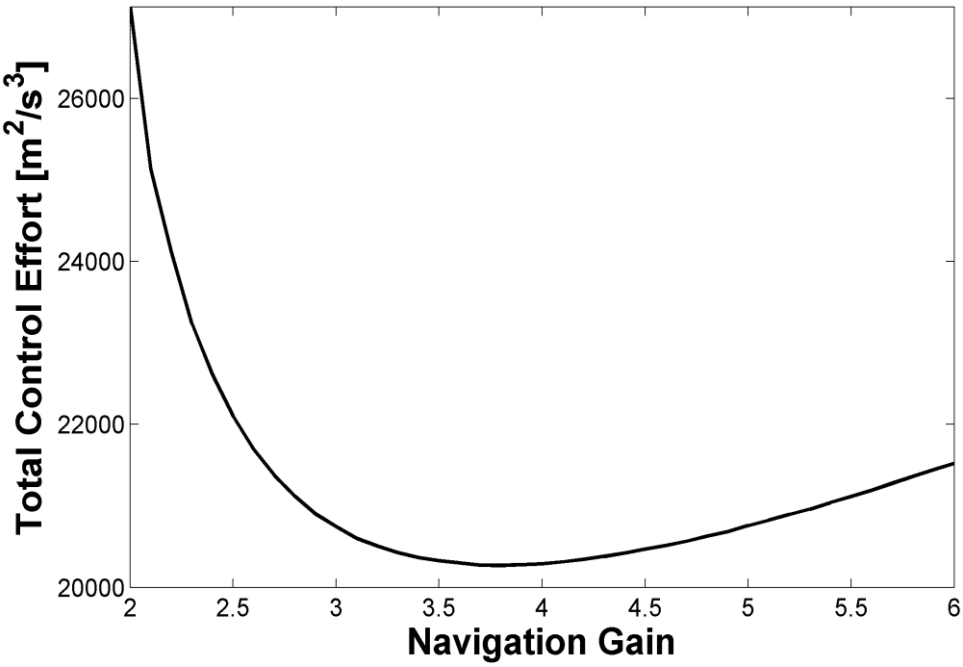

Figure 2.5 Cost of vertical impact as a function of navigation gain with continuous bias application strategy

Figure 2.6 shows the spatial trajectories created by these navigation gains. It is seen that there is a positive correlation between the gain value and the maximum altitude. The acceleration histories are presented in Figure 2.7. The minimum initial acceleration is created by $N = 2$; however, the price paid for using such a low gain is seen to be the very high value at the end of the engagement. This result is compatible with Eq. (2.31). On the other hand, $N = 4$ results in the highest initial and the lowest final acceleration values whereas $N = 3$ manages an intermediate response. The total control effort values obtained with these acceleration trends are: $E_2 = 27128 \text{ m}^2/\text{s}^3$, $E_3 = 20796 \text{ m}^2/\text{s}^3$, $E_{3.8} = 20334 \text{ m}^2/\text{s}^3$ and $E_4 = 20338 \text{ m}^2/\text{s}^3$. Due to its poor performance near the target as seen in Figure 2.7, the worst performance unsurprisingly belongs to $N = 2$. Being closer to the minimizing value, $N = 4$ performs slightly better than $N = 3$. Figure 2.8 presents the look angle behaviors to be compared with the state plane trajectories drawn in Figure 2.2, Figure 2.3 and Figure 2.4. Finally, the path angle variations are given in Figure 2.9. It is clearly seen that all four navigation gains are successful in leading the pursuer to the desired impact condition.

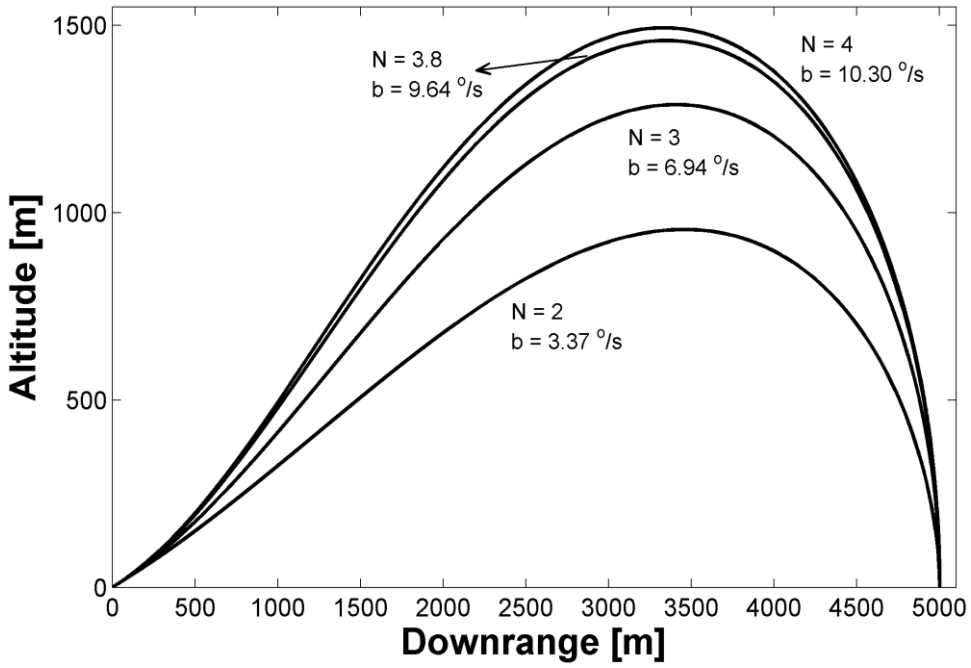

Figure 2.6 Spatial trajectories produced by the continuous bias application strategy

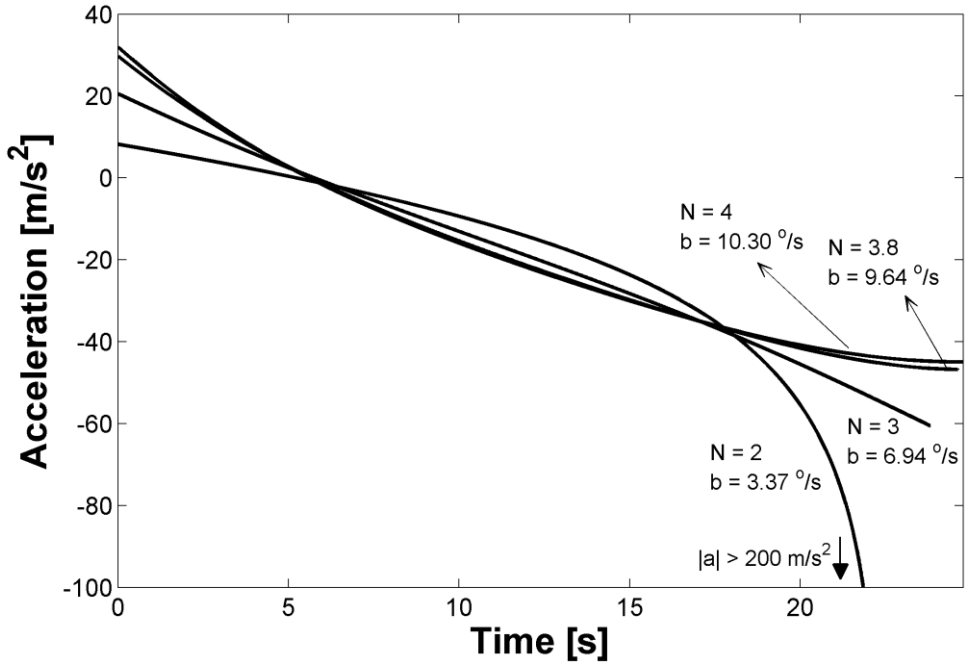

Figure 2.7 Acceleration histories produced by the continuous bias application strategy

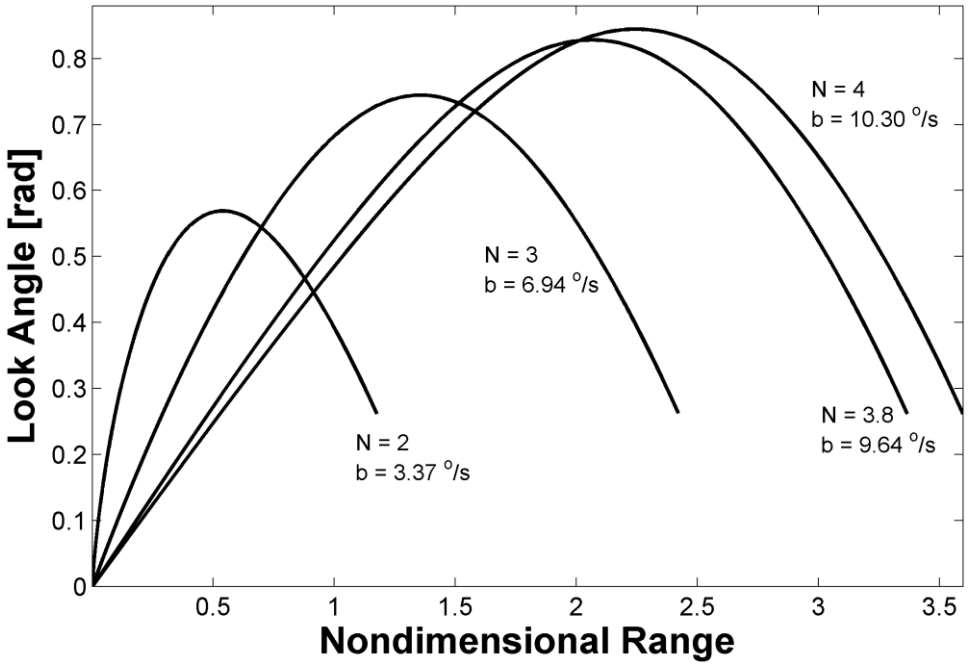

Figure 2.8 Look angle behaviors produced by the continuous bias application strategy

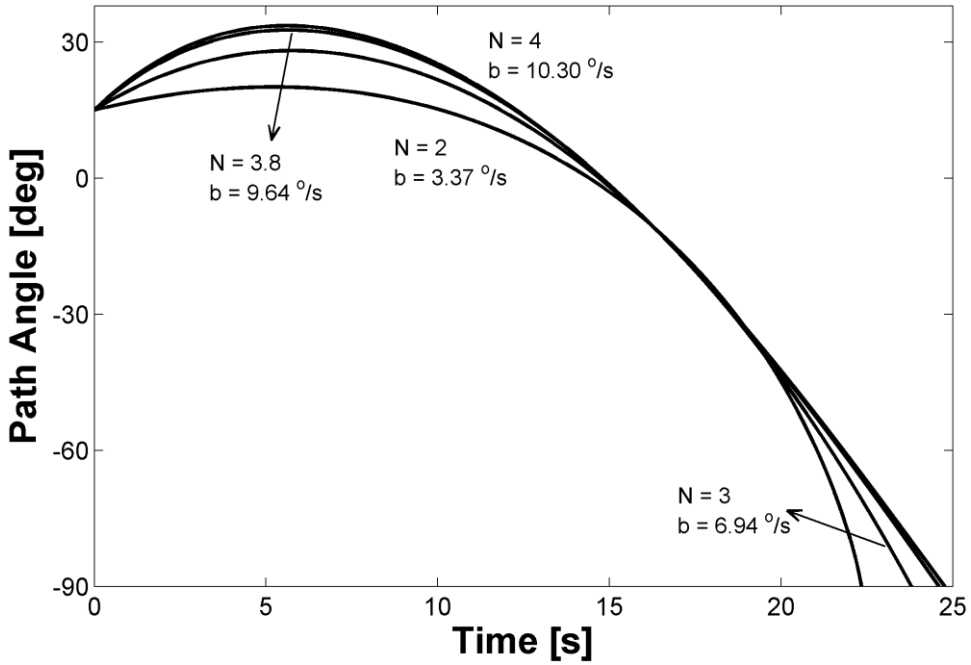

Figure 2.9 Path angle variations produced by the continuous bias application strategy

The benchmark scenario, which is to be used as a comparison criterion, is obtained by applying the optimal control procedure given in Appendix A to the reference engagement geometry. The following figures present the optimal results along with those produced by the cost-minimizing value of the BPPN gain. Figure 2.10 shows the spatial trajectories, which are not quite the same. In Figure 2.11, the acceleration histories are plotted. It is seen that the initial and final acceleration magnitudes produced by the continuous bias application scenario are both higher than those of the optimal control. In agreement with this, the total control effort values turn out to be 20167 m^2/s^3 and 20334 m^2/s^3 for the optimal and BPPN solutions, respectively. Lastly, Figure 2.12 shows the variations of the look and the path angles.

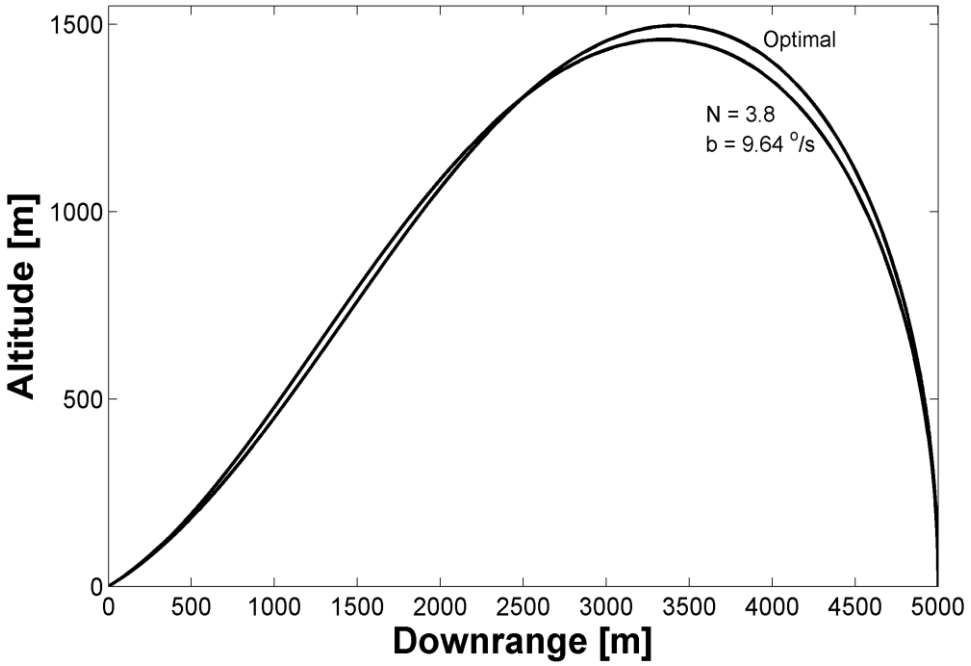

Figure 2.10 Comparison of spatial trajectories produced by the optimal and continuous bias application strategies

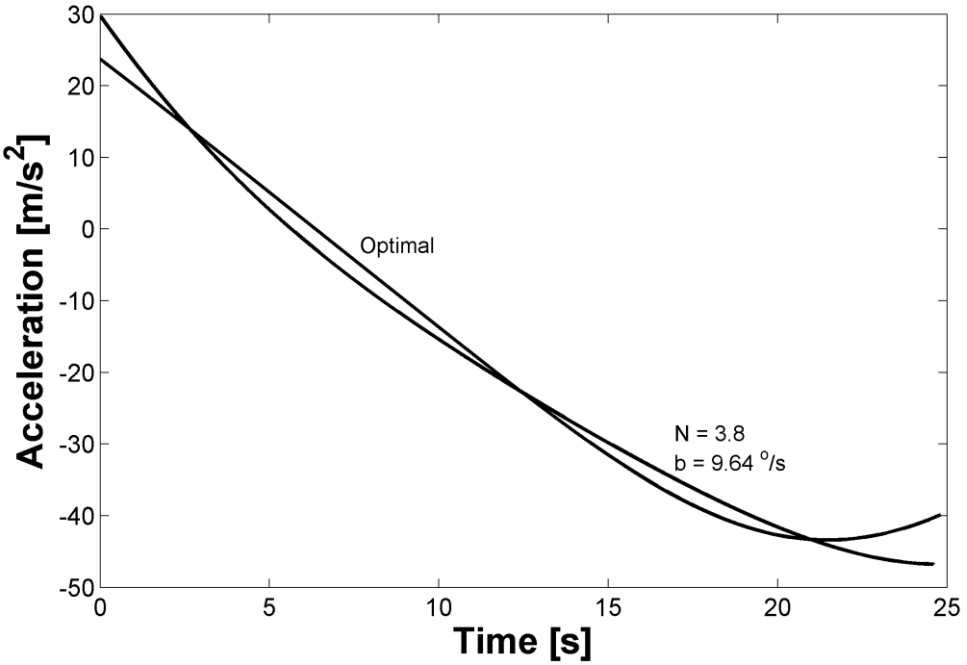

Figure 2.11 Comparison of acceleration histories produced by the optimal and continuous bias application strategies

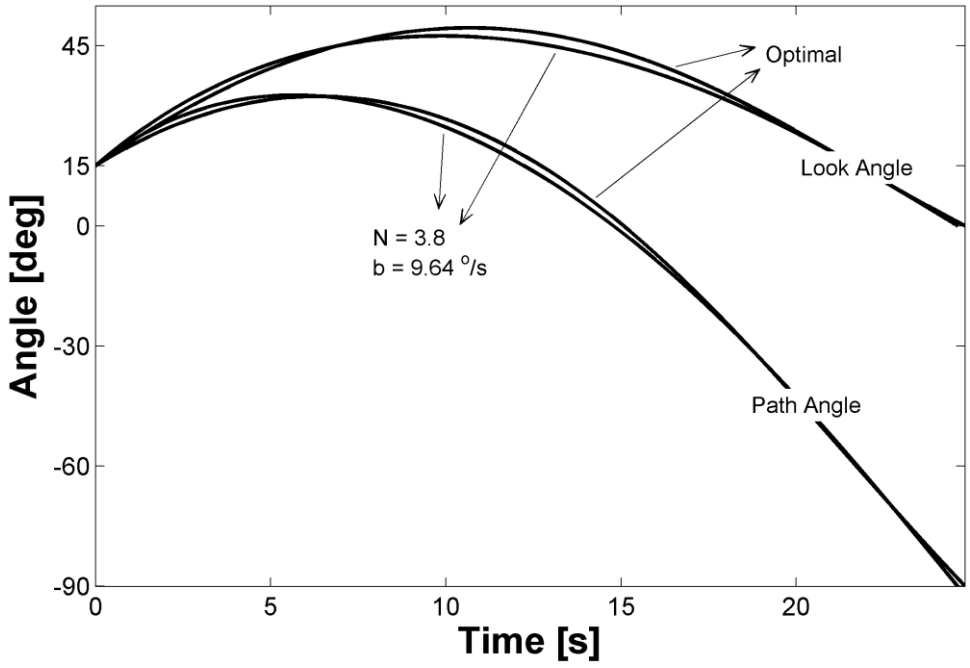

Figure 2.12 Comparison of look and path angle variations produced by the optimal and continuous bias application strategies

2.3. Linear Aspects

Mathematical tools to analyze linear systems are in general more direct than those that supply information about nonlinear counterparts. This section utilizes a linear point of view in order to provide more insight into the proposed guidance law. As the first item, the linear behavior of BPPN in the neighborhood of its equilibrium point will be analyzed. Then, the linear form of the biased PN (BPN) law will be obtained to compare it to the optimal control solution (the reader should note that in a linear world, the adjective *pure* accompanying PN is simply meaningless since there is only one direction the acceleration can be applied). Lastly, it will be shown that the bias term may be viewed as some kind of a disturbing factor in the PN guidance loop.

2.3.1. Equilibrium Analysis

A study of the equilibrium conditions of the system would be convenient to gain insight into the physics of the problem. The required partial derivatives of Eq. (2.18) to form the Jacobian matrix are as follows:

$$\frac{\partial}{\partial \rho}\rho' = 0 \tag{2.39}$$

$$\frac{\partial}{\partial \varepsilon}\rho' = \sin\varepsilon \tag{2.40}$$

$$\frac{\partial}{\partial \rho}\varepsilon' = \left(N-1\right)\frac{\sin\varepsilon}{\rho^2} \tag{2.41}$$

$$\frac{\partial}{\partial \varepsilon}\varepsilon' = -\left(N-1\right)\frac{\cos\varepsilon}{\rho} \tag{2.42}$$

Then the Jacobian matrix can be constructed as

$$\hat{J} = \begin{bmatrix} 0 & \sin\varepsilon_{\mathrm{e}} \\ \left(N-1\right)\dfrac{\sin\varepsilon_{\mathrm{e}}}{\rho_{\mathrm{e}}^2} & -\left(N-1\right)\dfrac{\cos\varepsilon_{\mathrm{e}}}{\rho_{\mathrm{e}}} \end{bmatrix} \tag{2.43}$$

Using Eq. (2.20) with positive range and bias, the final form of the matrix is

$$\hat{J} = \begin{bmatrix} 0 & 1 \\ \dfrac{1}{N-1} & 0 \end{bmatrix} \tag{2.44}$$

The eigenvalues can be shown to be

$$\Lambda_{1,2} = \pm\frac{1}{\sqrt{N-1}} \tag{2.45}$$

whereas the eigenvectors are

$$\bar{\Upsilon}_{1,2} = \begin{bmatrix} 1 \\ \pm \dfrac{1}{\sqrt{N-1}} \end{bmatrix} \tag{2.46}$$

Since the eigenvalues are equal in magnitude and of opposite sign, the singular point is a saddle point. The physical interpretation of such an equilibrium condition is that the target becomes the center of the pursuer's circular motion, which implies that the effects of the LOS angle rate and the bias term cancel each other; so, the pursuer neither converges to the target nor does it diverge away from it. Linear behaviors in the neighborhood of the equilibrium point for $N = 2$, $N = 3$ and $N = 4$ are presented respectively in Figure 2.13, Figure 2.14 and Figure 2.15. It is observed that the eigenvectors become more horizontal as N increases as predicted by Eq. (2.46).

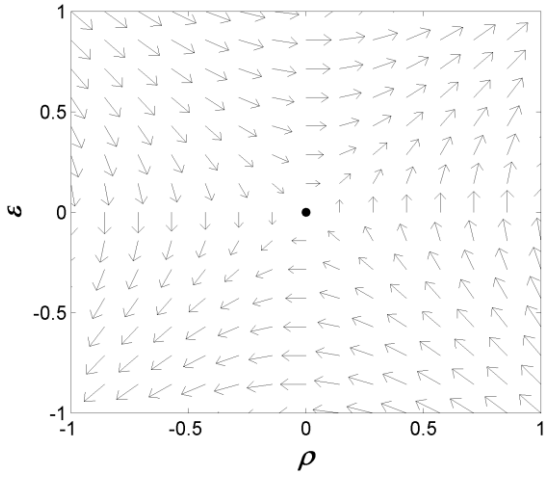

Figure 2.13 Neighborhood of the BPPN saddle point for $N = 2$

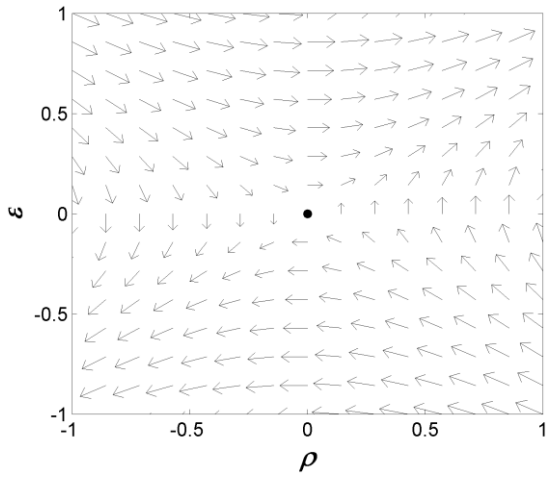

Figure 2.14 Neighborhood of the BPPN saddle point for $N = 3$

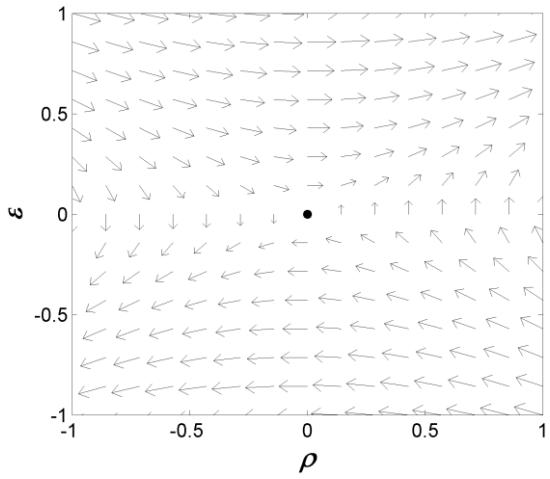

Figure 2.15 Neighborhood of the BPPN saddle point for $N = 4$

2.3.2. Optimality

The nonlinear engagement dynamics between a stationary target and its pursuer can be simplified by assuming that the horizontal velocity component V of the pursuer is constant. This is a commonly practiced simplification in guidance design [2] that enables the time to go ($t_{go} = t_f - t$) to be written as the range to go divided by the closing speed so that the remaining amount of time until the pursuer reaches the

target becomes available at any instant during the engagement. The only degree of freedom is associated with the pursuer, which is allowed to perform corrective maneuvers only in the vertical direction. Based on the geometry shown in Figure 2.16, the objective of this section is to solve the two-point linear optimal control problem and to compare the corresponding solution to the linear open-loop equivalent of the biased guidance law.

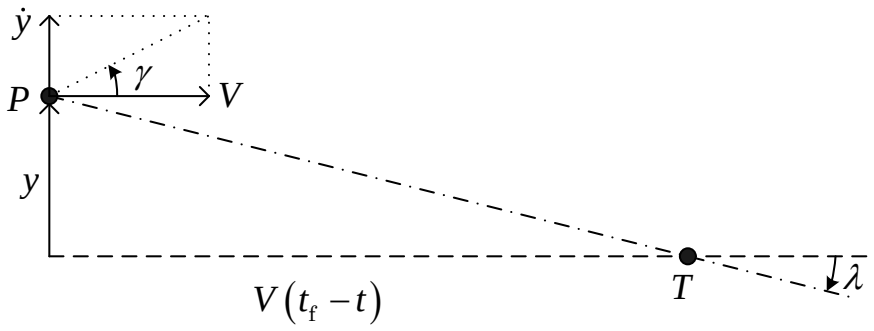

Figure 2.16 Linear engagement between a stationary target and its pursuer

2.3.2.1. Open Loop Optimal Control

Selecting the states and the control as

$$x_1 = y \tag{2.47}$$

$$x_2 = \dot{y} \tag{2.48}$$

$$u = \ddot{y} \tag{2.49}$$

the problem is to minimize the cost

$$E = \frac{1}{2}\int_0^{t_f} u^2 \mathrm{d}t \tag{2.50}$$

which is in the same form as Eq. (2.38), while satisfying the boundary conditions

$$\bar{x}(0) = \bar{x}_{\mathrm{i}} \tag{2.51}$$

$$\bar{x}(t_{\mathrm{f}}) = \bar{x}_{\mathrm{f}} \tag{2.52}$$

and the dynamic constraints

$$\dot{x}_1 = x_2 \tag{2.53}$$

$$\dot{x}_2 = u \tag{2.54}$$

The solution to this straightforward problem is (see Appendix B for the derivation)

$$u = \left\{ \frac{12}{t_{\mathrm{f}}^3}\left(x_{1,\mathrm{i}} - x_{1,\mathrm{f}}\right) + \frac{6}{t_{\mathrm{f}}^2}\left(x_{2,\mathrm{i}} + x_{2,\mathrm{f}}\right) \right\} t - \left\{ \frac{6}{t_{\mathrm{f}}^2}\left(x_{1,\mathrm{i}} - x_{1,\mathrm{f}}\right) + \frac{2}{t_{\mathrm{f}}}\left(2x_{2,\mathrm{i}} + x_{2,\mathrm{f}}\right) \right\} \tag{2.55}$$

and since $y_{\mathrm{f}} = 0$ is required in order to capture the target, the final result is

$$u = \left\{ \frac{12}{t_{\mathrm{f}}^3} x_{1,\mathrm{i}} + \frac{6}{t_{\mathrm{f}}^2}\left(x_{2,\mathrm{i}} + x_{2,\mathrm{f}}\right) \right\} t - \left\{ \frac{6}{t_{\mathrm{f}}^2} x_{1,\mathrm{i}} + \frac{2}{t_{\mathrm{f}}}\left(2x_{2,\mathrm{i}} + x_{2,\mathrm{f}}\right) \right\} \tag{2.56}$$

2.3.2.2. Linearization of BPN

Based on Figure 2.16, the path angle and its rate can be written as

$$\gamma = \frac{\dot{y}}{V} \tag{2.57}$$

$$\dot{\gamma} = \frac{\ddot{y}}{V} \tag{2.58}$$

The LOS angle and its rate are

$$\lambda = -\frac{y}{V\left(t_{\mathrm{f}} - t\right)} \tag{2.59}$$

$$\dot{\lambda} = -\frac{\dot{y}}{V\left(t_{\mathrm{f}} - t\right)} - \frac{y}{V\left(t_{\mathrm{f}} - t\right)^2} \tag{2.60}$$

So, the guidance law in Eq. (2.10) may be expressed as

$$\ddot{y} = -N\left\{\frac{\dot{y}}{\left(t_{\mathrm{f}} - t\right)} + \frac{y}{\left(t_{\mathrm{f}} - t\right)^2}\right\} + Vb \tag{2.61}$$

To find the equivalent of the bias term, the integrated form of Eq. (2.10) can be considered:

$$\gamma_{\mathrm{f}} - \gamma_{\mathrm{i}} = N\left(\lambda_{\mathrm{f}} - \lambda_{\mathrm{i}}\right) + bt_{\mathrm{f}} \tag{2.62}$$

Noting that the final values of the path and LOS angles are required to be equal for successful capture, the following becomes valid:

$$b = \frac{-\gamma_{\mathrm{i}} + N\lambda_{\mathrm{i}} - \left(N-1\right)\gamma_{\mathrm{f}}}{t_{\mathrm{f}}} \tag{2.63}$$

With the help of Eq. (2.57) and Eq. (2.59), the final form of *b* is

$$b = -\frac{Ny_{\mathrm{i}} + t_{\mathrm{f}}\dot{y}_{\mathrm{i}} + \left(N-1\right)t_{\mathrm{f}}\dot{y}_{\mathrm{f}}}{Vt_{\mathrm{f}}^2} \tag{2.64}$$

Using this result in Eq. (2.61) gives

$$\ddot{y} = -N\left\{\frac{\dot{y}}{t_\mathrm{f} - t} + \frac{y}{\left(t_\mathrm{f} - t\right)^2}\right\} - \frac{Ny_\mathrm{i} + t_\mathrm{f}\dot{y}_\mathrm{i} + \left(N-1\right)t_\mathrm{f}\dot{y}_\mathrm{f}}{t_\mathrm{f}^2} \tag{2.65}$$

The second term above, which is a constant, might as well be constructed using instantaneous variables. Replacing in this term t_f with $t_\mathrm{f} - t$ and the initial variables with instantaneous variables will do the trick. So Eq. (2.65) becomes

$$\ddot{y} = -2N\left\{\frac{\dot{y}}{t_\mathrm{f} - t} + \frac{y}{\left(t_\mathrm{f} - t\right)^2}\right\} + \left(N-1\right)\frac{\dot{y} - \dot{y}_\mathrm{f}}{t_\mathrm{f} - t} \tag{2.66}$$

This same form was obtained in [16] using a different approach, where it was shown that Eq. (2.66) gave the optimal control corresponding to a cost function whose integrand was that of Eq. (2.38) divided by some power of the time to go. A special form of Eq. (2.66) with $N = 3$, $y_\mathrm{f} = 0$ and $\dot{y}_\mathrm{f} = 0$ was reported in [9] as

$$\ddot{y} = -\frac{4\dot{y}}{t_\mathrm{f} - t} - \frac{6y}{\left(t_\mathrm{f} - t\right)^2} \tag{2.67}$$

According to [2], this is "the guidance law that landed the Apollo spacecraft on the moon in 1969". Using Eq. (2.57), Eq. (2.59) and Eq. (2.60), Eq. (2.66) can be manipulated into the following forms:

$$\dot{\gamma} = 2N\dot{\lambda} + \left(N-1\right)\frac{\gamma - \gamma_\mathrm{f,d}}{t_\mathrm{go}} \tag{2.68}$$

$$\dot{\gamma} = N\dot{\lambda} + \frac{N\lambda - \gamma - \left(N-1\right)\gamma_\mathrm{f,d}}{t_\mathrm{go}} \tag{2.69}$$

$$\dot{\gamma} = \frac{2N\lambda - \left(N+1\right)\gamma - \left(N-1\right)\gamma_\mathrm{f,d}}{t_\mathrm{go}} \tag{2.70}$$

which respectively appear in [39], [2] and [15] with $N=3$. It is interesting to note that the coefficients of the LOS angle rate in the first two equations are different from each other and the LOS rate itself does not even exist in the last equation. The guidance designer should take into account the feedback availability of the signals in the actual system when selecting among these alternatives.

2.3.2.3. Optimality of Biased Proportional Navigation

The second-order differential equation presented in Eq. (2.65) can be rewritten as

$$\ddot{y} = -N\left\{\frac{\dot{y}}{t_{\mathrm{f}}-t}+\frac{y}{\left(t_{\mathrm{f}}-t\right)^{2}}\right\}+C \tag{2.71}$$

where C is a constant. If the transformation

$$\chi = t_{\mathrm{f}}-t \tag{2.72}$$

is applied, Eq. (2.71) can be written as

$$\chi^{2}y''(\chi)-N\chi y'(\chi)+Ny(\chi)=C\tau^{2} \tag{2.73}$$

which is a nonhomogeneous Euler-Cauchy type differential equation. Its general solution can be shown to be

$$y(\chi)=d_{1}\chi^{N}-\frac{C}{N-2}\chi^{2}+d_{2}\chi \tag{2.74}$$

where d_1 and d_2 are the integration constants. The corresponding first and second derivatives are

$$y'(\chi) = Nd_1\chi^{N-1} - \frac{2C}{N-2}\chi + d_2 \tag{2.75}$$

$$y''(\chi) = N(N-1)d_1\chi^{N-2} - \frac{2C}{N-2} \tag{2.76}$$

At $\chi = t_\mathrm{f}$, i.e. $t = 0$, the conditions $y(t_\mathrm{f}) = y_\mathrm{i}$ and $y'(t_\mathrm{f}) = -\dot{y}_\mathrm{i}$ are applicable. This, using Eq. (2.74) and Eq. (2.75), leads to the following set of equations

$$\begin{bmatrix} t_\mathrm{f}^N & t_\mathrm{f} \\ Nt_\mathrm{f}^{N-1} & 1 \end{bmatrix}\begin{bmatrix} d_1 \\ d_2 \end{bmatrix} = \begin{bmatrix} y_\mathrm{i} + \dfrac{C}{N-2}t_\mathrm{f}^2 \\ -\dot{y}_\mathrm{i} + \dfrac{2C}{N-2}t_\mathrm{f} \end{bmatrix} \tag{2.77}$$

The first integration constant can then be solved as

$$d_1 = -\frac{2y_\mathrm{i} + t_\mathrm{f}\dot{y}_\mathrm{i} + t_\mathrm{f}\dot{y}_\mathrm{f}}{(N-2)t_\mathrm{f}^N} \tag{2.78}$$

Hence the second derivative in Eq. (2.75) can be written in open form as

$$y''(\chi) = -N(N-1)\left\{\frac{2y_\mathrm{i} + t_\mathrm{f}\dot{y}_\mathrm{i} + t_\mathrm{f}\dot{y}_\mathrm{f}}{(N-2)t_\mathrm{f}^N}\right\}\chi^{N-2} + \frac{2}{N-2}\left\{\frac{Ny_\mathrm{i} + t_\mathrm{f}\dot{y}_\mathrm{i} + (N-1)t_\mathrm{f}\dot{y}_\mathrm{f}}{t_\mathrm{f}^2}\right\} \tag{2.79}$$

Transforming back to the original variable yields

$$\ddot{y} = -N(N-1)\left\{\frac{2y_\mathrm{i} + t_\mathrm{f}\dot{y}_\mathrm{i} + t_\mathrm{f}\dot{y}_\mathrm{f}}{(N-2)t_\mathrm{f}^N}\right\}(t_\mathrm{f} - t)^{N-2} + \frac{2}{N-2}\left\{\frac{Ny_\mathrm{i} + t_\mathrm{f}\dot{y}_\mathrm{i} + (N-1)t_\mathrm{f}\dot{y}_\mathrm{f}}{t_\mathrm{f}^2}\right\} \tag{2.80}$$

If $N = 3$, it can be shown after some straightforward arrangement that Eq. (2.80) is in fact equivalent to Eq. (2.56). This proves that the BPN scheme with $N = 3$ is optimal with respect to Eq. (2.50) in a linear setting.

2.3.3. Equivalency of Inputs

The implementation of the PN guidance requires the LOS angle rate. When the LOS angle rate is measured by an onboard sensor such as a gyro, it is likely that one of the dominant error types will be the bias error. Appointing b_s to denote the seeker bias error, the realized path angle rate using the intended law of Eq. (2.10) happens to be

$$\dot{\gamma} = N\left(\dot{\lambda} + b_s\right) + b \tag{2.81}$$

If the target acts evasively in the vertical direction, $\ddot{y}_r = \ddot{y} - \ddot{y}_T$ will be valid, where y_r is the relative vertical displacement. Thus, making use of Eq. (2.58) and Eq. (2.60) where *y* is replaced with y_r, Eq. (2.81) may be written as

$$\ddot{y}_r + N\frac{\dot{y}_r}{t_f - t} + N\frac{y_r}{\left(t_f - t\right)^2} = Vb + NVb_s - \ddot{y}_T \tag{2.82}$$

The seemingly simple equation above has the following important implications:

- The intentional bias, the unintentional bias error and the target acceleration are equivalent in effect to the PN guidance loop.
- The bias error due to the seeker is *N* times as effective as the trajectory-shaping bias value.
- Unlike the bias errors, the target maneuver in one direction disturbs the loop in the opposite direction.

This short section tries to underline the significance of having high quality LOS angle rate estimates available so that the pursuer may shape its trajectory properly. To give an exaggerated example; an anti-tank missile that obtains low quality outputs from its seeker might judge that its target is maneuvering in the same way the target of an air defense missile maneuvers.

CHAPTER 3

IMPACT ANGLE CONTROL WITH BIASED PURE PROPORTIONAL NAVIGATION

The examples presented in Section 2.2 show that a desired impact angle can be achieved by the continuous application of a predetermined amount of bias. Since the bias value needs to be found by iterative means, such an approach is not feasible. Several alternative and feasible solutions to this problem are presented in this chapter, which is the one where the outcomes of the previous chapter will be put to practical use.

3.1. BPPN Impact Angle

The integrated form of Eq. (2.10) is

$$\gamma_{\mathrm{f}} - \gamma_{\mathrm{i}} = N\left(\lambda_{\mathrm{f}} - \lambda_{\mathrm{i}}\right) + \int_{t_{\mathrm{i}}}^{t_{\mathrm{f}}} b \, \mathrm{d}t \tag{3.1}$$

Making use of (2.4), this can be written as

$$\gamma_{\mathrm{f}} - \gamma_{\mathrm{i}} = N\left(\gamma_{\mathrm{f}} - \varepsilon_{\mathrm{f}} - \lambda_{\mathrm{i}}\right) + \int_{t_{\mathrm{i}}}^{t_{\mathrm{f}}} b \, \mathrm{d}t \tag{3.2}$$

As per Eq. (2.23), the look angle is zero when the range is zero. This means that the final value of the look angle must be zero if the target is to be captured. This is also

intuitively obvious: The final velocity vector must be on the LOS to capture a stationary target. Therefore, Eq. (3.2) can be written as

$$\gamma_{\mathrm{f}} = \frac{N\lambda_{\mathrm{i}} - \gamma_{\mathrm{i}} - B}{N-1} \tag{3.3}$$

where the impact angle is seen to be a function of the following: the navigation gain, the initial angular conditions and the total value of the bias integral denoted by *B*. This seemingly simple equation, which is the backbone of the impact angle control logic developed in this study, has a very important implication: The impact angle can be controlled by adjusting the bias integral.

If there was no bias, the impact angle would be the result of the undisturbed flow of the PPN guidance law instead of the BPPN law. Erasing the bias integral and replacing the initial variables with instantaneous ones, Eq. (3.3) can be transformed into

$$\Gamma = \frac{N\lambda - \gamma}{N-1} \tag{3.4}$$

or via Eq. (2.4) into

$$\Gamma = \gamma - \frac{N}{N-1}\varepsilon \tag{3.5}$$

This equation gives the potential impact angle function, which is defined as the impact angle that will be obtained if the pursuer maintains a PPN course from the moment the function value is calculated until the very end, independent of the guidance law it has been performing. This suggests that the potential impact angle function remains constant during the PPN process.

3.2. Bias Application Alternatives

According to Eq. (3.3), the bias integral must have a specific value at the end of the engagement so that a desired impact angle can be obtained, i.e. $\gamma_{\mathrm{f}} = \gamma_{\mathrm{f,d}}$. This desired value happens to be

$$B_{\mathrm{d}} = N\lambda_{\mathrm{i}} - \gamma_{\mathrm{i}} - \left(N-1\right)\gamma_{\mathrm{f,d}} \tag{3.6}$$

This equation represents the single condition to reach a desired impact angle via BPPN. It imposes a constraint on *B*; however, it does not tell anything about *b*. So, the designer seems to be free to shape the bias profile. The shaping would probably be based on some design requirement; yet at the same time, the designer should be aware of the stability considerations explained in Section 2.1.2 especially if the bias is still to be present when the pursuer is in the vicinity of the target.

The fundamental issue that needs attention is the fact that the pursuer does not know in advance how much time there is to reach the target. If the total engagement time *L* was known, the most direct choice would be to invoke the constant bias concept and to write Eq. (3.6) as

$$b = \frac{N\lambda_{\mathrm{i}} - \gamma_{\mathrm{i}} - \left(N-1\right)\gamma_{\mathrm{f,d}}}{L} \tag{3.7}$$

which, as shown in Section 2.3.2.3, is the optimal strategy in a linear setting and would be expected to work also well in a nonlinear environment. However, the time to go is almost never available in practice. Even if the target position was known precisely and the assumption of constant pursuer speed was valid, the highly curved shape of the trajectory to be produced by BPPN would not allow an efficient calculation. Hence, Eq. (3.7) has little use in its current form.

In what follows, alternative strategies for impact angle control will be explored in the framework of the BPPN guidance law. The first two strategies are the discontinuous

and range-driven bias application tactics based on Eq. (3.7). The distinct advantage of the former approach, which involves at least one switching between the BPPN and PPN (the reader is advised to refer to Appendix C for analytical solutions) guidance laws, is the fact that it does not require the time-to-go information. The latter approach, on the other hand, makes use of the time-to-go estimation supplied via the range observer to be introduced in Chapter 5 and provides an acceleration command profile with no phase switching. As far as the impact angle control logics are concerned, the superiority of the second strategy is its closed loop nature as opposed to the open loop nature of the first strategy during the terminal PPN phase. The third and the last strategy is based on the concept of error dynamics inspired by Eq. (3.4). Like the first strategy, it does not require the time to go; and, like the second strategy, it regulates the impact angle error in a closed loop manner. The control action is achieved by means of a single constant gain, which needs to be sufficiently high so that the error can safely diminish before the engagement ends.

3.2.1. Discontinuous Bias Application

As stated above, the only critical parameter is the final value of the bias integral as presented in Eq. (3.6). It then seems reasonable to increase the bias value given in Eq. (3.7) by using a shorter interval Δt than the total engagement time L. This Δt value is in practice far easier to obtain than the L value because it is not unique; any value can be utilized provided that it is guaranteed to be lower than L. This reasoning enables Eq. (3.7) to be written as

$$b = \frac{N\lambda_{\mathrm{i}} - \gamma_{\mathrm{i}} - (N-1)\gamma_{\mathrm{f,d}}}{\Delta t} \tag{3.8}$$

The equation above implies that the constant bias can be applied on any interval during the engagement. In fact, the total biasing effort may even be divided into several intervals. Multiple intervals, however, would complicate the guidance logic and there must definitely be some solid reasoning for resorting to such a practice. To

keep things simple, the current focus is maintained on using a single interval of biasing as exemplified in [2].

Now, based on the guidance laws in Eq. (2.9) and Eq. (2.10), the discontinuous guidance strategy to control the impact angle can be proposed as

$$\dot{\gamma} = \begin{cases} N\dot{\lambda} + b & \text{if } t_{\mathrm{b}} \le t \le t_{\mathrm{b}} + \Delta t \\ N\dot{\lambda} & \text{otherwise} \end{cases} \tag{3.9}$$

where b is defined in Eq. (3.8). As seen, the logic dictates switching between guidance laws when the appropriate time comes. This is clearly a two phased structure; the BPPN phase may be regarded as the *midcourse* phase and the PPN phase may be regarded as the *terminal* phase. It can be said that the bias application logic is open loop; that is, it purely depends on time, t_{b} indicating the beginning time of the bias interval. By resorting to such a guidance structure, the designer expects that Eq. (3.4) will yield $\Gamma = \gamma_{\mathrm{f,d}}$ after the duration of $t_{\mathrm{b}} + \Delta t$ has elapsed and that at the end of the unbiased terminal phase, the desired impact angle will be obtained.

Besides the guidance objective $\gamma_{\mathrm{f,d}}$, there are two user-specified parameters in Eq. (3.9) that are N and t_{b}. The effect of the navigation gain will be investigated shortly. As for the bias start time, the following reasoning is considered: One may appreciate the fact that there are two opposing forces at work when using the BPPN guidance law. The LOS angle rate drives the velocity vector toward the LOS while the bias tries to do just the opposite. Hence, the shaping of the trajectory by means of bias addition would be easier when the target is still far away owing to the low levels of the LOS angle rate. This implies that the bias application interval should start as early as possible if the pursuer wants to avoid high control effort. To briefly demonstrate this situation, the case with $N = 3$ is simulated for $t_{\mathrm{b}} = 0,\ 1,\ 2$ s. For the reference engagement geometry introduced in Section 2.2, $\Delta t = 20$ s, for instance, is guaranteed to be shorter than the total time. For $N = 3$, Eq. (3.14) yields $b = 8.25$ °/s.

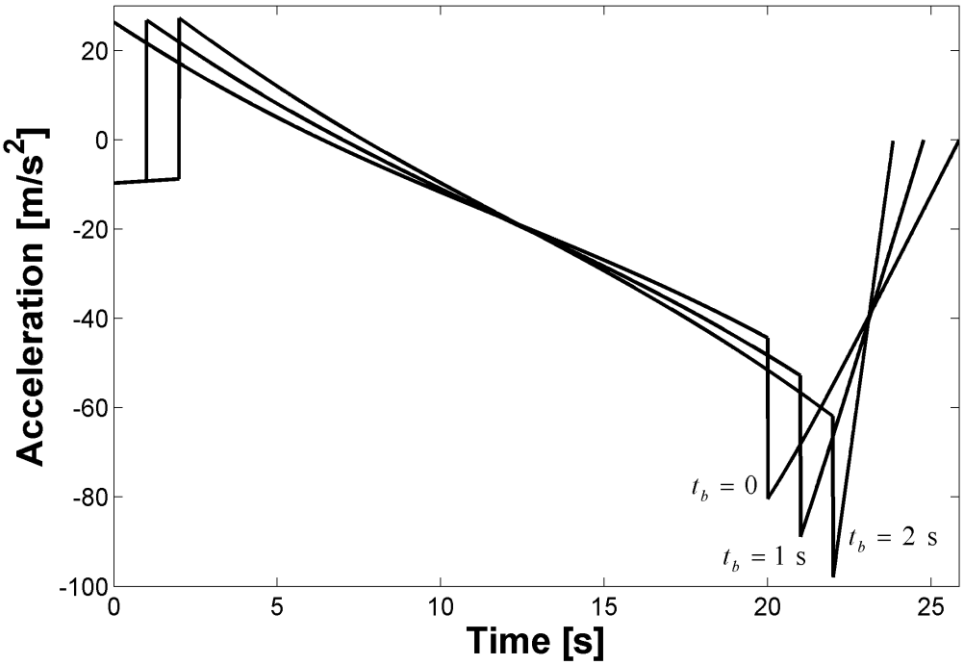

Figure 3.1 Acceleration histories for various delay times produced by the discontinuous bias application strategy

Figure 3.1 presents the acceleration trends. It is observed that the levels are almost the same at the beginnings of the biased intervals. When the bias is removed, however, the responses happen to be quite different. It can be concluded that the more the application of the bias is delayed the higher the acceleration magnitude will be at the switching instant. In accordance with this fact, the control effort values from Eq. (2.38) are 23127 m^2/s^3, 23693 m^2/s^3 and 24242 m^2/s^3. Another important point that needs attention is associated with the end game duration. As seen in the figure, the pursuer is expected to accommodate a discrete jump in the acceleration command when it nears the target. If the time constant of the pursuer is not sufficiently lower than the amount of time left after the switching, certain problems in its acceleration response are very likely to arise. Because the pursuer considered here is ideal with no time lag, there seem to be no problems at all in Figure 3.1. However, for the case where the biasing starts at $t = 2$ s, the time allocated for the end game is about 1.8 s, which might be quite short to experience a discrete jump followed by a ramp-like trend that leads to zero acceleration. As opposed to this, the

pursuer has almost 6 s to complete its terminal maneuver when the bias starts at the very beginning.

Having settled the issue of bias start time, it is now time to revisit the guidance logic given in Eq. (3.9). With $t_b = 0$, the following form appears:

$$\dot{\gamma} = \begin{cases} N\dot{\lambda} + b & \text{if } t \le \Delta t \\ N\dot{\lambda} & \text{otherwise} \end{cases} \tag{3.10}$$

During a typical ground-to-ground scenario governed by Eq. (3.10), the potential impact angle is expected to become more negative with increasing time until $\Gamma = \gamma_{f,d}$ holds at $t = \Delta t$. This is the instant when BPPN leaves the stage to PPN. This reasoning makes it possible to write the following:

$$\dot{\gamma} = \begin{cases} N\dot{\lambda} + b & \text{if } \dfrac{N\lambda - \gamma}{N-1} > \gamma_{f,d} \\ N\dot{\lambda} & \text{otherwise} \end{cases} \tag{3.11}$$

It should here be noted that unlike Eq. (3.10), the equality is embedded in the second condition because PPN maintains $\Gamma = \gamma_{f,d}$. Also, It is seen that instead of the time dependent switching condition in Eq. (3.10), Eq. (3.11) includes another one based on the potential impact angle function defined in Eq. (3.4) with Γ replaced with $\gamma_{f,d}$. This alternative form of decision making brings about an important improvement for the midcourse phase: If, for some reason, the pursuer cannot realize $\Gamma = \gamma_{f,d}$ at $t = \Delta t$, the desired impact angle should not be obtained if the switching condition was as seen in Eq. (3.10). The upgraded condition in Eq. (3.11) ensures that the pursuer will not remove the bias until the potential function value is as desired. Also, it needs to be stated that the switching from midcourse to terminal should be one way. In other words, no return to the biased guidance phase should be allowed in practice even if Γ does not remain constant due to some disturbance the pursuer is likely to struggle with. This is because of the limited time allocated to terminal maneuvers; it would just not be wise to risk a switching back to BPPN when the

pursuer has already commenced PPN. So, the impact angle control structure in Eq. (3.11) may be thought to be closed loop during the midcourse guidance and open loop during the terminal guidance in terms of impact angle control.

At this point, the following question might arise: Does the operator have to use the same navigation gains for both phases? The answer is simply *no*. In fact, the flexibility can be increased by increasing the number of user specified parameters by one. In short, by introducing the midcourse gain N_{M} and the terminal gain N_{T}, Eq. (3.11) can be converted into

$$\dot{\gamma} = \begin{cases} N_{\mathrm{M}}\dot{\lambda} + b & \text{if } \dfrac{N_{\mathrm{T}}\lambda - \gamma}{N_{\mathrm{T}} - 1} > \gamma_{\mathrm{f,d}} \\ N_{\mathrm{T}}\dot{\lambda} & \text{otherwise} \end{cases} \tag{3.12}$$

where the bias term satisfies Eq. (3.8).

It is now time to deal with the ambiguity inherent in the Δt term in Eq. (3.8). It is simply suggested here that division of the initial range to the initial speed would provide a conservative value for the duration of bias application:

$$\Delta t = \frac{r_{\mathrm{i}}}{v_{\mathrm{i}}} \tag{3.13}$$

Prior to a real engagement, it is often possible to get a rough estimate of the range to go using unsophisticated techniques such as triangulation or constructing similar triangles based on the target's apparent and expected sizes. It might be even possible to start the biased guidance after estimating the range with an estimator such as the one to be presented in Chapter 5.

It should be noted that the approach in Eq. (3.13) might fail if the pursuer accelerates after the engagement starts. Assuming that it will not fail, Eq. (3.8) can be written as

$$b = \frac{N_{\mathrm{M}}\lambda_{\mathrm{i}} - \gamma_{\mathrm{i}} - \left(N_{\mathrm{M}} - 1\right)\gamma_{\mathrm{f,d}}}{r_{\mathrm{i}}/v_{\mathrm{i}}} \tag{3.14}$$

So, Eq. (3.12) can be written as

$$\dot{\gamma} = \begin{cases} N_{\mathrm{M}}\dot{\lambda} + \dfrac{N_{\mathrm{M}}\lambda_{\mathrm{i}} - \gamma_{\mathrm{i}} - \left(N_{\mathrm{M}} - 1\right)\gamma_{\mathrm{f,d}}}{r_{\mathrm{i}}/v_{\mathrm{i}}} & \text{if } \dfrac{N_{\mathrm{T}}\lambda - \gamma}{N_{\mathrm{T}} - 1} > \gamma_{\mathrm{f,d}} \\ N_{\mathrm{T}}\dot{\lambda} & \text{otherwise} \end{cases} \tag{3.15}$$

Next, simulations governed by the guidance law in Eq. (3.15) with different navigation gains are performed to compare them against each other and against the benchmark scenario presented in Section 2.2. For the reference engagement geometry with $\Delta t = r_{\mathrm{i}}/v_{\mathrm{i}} = 20$ s, Eq. (3.14) yields $b = 3.75, 8.25, 12.75$ °/s for $N_{\mathrm{M}} = 2,\ 3,\ 4$, respectively. Before showing the corresponding figures, the summary of the simulation results is presented in Table 3.1 for quick referencing. The first column of the table indicates the scenarios: O stands for the benchmark optimal control and D stands for the discontinuous bias application. The next two columns respectively include the midcourse and terminal navigation gain values, if applicable. The fourth column presents the bias value, again if applicable. The fifth column shows the extreme acceleration values. The negative values suggest that the extreme values occur near the end of the engagement. On the other hand, a positive sign would mean that the extreme acceleration occurs near the beginning. Maximum look angle values are given in the next column. The seventh column is for the total control effort values calculated from Eq. (2.38) and the last column presents the impact angles achieved.

Table 3.1 Summary of the simulation results produced by the discontinuous bias application strategy

Scn.	N_M	N_T	b [deg/s]	a_{ext} [m/s^2]	ε_{max} [deg]	E [m$^{2/}$s^3]	γ_f [deg]
O	N/A	N/A	N/A	−43.4	49.5	20167	−90.0
D_1	2	2	3.75	−71.5	35.9	23323	−90.0
D_2	3	3	8.25	−80.4	52.3	23127	−90.0
D_3	4	4	12.75	−92.1	65.7	28237	−90.0
D_4	3	2	8.25	−39.4	52.3	20453	−90.0

The detailed simulation results are presented in the upcoming figures. The important points will be highlighted firstly without paying attention to D_4. This is because D_4, which is the only scenario with different midcourse and terminal navigation gains, can only be appreciated with clues to be gathered from the other scenarios. The first figure is Figure 3.2 presenting the spatial trajectories. D_1 results in the lowest maximum altitude whereas D_3 has the most elevated trajectory. D_2 with its intermediate navigation gain performs in between. In Figure 3.3, the initial and final acceleration magnitudes are seen to be positively correlated with the navigation gain values. Until the switching, D_2 performs similarly to O but like D_1 and D_3, it causes a severe peak right after the switching. The worst performance belongs to D_3 with its highest navigation gain as also evidenced by the control effort values in Table 3.1. It is interesting to observe D_1 maintains fairly low levels until the switching instant; yet, it pays the price of its poor trajectory shaping during the midcourse phase by having to pull a high acceleration magnitude constantly over the entire terminal phase. Next, the look angle variations are shown in Figure 3.4. It is seen that D_1 has the lowest maximum value, which is an advantage in practice where the look angle will certainly be limited. Again, D_2 is similar to O during the midcourse guidance and D_3 performs the worst. Lastly, Figure 3.5 shows that the desired vertical impact is achieved in all scenarios.

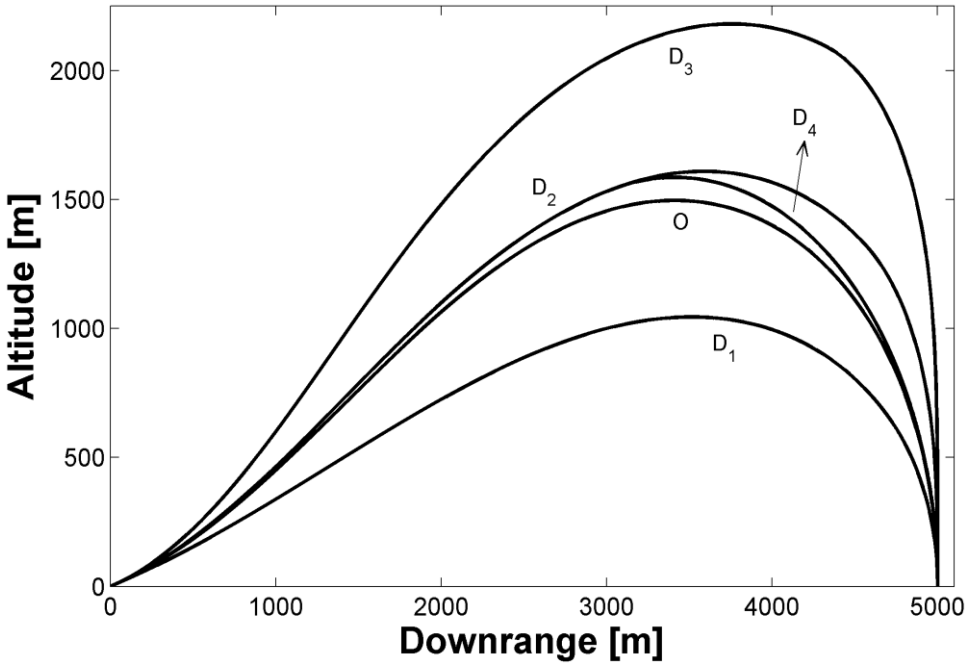

Figure 3.2 Spatial trajectories produced by the discontinuous bias application strategy (see Table 3.1 for details)

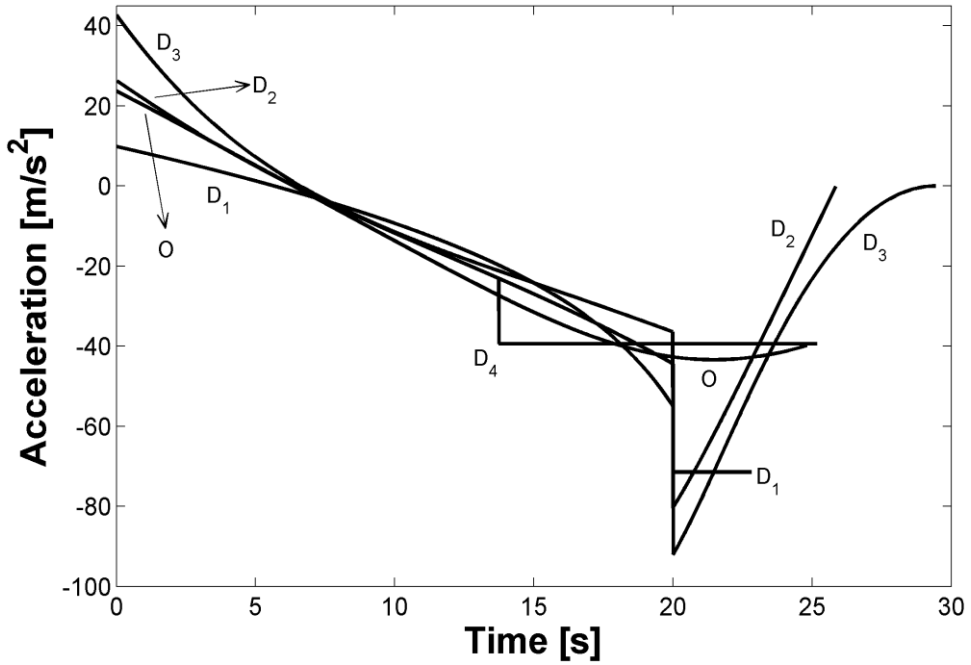

Figure 3.3 Acceleration histories produced by the discontinuous bias application strategy (see Table 3.1 for details)

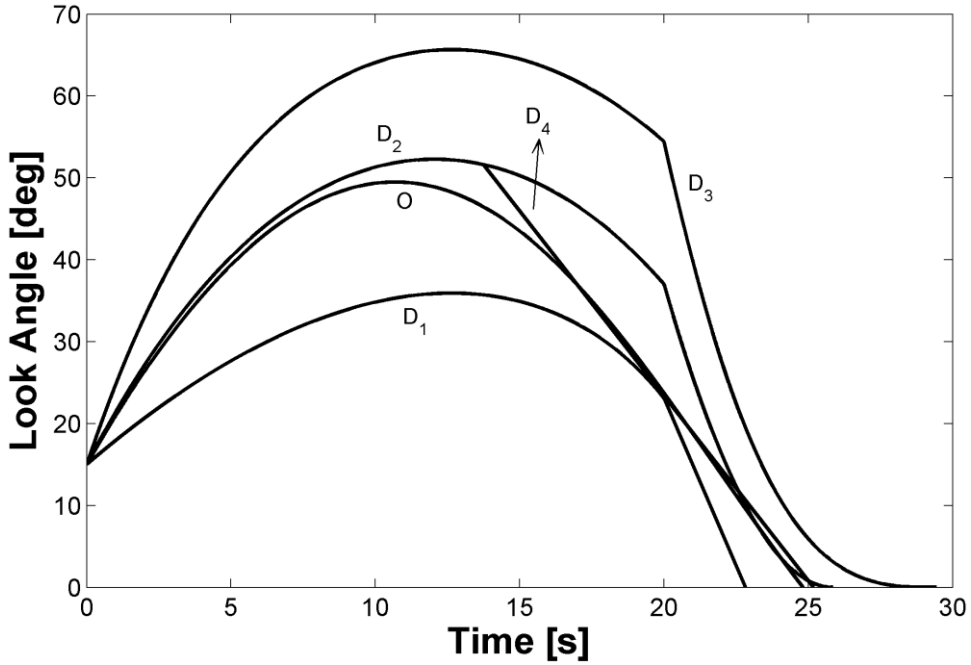

Figure 3.4 Look angle variations produced by the discontinuous bias application strategy (see Table 3.1 for details)

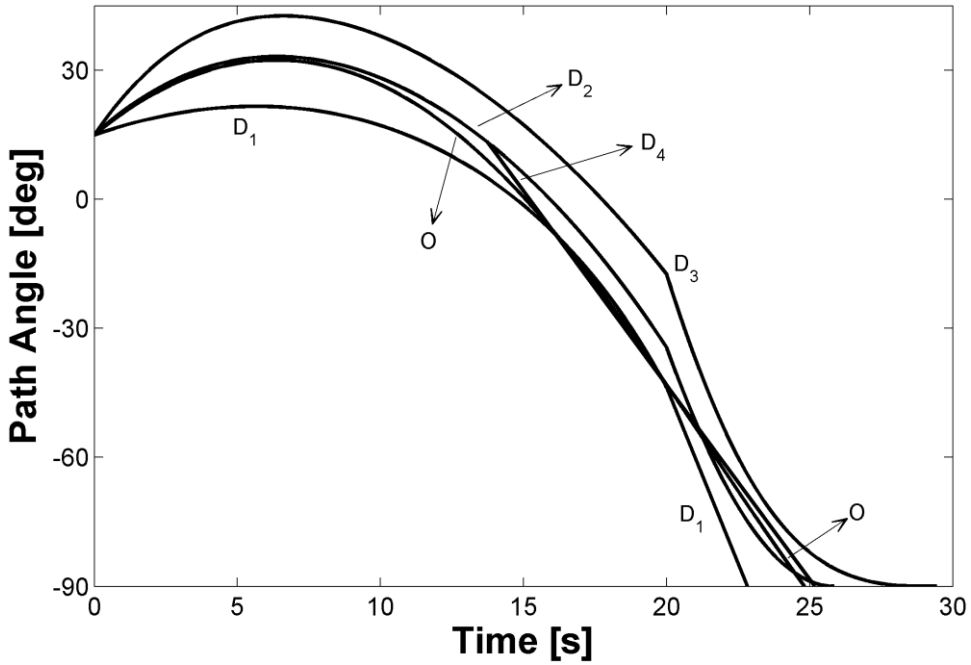

Figure 3.5 Path angle trends produced by the discontinuous bias application strategy (see Table 3.1 for details)

The trends in all these figures hint that D_2 approaches to the optimal performance during the midcourse guidance phase, which is not surprising as shown in Section 2.3.2.3 for the linear case. As for the terminal phase, Figure 3.3 shows that D_1 uses the least control effort. Also, it is true that if the switching happened earlier than it does, the terminal acceleration level would even be less. In other words, the total control effort of D_1 would turn out to be considerably less if its trajectory was more properly shaped during the midcourse phase. Based on this discussion, it could be wise to choose $N_M = 3$ and $N_T = 2$. So finally, D_4 is the scenario undergone with these specific gain values. The figures and the seventh column of Table 3.1 confirm that its performance approaches that of O. It is also very important to note that the maximum absolute acceleration of D_4 is even less than that of O. The switching occurs after 13.7 seconds has elapsed, which leaves much more time for the terminal phase. For the realistic case, where the pursuer will have a response lag, this additional time interval will help reduce the miss distance.

The hypothesis that a configuration with $N_M = 3$ and $N_T = 2$ performs similarly to the optimal solution requires further evidence. For this purpose, two additional engagement geometries are simulated for a desired impact angle of 60°. In the first case, the starting point of the pursuer is elevated to an altitude of 500 m and it is given an initial path angle of −10°. In the second case, the target is brought 2 km nearer to the pursuer, which is launched with an initial path angle of 10°. In each case, the proposed guidance configuration is compared with the numerical optimal solution and the continuously biased PPN solution based on trial and error. The bias values used by the proposed and continuous guidance methods are respectively 5.615 °/s and 5.306 °/s in the first case and 9.167 °/s and 8.480 °/s in the second case. Figure 3.6 presents the spatial trajectories. It is encouraging to observe that the spatial trajectories created by the configuration under test are closer to the optimal ones than those produced by continuous biasing. In Figure 3.7, the corresponding acceleration histories are given. It is seen that the proposed configuration requires the least amount of acceleration capacity when the pursuer approaches the target, which would be quite an advantage for a realistic pursuer. As for the total control effort values, they happen to be 11142 m^2/s^3 and 17501 m^2/s^3 for the optimal solutions, 11167 m^2/s^3 and 17560 m^2/s^3 for the continuously biased solutions, and 11194 m^2/s^3

and 17609 m^2/s^3 for the proposed solution; the lower values naturally belonging to the first engagement case. As seen, the control efforts are very close to each other. The number of examples can be increased with no difference in the general picture. So, this concludes that the proposed configuration would indeed be useful as a practical guidance law.

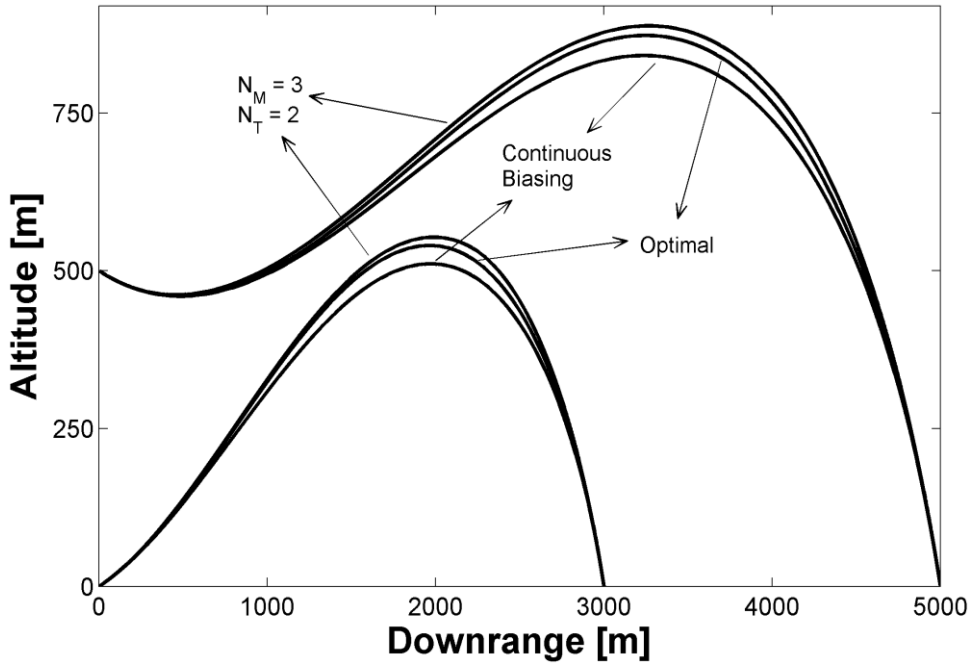

Figure 3.6 Comparison of spatial trajectories produced by the optimal, continuous bias application and discontinuous bias application strategies

As a final note, it should be realized that if the pursuer speed is not constant, β must still be kept constant according to Eq. (2.17). This can simply be achieved by applying the following speed weighting:

$$b = b_i \frac{v}{v_i} \tag{3.16}$$

An example of what would happen without the weighting can be found in [32].

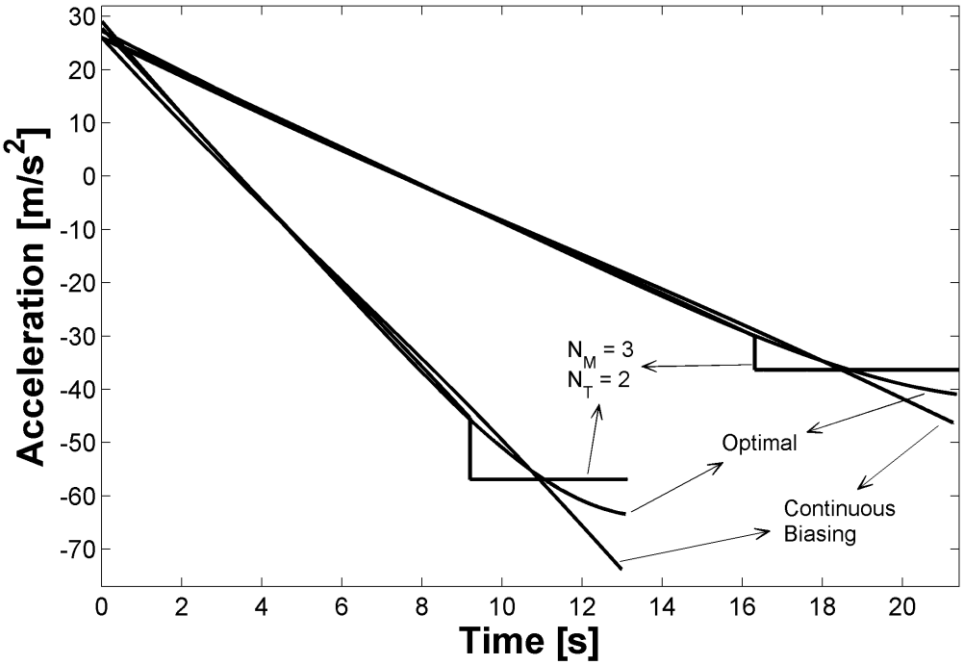

Figure 3.7 Comparison of acceleration histories produced by the optimal, continuous bias application and discontinuous bias application strategies

3.2.2. Range-Driven Bias Application

Replacing the initial conditions with instantaneous variables and converting the total time to the time to go, Eq. (3.7) may be written as

$$b = n\frac{N\lambda - \gamma - (N-1)\gamma_{\mathrm{f,d}}}{t_{\mathrm{go}}} \tag{3.17}$$

where n is a parameter that determines the shape of the bias profile. In the linear domain, where the time to go is assumed to be available, the bias would stay constant when $n=1$ and the profile would be a straight line starting from a value two times the constant bias and ending at zero when $n=2$. This is because of the fact that the same amount of the bias integral is needed to reach the same impact angle. Other values may be employed as well; but, the current scope is limited with these values as they have direct linear interpretations.

The guidance strategy can be obtained by using (4.17) in Eq. (2.10) as

$$\dot{\gamma} = N\dot{\lambda} + n\frac{N\lambda - \gamma - (N-1)\gamma_{\mathrm{f,d}}}{t_{\mathrm{go}}} \tag{3.18}$$

It is seen that when $n=1$ this guidance law becomes the same as Eq. (2.69), which is a commonly appearing form in the literature as expressed in Section 2.3.2.2. To avoid the problematic time-to-go term, Eq. (5.2), which is to be derived later, may be utilized to transform Eq. (3.18) into the following form:

$$\dot{\gamma} = N\dot{\lambda} + n\frac{v\cos\varepsilon}{r}\left\{N\lambda - \gamma - (N-1)\gamma_{\mathrm{f,d}}\right\} \tag{3.19}$$

where a range estimator such as the one to be introduced in Chapter 5 may be employed to obtain an estimate of the range value. Coincidentally, this guidance law happens to be the same as what appeared in a recent paper [41], where the simulations were performed only with a fixed set of guidance gains; more time was spent dealing with the time-to-go estimation than studying the guidance law.

Now, simulations governed by the guidance law in Eq. (3.19) with different guidance gains are performed to compare them against each other and against the benchmark scenario. The summary of the simulation results is presented in Table 3.2, where the first column indicates the scenarios: O stands for the benchmark optimal control and R stands for the range-driven bias application. The second and third columns of the table are respectively reserved for *N* and *n* values. The remaining columns are the same of those in Table 3.1. As seen, $n=1$ with $N=2$ is not utilized since the bias should not be present at the end when $N<3$ as indicated in Eq. (2.31). $n=2$ with $N=4$ is not utilized as well because the results obtained via such a configuration do not agree well with the others.

Table 3.2 Summary of the simulation results with range-driven bias application

Scn.	***N***	***n***	a_{ext} [m/s^2]	ε_{max} [deg]	***E*** [m^2/s^3]	γ_f [deg]
O	N/A	N/A	−43.4	49.5	20167	−90.0
R_1	2	2	−61.9	42.5	20833	−90.0
R_2	3	1	−71.9	41.0	21305	−90.0
R_3	3	2	+59.8	55.8	22551	−90.0
R_4	4	1	−55.6	45.3	21075	−90.0

Figure 3.8 presents the spatial trajectories. It is clearly seen that the trajectory becomes more lofted as *N* or *n* is increased. As opposed to the trends in Figure 3.3, Figure 3.9 reveals the smooth acceleration curves obtained. It is observed that increased gain values result in increased initial accelerations. The extreme values occur either at the beginning or at the end of the engagement depending on the gain configuration. R_3 achieves zero acceleration at the final instant. R_1 and R_2 agree quite well with each other and reasonably well with O up until the pursuer gets close to the target. The look angle variations are displayed in Figure 3.10, where it is seen that higher gains give rise to higher maximum look angle values in harmony with what is presented in Figure 3.8. Next, Figure 3.11 shows that the intended vertical impact is achieved in all cases. It is interesting to note that R_1 and R_2 are almost indistinguishable. Judging by these figures and the control effort values in Table 3.2, the behaviors are in harmony with O except for, perhaps, R_3. As opposed to lower values, $N = 4$ shapes the trajectory more when the target is far and less when it is near. This could be an advantage in terms of the required acceleration capacity, but also could be a disadvantage in terms of the required look angle capacity as can be seen in the fourth and fifth columns of Table 3.2. Finally, the bias profiles are presented in Figure 3.12. The figure confirms that the selected *n* values work as intended: The bias aspires to stay constant with $n = 1$ and decreases monotonically to zero with $n = 2$.

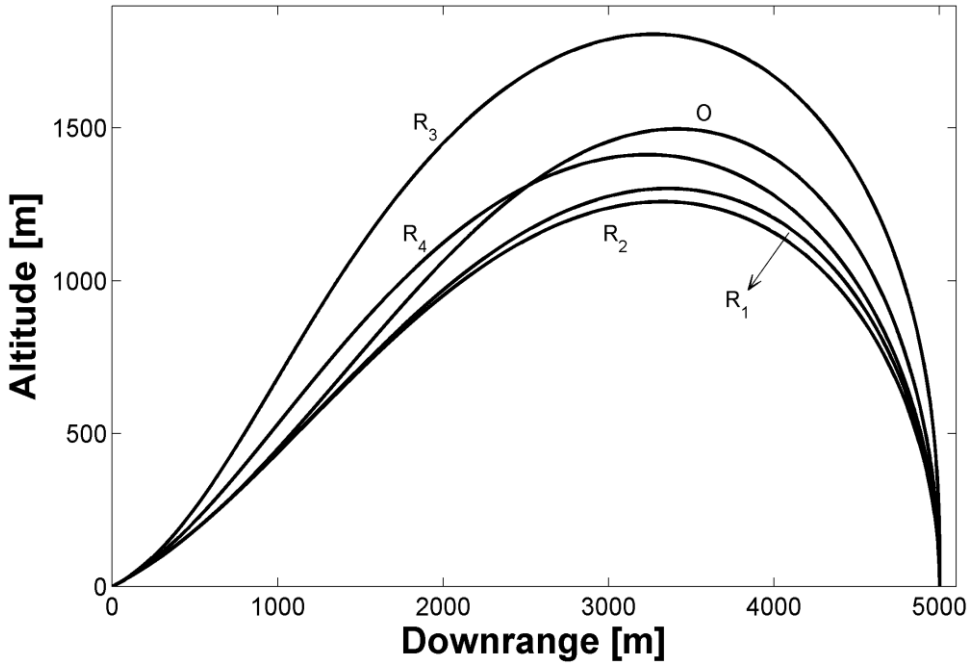

Figure 3.8 Spatial trajectories produced by the range-driven bias application strategy (see Table 3.2 for details)

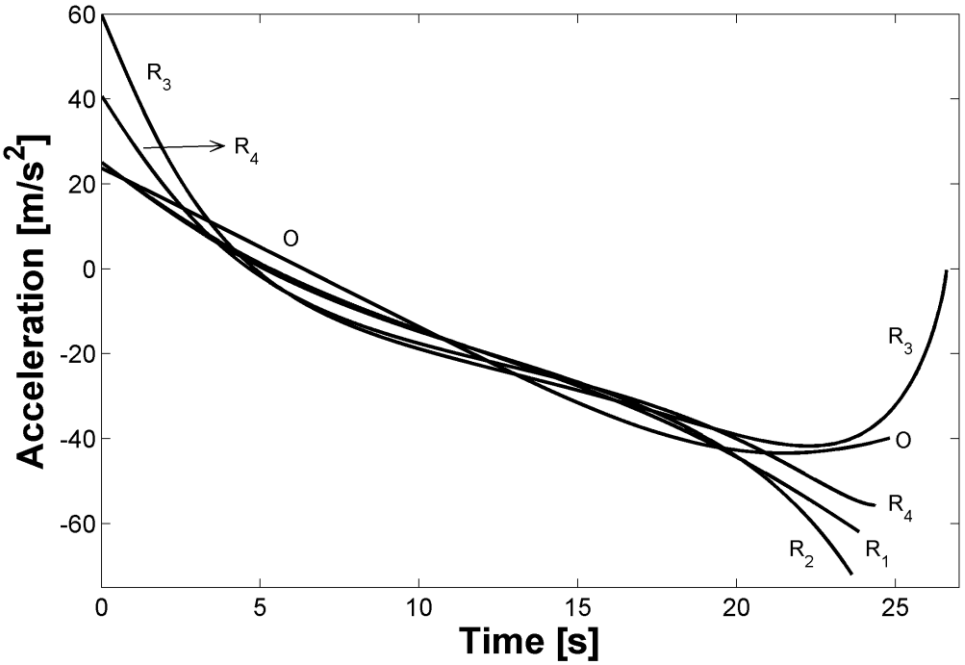

Figure 3.9 Acceleration histories produced by the range-driven bias application strategy (see Table 3.2 for details)

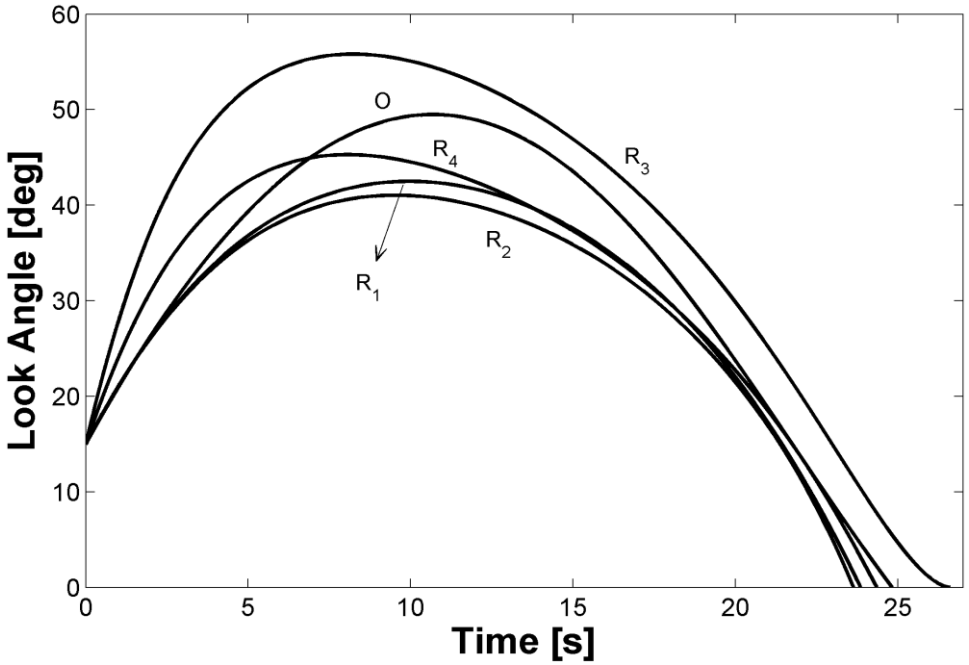

Figure 3.10 Look angle variations produced by the range-driven bias application strategy (see Table 3.2 for details)

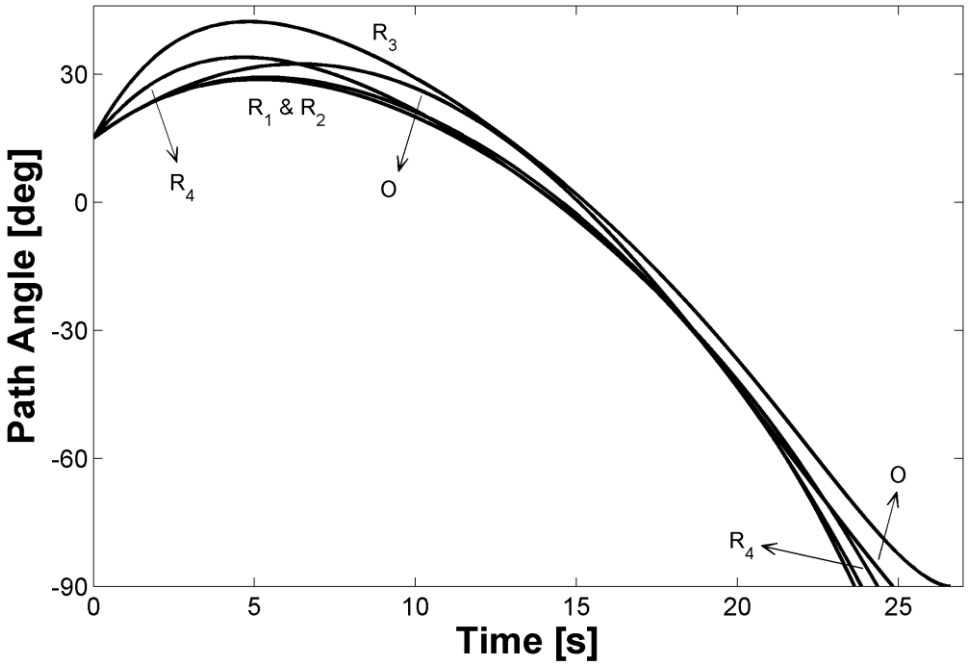

Figure 3.11 Path angle trends produced by the range-driven bias application strategy (see Table 3.2 for details)

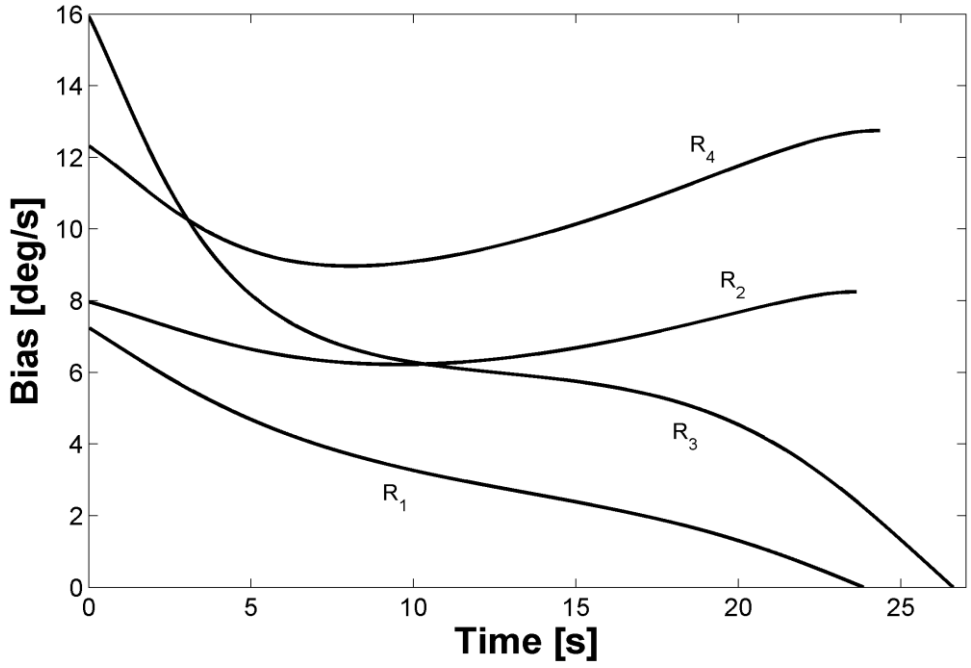

Figure 3.12 Bias profiles produced by the range-driven bias application strategy (see Table 3.2 for details)

3.2.3. Error-Based Bias Application

The driving factor for the guidance laws represented by Eq. (3.15) and Eq. (3.19) is the bias integral defined in Eq. (3.6), which needs to be filled up to the required value before the engagement comes to an end. An alternative formulation may be obtained by considering the PPN potential impact angle function given in Eq.(3.4). Collecting everything on one side of the equal sign and replacing Γ with $\gamma_{\mathrm{f,d}}$, the equation can be written as

$$N\lambda - \gamma - (N-1)\gamma_{\mathrm{f,d}} = 0 \tag{3.20}$$

This implies that if the PPN guidance process goes as intended, the desired impact angle will eventually be obtained. However, if this is not the case; that is, if the

pursuer has somehow deviated from the preferred PPN trajectory, the equation will not anymore be equal to zero. Accordingly, an error term may be defined as

$$\psi = N\lambda - \gamma - \left(N-1\right)\gamma_{\mathrm{f,d}} \tag{3.21}$$

With the objective of driving this error to zero, the following BPPN-type guidance law is now proposed:

$$\dot{\gamma} = N\dot{\lambda} + m\psi \tag{3.22}$$

where m is the error gain. Replacing ψ from Eq. (3.21), the open form of the law is

$$\dot{\gamma} = N\dot{\lambda} + m\left\{N\lambda - \gamma - \left(N-1\right)\gamma_{\mathrm{f,d}}\right\} \tag{3.23}$$

From Eq. (3.21), the derivative of the error is

$$\dot{\psi} = N\dot{\lambda} - \dot{\gamma} \tag{3.24}$$

Combining this with Eq. (3.22) yields the error dynamics:

$$\dot{\psi} + m\psi = 0 \tag{3.25}$$

As seen, this is a first-order linear system which is stable when $m > 0$. There is yet another constraint on the interval of values that m, whose reciprocal acts as the time constant of the error dynamics, may assume: At the very end, ψ must be sufficiently small so that the desired impact angle can be said to be reached. It is well known that the impulse response magnitude of a first-order system diminishes approximately to 5 % of its initial value after a time interval of 3 times of its time constant has elapsed [46]. This value drops to 1.8 % and to 0.7 % for durations of respectively 4 times and 5 times of the time constant. So, it is obvious that the impact angle performance with

Eq. (3.23) will be satisfactory as long as the reciprocal of *m* is much smaller than the total engagement time. Equivalently, the condition

$$m \gg 1/L \tag{3.26}$$

should be satisfied. This implies that the operator needs to have a rough idea about the total time before the engagement starts as practiced in Section 3.2.1. Here, it should be noted that there is positive correlation between *N* and *L*: In the context of BPPN, a higher *N* produces a more curved trajectory and a consequently higher *L*. Therefore, the choice of *m* is not independent of *N*.

If the designer does not want a sluggish first-order error response, the order can be doubled with the following strategy:

$$\dot{\gamma} = N\dot{\lambda} + m_1\psi + m_2\dot{\psi} + \ddot{\psi} \tag{3.27}$$

The error dynamics then happens to be

$$\ddot{\psi} + \left(m_2 + 1\right)\dot{\psi} + m_1\psi = 0 \tag{3.28}$$

A comparison of Eq. (3.22) and Eq. (3.28) shows that the price paid for doubling the order is twofold: The first and second error derivatives are both required. Leaving the more reasonable first derivative aside, the second derivative involves the derivatives of the LOS angle rate and the path angle rate, which are very unlikely to be available in practice. This is the reason why this case of increased order will not be pursued further in this text.

In what follows, simulations governed by the guidance law in Eq. (3.23) with various guidance gain values are performed to compare them against each other and against the benchmark scenario. The summary of the simulation results is presented in Table 3.3, where the first column indicates the scenarios: O stands for the benchmark

optimal control and E stands for the error-based bias application. The second and third columns of the table are respectively reserved for N and m values. The remaining columns are the same of those in Table 3.2. The table is dominated by $N = 2$ because higher integer values do not result in convenient solutions as will be demonstrated by the last example scenario. Since in the final moments, the bias is expected to be sufficiently small according to Eq. (3.25), the pursuer with this specific gain value should not experience any trouble associated with the rate of its acceleration as predicted by Eq. (2.31).

Table 3.3 Summary of the simulation results produced by the error-based bias application strategy

Scn.	$\boldsymbol{N}$	$\boldsymbol{m}$ [s^{-1}]	$\boldsymbol{a}_{\mathbf{ext}}$ [m/s^2]	$\boldsymbol{\varepsilon}_{\mathbf{max}}$ [deg]	$\boldsymbol{E}$ [m^2/s^3]	$\boldsymbol{\gamma}_{\mathbf{f}}$ [deg]
O	N/A	N/A	−43.4	49.5	20167	−90.0
E_1	2	0.150	−56.9	49.9	20267	−88.2
E_2	2	0.200	+59.0	55.7	22041	−89.6
E_3	2	0.250	+75.3	60.0	24011	−89.9
E_4	3	0.125	+80.3	76.3	27782	−88.3

As seen in Figure 3.13, higher guidance gains produce higher trajectories. It is important to note that E_4 has the highest maximum altitude among all the example scenarios presented in this text. The acceleration histories displayed in Figure 3.14 reveal that all of the initial values are higher than that of O; however, the final trends behave more reasonably. When $N = 2$, the final accelerations are close to the optimal value whereas E_4 converges towards zero, which might be an advantage in terms of control action. The sixth column of Table 3.3 indicates that the total control effort gets higher as the guidance gains are increased. The look angle variations are shown in Figure 3.15, where E_1 and E_4 are seen to require the lowest (almost as low as O) and highest capacities, respectively. Figure 3.16 presents the path angle trends, where it might not be possible to discern that almost all of the impact angle values

fall short of the guidance objective. The final path angle values are included in the last column of Table 3.3 and the performance should not be evaluated independent of the previous column. It is true that the cost function value of E_1 is almost as low as that of O; yet like E_4, it cannot fully achieve the desired impact angle. On the other hand, E_2 and E_3 produce higher costs that enable them to perform better in achieving the vertical impact condition. Here, the designer has to reach a compromise between the impact angle performance and the control expenditure. In fact, the impact angle error of E_1 is only 2 %, which is likely to be negligible in a real situation. It is also important to note that the total control effort of this scenario is the nearest to the optimal one among others including discontinuous and range-driven bias application scenarios. Lastly, Figure 3.17 shows the diminishing bias profiles. Unlike those with $n = 2$ in Figure 3.12, the bias curves do not reach to zero as expected. The lower the bias value becomes the better the impact angle objective will be met.

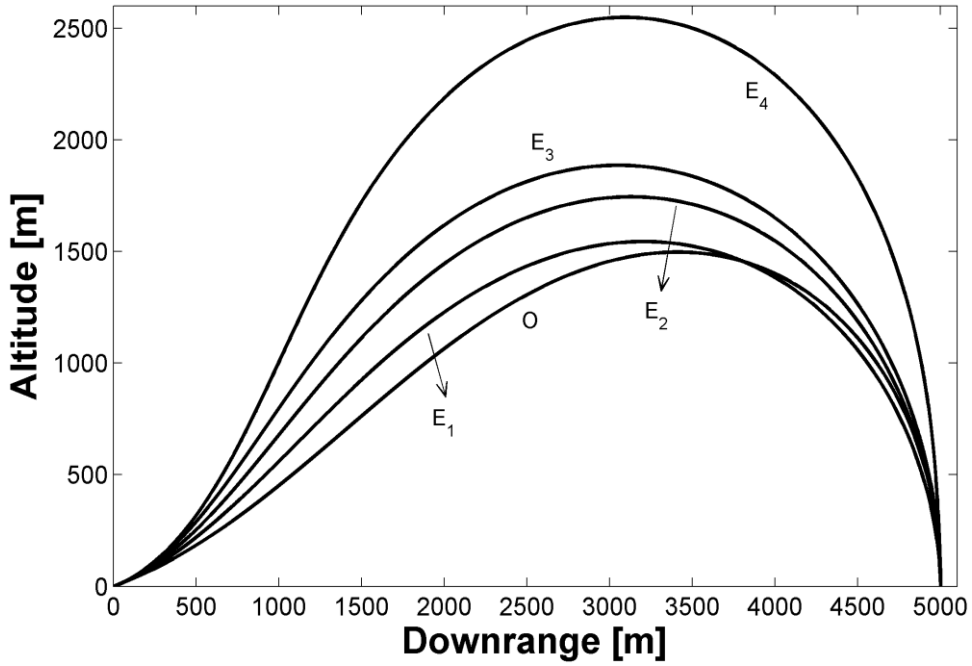

Figure 3.13 Spatial trajectories produced by the error-based bias application strategy (see Table 3.3 for details)

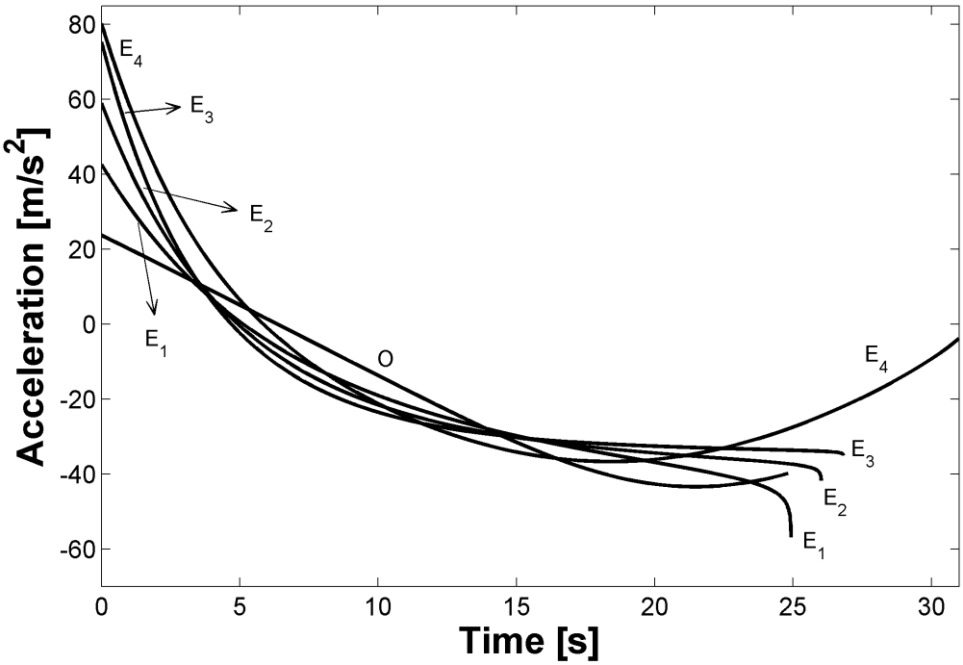

Figure 3.14 Acceleration histories produced by the error-based bias application strategy (see Table 3.3 for details)

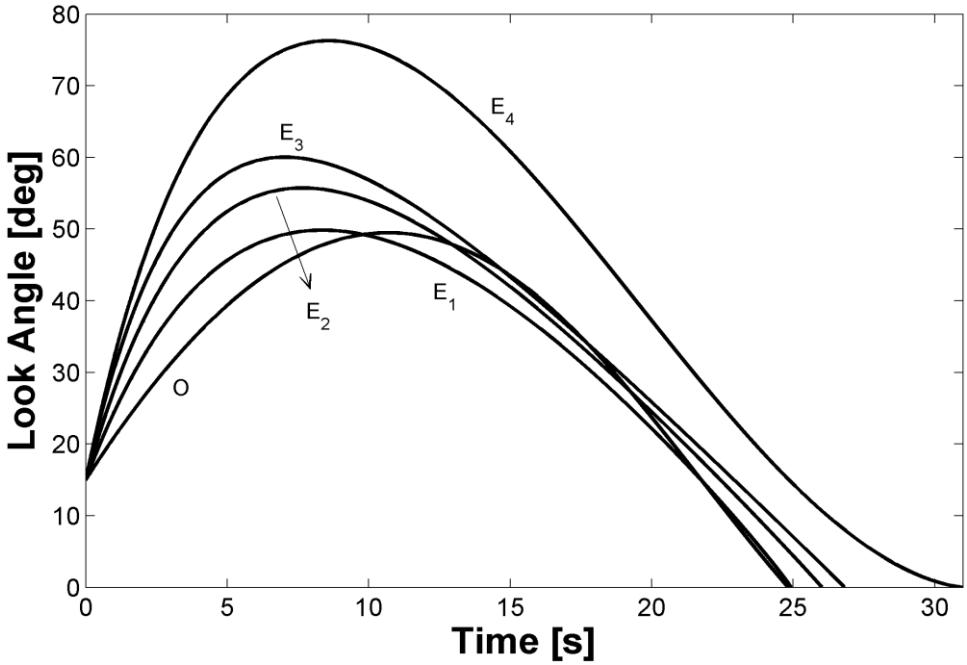

Figure 3.15 Look angle variations produced by the error-based bias application strategy (see Table 3.3 for details)

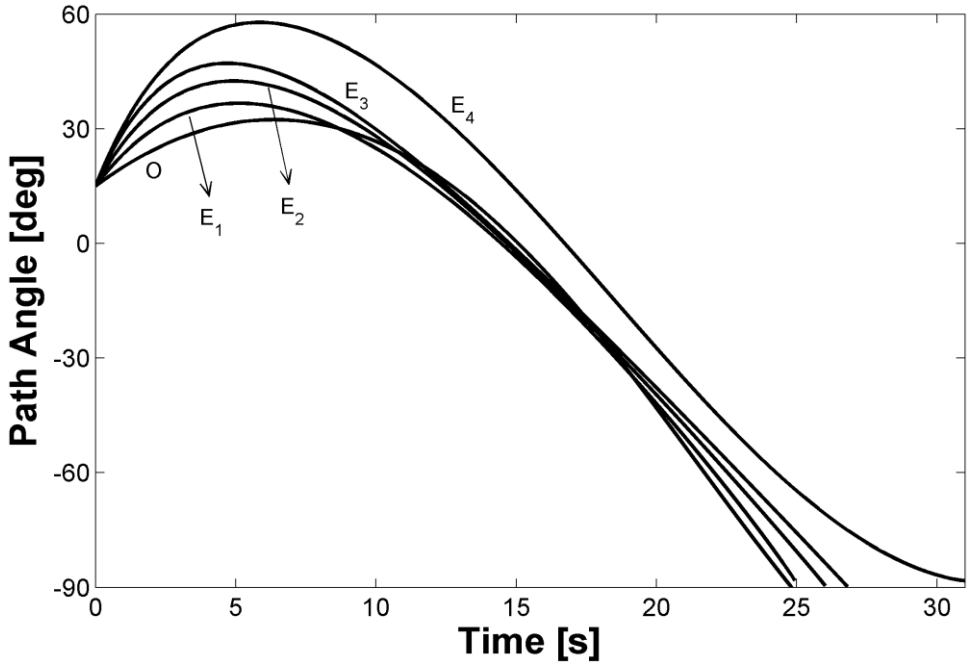

Figure 3.16 Path angle trends produced by the error-based bias application strategy (see Table 3.3 for details)

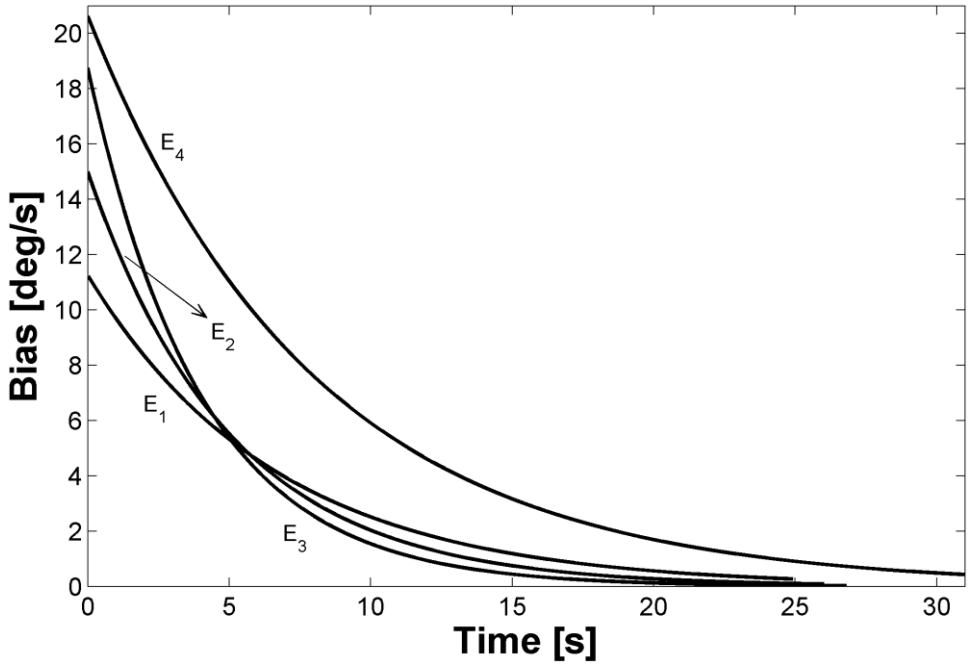

Figure 3.17 Bias profiles produced by the error-based bias application strategy (see Table 3.3 for details)

3.3. Performance of Guidance Laws under Disturbance

Having witnessed above the idealistic performance of the proposed guidance methods, it is now time to present how they perform under several types of disturbance. One of the unavoidable types of disturbance is the noise in the measured LOS angle rate. This is kind of disturbance is not considered in this text because it is known that the noise effect on the BPPN loop is not severe [32]. The first type of disturbance investigated here is the pursuer dynamics accompanied by the existence of gravity, to which all real pursuers are subject to in varying degrees determined by their airframe and/or autopilot characteristics. In the second disturbance case examined, the pursuer experiences a time interval where no measurements are available from the seeker. Such situations might occur in practice if the target has the ability to take countermeasures that might disable the target tracking for a while. The last disturbance is the case of a slowly moving target. Although an extension to cover the moving targets will be made in Chapter 6, it is still necessary to see how much the performance deteriorates because the information required to handle a moving target may not be available to the pursuer.

The reference engagement geometry is again considered. Based on the examples presented in Section 3.2 with the same geometry, the following guidance gain configurations are *subjectively* selected by considering the need for both impact angle accuracy and low control effort: $N_{\mathrm{M}} = 3$ and $N_{\mathrm{T}} = 2$ to be used in Eq. (3.15), $N = 2$ and $n = 2$ to be used in Eq. (3.19) and, $N = 2$ and $m = 0.15$ to be used in Eq. (3.23). So firstly, the discontinuous guidance law becomes

$$\dot{\gamma}_{\mathrm{D}} = \begin{cases} 3\dot{\lambda} + \dfrac{3\lambda_{\mathrm{i}} - \gamma_{\mathrm{i}} - 2\gamma_{\mathrm{f,d}}}{r_{\mathrm{i}}} v & \text{if } \ 2\lambda - \gamma > \gamma_{\mathrm{f,d}} \\ 2\dot{\lambda} & \text{otherwise} \end{cases} \tag{3.29}$$

where it should be realized that Eq. (3.16) is used in Eq. (3.15) because the speed will not be constant anymore due to gravity. Secondly, the range-driven guidance law becomes

$$\dot{\gamma}_{\mathrm{R}} = 2\dot{\lambda} + 2\frac{v\cos\varepsilon}{r}\left(2\lambda - \gamma - \gamma_{\mathrm{f,d}}\right) \tag{3.30}$$

Lastly, the error-based guidance law becomes

$$\dot{\gamma}_{\mathrm{E}} = 2\dot{\lambda} + 0.15\left(2\lambda - \gamma - \gamma_{\mathrm{f,d}}\right) \tag{3.31}$$

It should be noted that E, unlike D and R, does not yield a negligible impact angle error when there is no disturbance. However, an experienced designer can surmise that the lagged response of the pursuer, albeit it acts as a disturbing factor, could compensate for this error by forcing the trajectory to bend more at the final moments.

3.3.1. Pursuer Dynamics and Gravity

The response of the pursuer to the guidance command is modeled as a first-order lag represented by the transfer function $1/(\tau_{\mathrm{a}}s+1)$ so that the following can be written:

$$\tau_{\mathrm{a}}\ddot{\gamma}_{\mathrm{IMU}} = \dot{\gamma}_{\substack{\mathrm{IMU}\\\mathrm{com}}} - \dot{\gamma}_{\mathrm{IMU}} \tag{3.32}$$

where τ_{a} is the autopilot time constant. $\dot{\gamma}_{\mathrm{IMU}}$ is the path angle rate due to those acceleration components measurable by an onboard inertial measurement unit (IMU); i.e. the acceleration of the pursuer excluding the gravitational acceleration, which cannot be measured by accelerometers [47]. It should be remembered that the acceleration and the path angle rate are related through Eq. (2.11). The command to be sent to the autopilot is

$$\dot{\gamma}_{\substack{\mathrm{IMU}\\\mathrm{com}}} = \dot{\gamma}_{\mathrm{com}} + \frac{g}{v}\cos\gamma \tag{3.33}$$

which, after being realized via Eq. (3.32), leads to the true path angle rate as follows:

$$\dot{\gamma} = \dot{\gamma}_{\text{IMU}} - \frac{g}{v}\cos\gamma \tag{3.34}$$

In addition, the effect of gravity on the speed is modeled as

$$\dot{v} = -g\sin\gamma \tag{3.35}$$

To provide a more realistic simulation environment, the seeker is assumed to be unable to function properly when the range is below 30 m [25]. The last guidance command is held when this happens.

The summary of the simulations are presented in Table 3.4. The first column indicates the guidance law utilized: D refers to the discontinuous structure in Eq. (3.29), R is the continuous one in Eq. (3.30) and E stands for the error-based method in Eq. (3.31). The second column shows the autopilot lag values. The values in the third and fifth columns are based on the IMU accelerations. This is why the total control effort values are seen to be considerably lower than their counterparts in Table 3.1, Table 3.2 and Table 3.3; since the pursuer attacks a ground target, gravity assists the guidance process. The other columns are the same as those in the previous tables.

Table 3.4 Summary of the simulation results produced by the three alternative bias application strategies under pursuer dynamics and gravity

Law	τ_a [s]	$a_{\underset{\text{ext}}{\text{IMU}}}$ [m/s^2]	$\varepsilon_{\max}$ [deg]	E_{IMU} [m^2/s^3]	γ_f [deg]
D	0.2	−49.6	52.6	9774	−91.8
R	0.2	−55.4	42.9	11504	−89.9
E	0.2	−48.6	52.6	10441	−90.2
D	0.5	−82.6	53.0	11134	−95.3
R	0.5	−53.1	43.5	11295	−89.5
E	0.5	−61.5	53.5	10980	−91.8

The acceleration histories are presented in Figure 3.18. The plots of the spatial trajectories, the look angles and the path angles are not given because they are virtually the same as those presented earlier in Section 3.2. The trends in Figure 3.18 show that the slow autopilot gets into trouble during the final instants. This is especially apparent when D is used as the guidance law. With the slow autopilot, the response goes rapidly towards more negative values just before the pursuer captures the target. This unfavorable behavior manifests itself in the form of high total control effort and high impact angle error, which is seen to be more than 5° in Table 3.4. The table indicates that this is the only problematic case; other error values stay within reasonable limits. While this is so, it is seen that neither D with the fast autopilot and E with the slow one performs very well. The fact that D is not able to yield a negligible error value even with the fast autopilot is attributable its open loop nature during the terminal phase. Overall, R seems to exhibit the best performance at the expense of slightly increased total control effort.

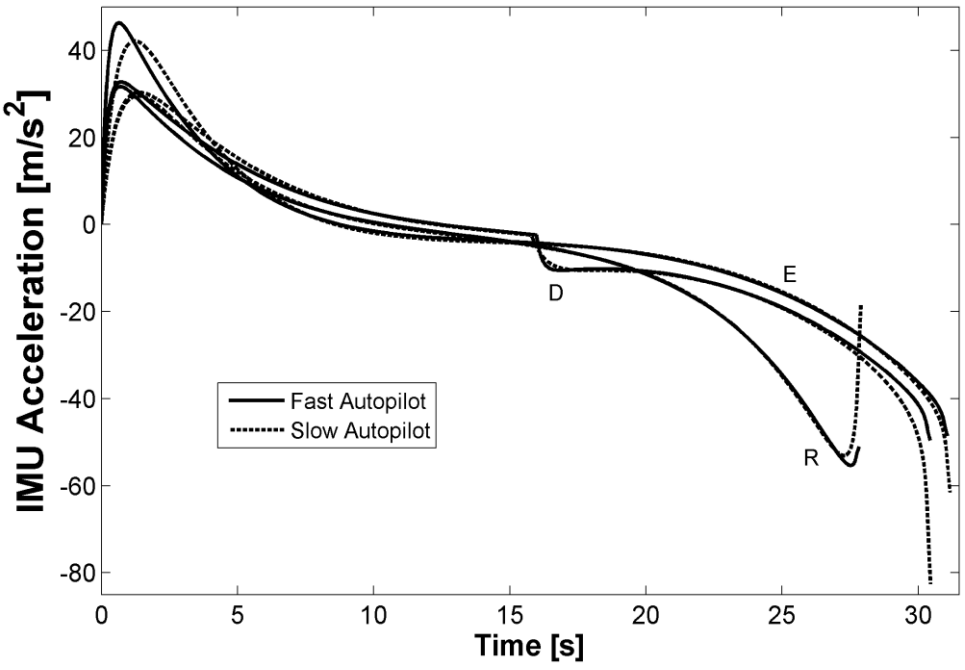

Figure 3.18 Acceleration histories produced by the three alternative bias application strategies under pursuer dynamics and gravity (see Table 3.4 for details)

In Figure 3.19, the bias profiles can be seen. Unlike those in Figure 3.12 and Figure 3.17, R and E are seen to produce negative values due to the lagged autopilot response. As for D, its profiles do not stay constant but change according to Eq. (3.16) as the speed changes.

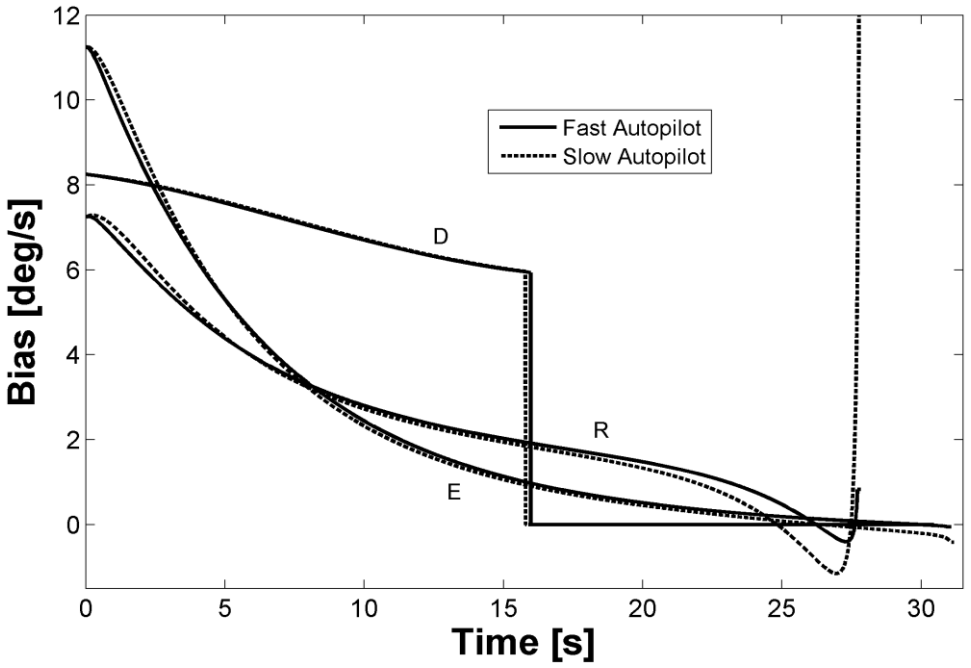

Figure 3.19 Bias profiles produced by the three alternative bias application strategies under pursuer dynamics and gravity (see Table 3.4 for details)

3.3.2. Temporarily Unavailable Seeker Data

In this case, the seeker data is made unavailable to the pursuer for a certain period of time while the engagement is in progress with the aim of testing whether or not it can recover and capture the target with a vertical velocity vector. The first period is denoted by letter A and covers $5\text{ s} < t < 10\text{ s}$. The second period is denoted by letter B and covers $15\text{ s} < t < 20\text{ s}$. The former period constitutes an early disturbance whereas the latter one constitutes a late disturbance; hence, their effects are expected to be different. The pursuer tries to achieve zero accelerometer reading when the

seeker data becomes lost. The autopilot time constant is 0.2 s and gravity exists. Again, the last guidance command is held when the range is below 30 m.

The summary of the simulations performed can be found in Table 3.5. The first column indicates the guidance law employed, D or R or E, along with the disturbance interval, A or B. The rest of the columns are the same as those in Table 3.4.

Table 3.5 Summary of the simulation results produced by the three alternative bias application strategies under temporarily unavailable seeker data

Sc.	$a_{\underset{\text{ext}}{\text{IMU}}}$ [m/s^2]	ε_{max} [deg]	E_{IMU} [m^2/s^3]	γ_{f} [deg]
D_A	−57.8	44.5	11495	−91.7
R_A	−62.1	38.6	12898	−89.9
E_A	−53.7	48.5	10921	−90.0
D_B	−64.4	54.2	14376	−109.2
R_B	−36.3	42.9	11003	−90.0
E_B	+46.3	52.6	10254	−91.6

Figure 3.20 presents the spatial trajectories, where it is seen that higher trajectories are produced if the unavailability of the data occurs late. The acceleration histories are shown in Figure 3.21. Intervals of zero acceleration are clearly observed. For guidance laws R and E, interval B results in more relaxed response levels as the target gets closer. This is only to be expected since the trajectory happens to be already shaped when the target tracking fails. However, D behaves differently. Referring to Figure 3.18, interval B can be seen to be positioned after the switching instant of D, which is known to be open loop in terms of impact angle control during the terminal phase. This is why D with interval B tends to pull more terminal acceleration than necessary. Moreover, the total control efforts in Table 3.5 are seen to be more than those in the first three rows of Table 3.4, which is the natural result

of a severely disturbed guidance loop. The next figure, Figure 3.22, presents the look angle variations, where in harmony with the spatial trajectories, lower maximum values are observed with interval A. As also shown in Table 3.5, D_B is seen in Figure 3.22 to fail to reach the desired impact angle in contrast to D_A, which exhibits a fine performance. This failure, which is due to the open loop terminal nature of D, is not unexpected as explained above. R and E perform well, especially when the disturbance happens early; this gives more time to the guidance law to recover. Finally, bias profiles are displayed in Figure 3.24.

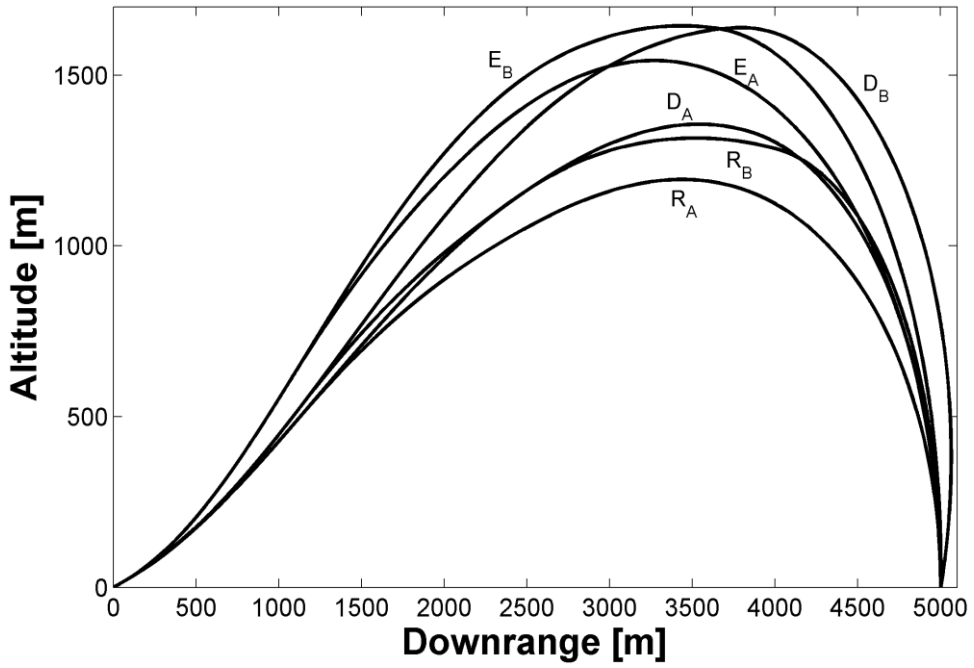

Figure 3.20 Spatial trajectories produced by the three alternative bias application strategies under temporarily unavailable seeker data (see Table 3.5 for details)

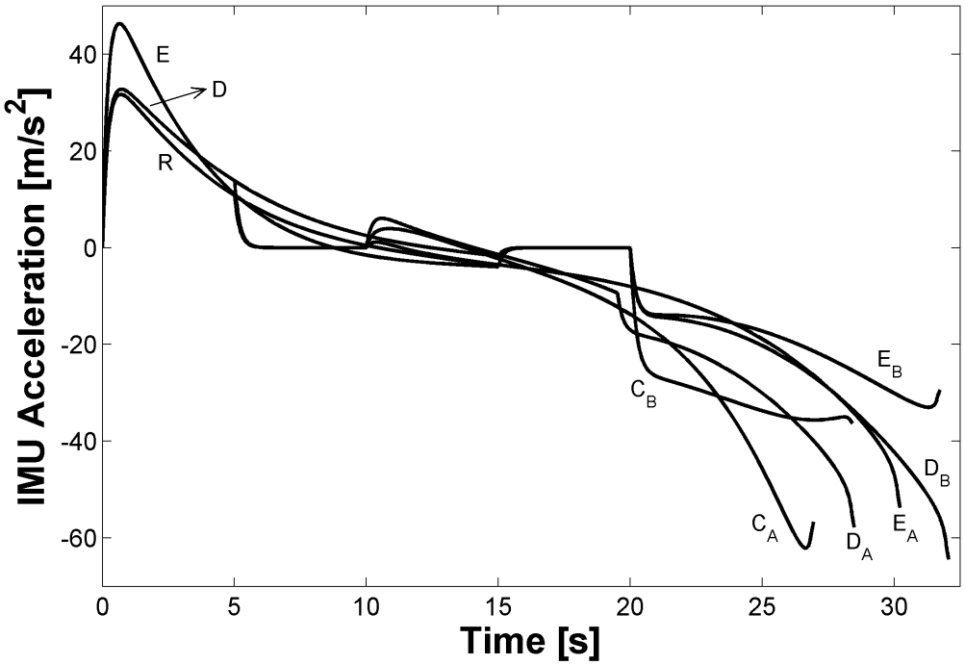

Figure 3.21 Acceleration histories produced by the three alternative bias application strategies under temporarily unavailable seeker data (see Table 3.5 for details)

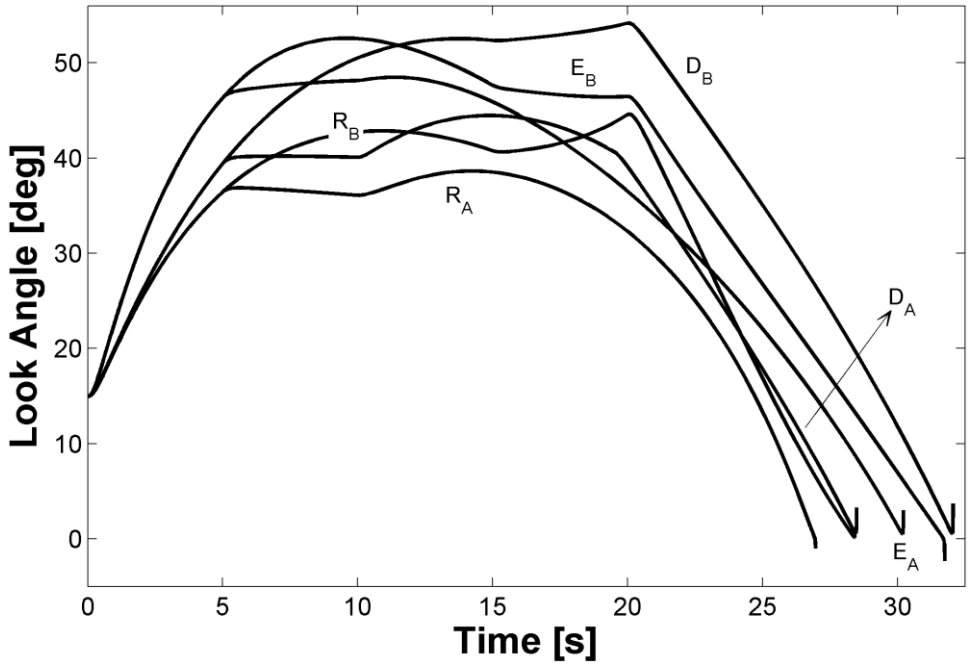

Figure 3.22 Look angle variations produced by the three alternative bias application strategies under temporarily unavailable seeker data (see Table 3.5 for details)

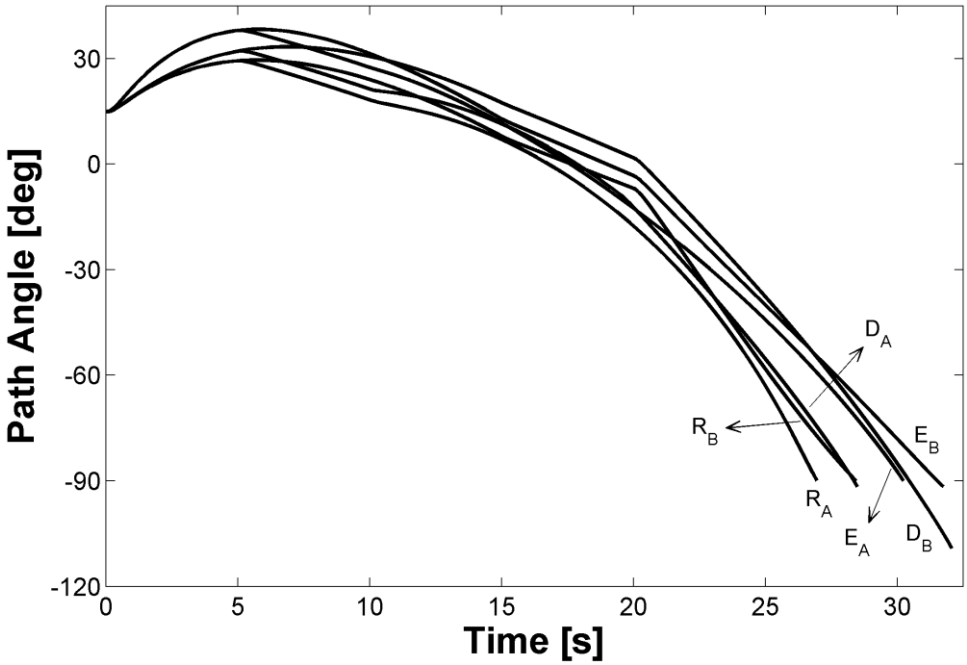

Figure 3.23 Path angle trends produced by the three alternative bias application strategies under temporarily unavailable seeker data (see Table 3.5 for details)

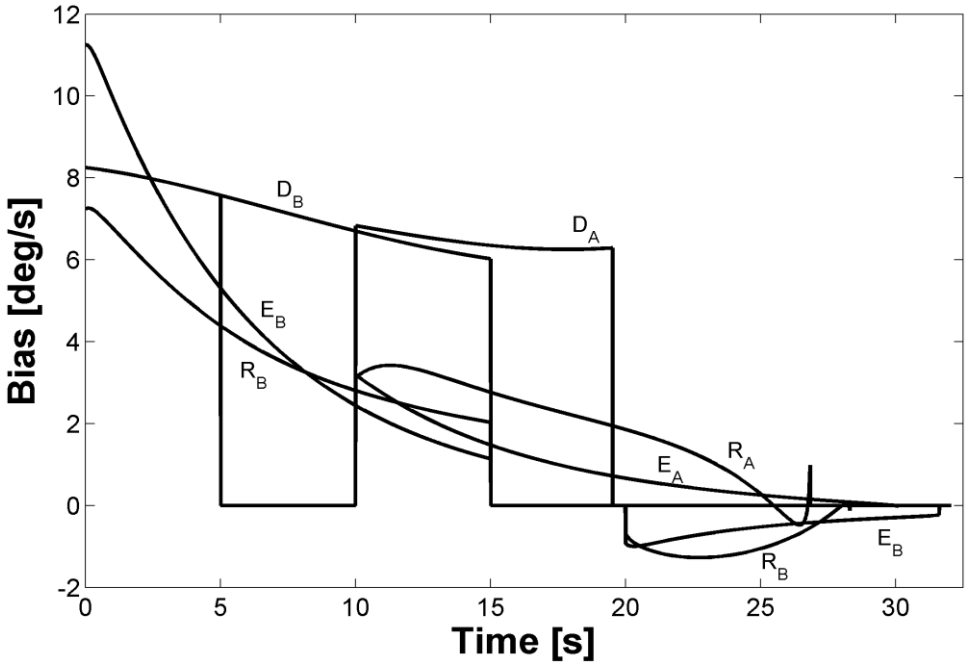

Figure 3.24 Bias profiles produced by the three alternative bias application strategies under temporarily unavailable seeker data (see Table 3.5 for details)

3.3.3. Target Movement

Although the guidance laws developed in this chapter are meant for stationary targets, it would be wise to see how they perform against moving ground targets because one may not be able to guarantee that the target will not start moving at some point during the engagement. For this purpose, a series of simulations with no disturbance are performed for each law to find out how the impact angle is distributed as a function of the target velocity. Figure 3.25 shows the results, where the letters D, R and E respectively correspond to Eq. (3.29), Eq. (3.30) and Eq. (3.31) as before. A negative target velocity means an approaching target whereas a positive velocity indicates that the target moves away from the pursuer. It is seen that R, which is fed the true range in this case, produces an error line that passes through the origin with a slope of approximately 45°. The origin repeats the information previously given in Table 3.2; there is no error if the target is stationary. The value of the slope, on the other hand, states that the guidance law results in almost the same amount of error for the same target speed independent of its direction. As for E, it is seen to produce another line that approaches line R as the target velocity becomes more positive. Table 3.3 implies that line E could almost be made to pass through the origin if m was larger than 0.25 s^{-1} so that R and E would lead to the same result. The remaining guidance law D behaves differently. After following a peculiar trend for an interval of negative velocity values, it creates a line that is almost the same as line R. This behavior can be demystified by considering the bias profile. From Figure 3.3, it is known that D applies the bias no longer than 14 s; so, the irregular portion of the curve simply corresponds to the scenarios where the target is captured with the bias still on. In short, it is not surprising to witness that these three different guidance laws lead to the almost same result against moving targets since they all rely on the bias integral given in Eq. (3.6); one should note that the term $2\lambda - \gamma - \gamma_{f,d}$ is common to Eq. (3.29), Eq. (3.30) and Eq. (3.31). To conclude with numerical figures; if the absolute impact angle error is not to exceed 10°, the target speedy needs to remain below 20 m/s, which is 12.5 % of the pursuer speed.

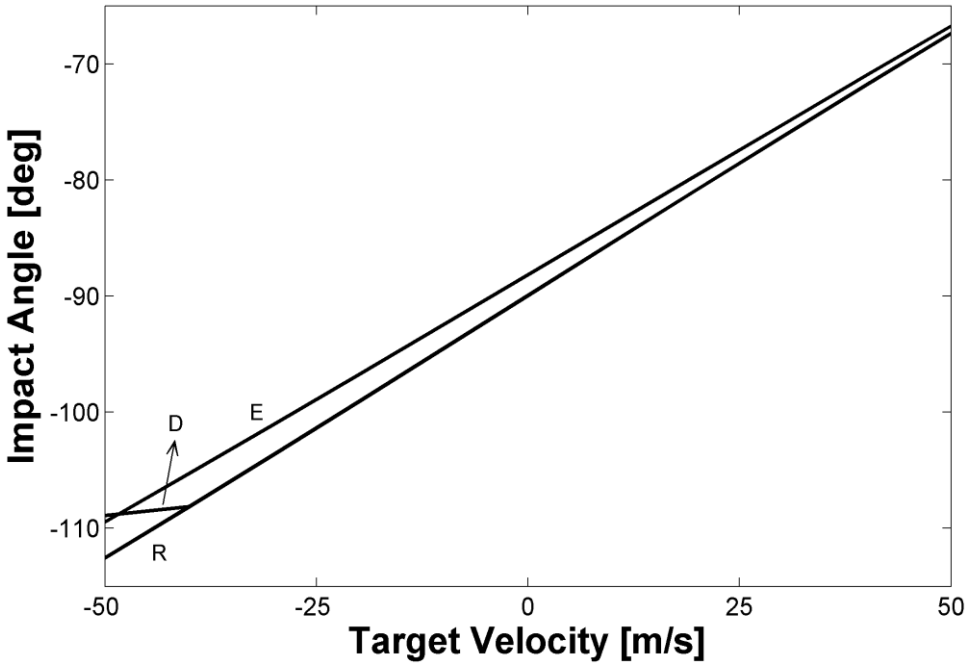

Figure 3.25 Impact angle sensitivities of the discontinuous, range-driven and error-based bias application strategies to target velocity

CHAPTER 4

CONSTRAINED GUIDANCE PROBLEM

Two of the most important constraints that a guidance law must not violate are the seeker angle and the acceleration limits; and, the risk of these constraints getting violated increases when a trajectory shaping guidance law is utilized. If the angle of attack is sufficiently small, the seeker angle may be approximated by the look angle so that the first constraint may be thought of as the look angle constraint. Since it would not be an understatement to say that the analytical treatment of the BPPN guidance law as adopted in this study is structured upon the concept of look angle, the constraint associated with this variable can be dealt with in a more straightforward manner. Another contributing factor is the fact that the look angle constraint is unchanging. The acceleration constraint, on the other hand, is a more challenging opponent because the acceleration capacity of a realistic pursuer is a function of its speed, which, in turn, is a function of the trajectory to be travelled on under the action of the guidance law.

It would here be convenient to state that, at the time of writing, the author was aware of only one published work on the subject of impact angle control that provided a proper treatment of the aforementioned physical limitations. The switched-gain PPN scheme proposed in [43] led to a numerically cooperative set of algebraic equations, using which the navigation gains were calculated. This was mostly owing to the fact that the look angle and the acceleration constraints happened to be satisfied simultaneously. Unfortunately, as will be shown below, the BPPN-based equations do not turn out to be as cooperative. Nonetheless, the BPPN approach might still be preferable owing to the fact that it approaches to the optimal solution as demonstrated at the end of Section 3.2.1. Indeed, it was shown in [44] that for the same impact angle and under the same look angle constraint, this tactic produced a lower maximum acceleration magnitude than the switched-gain approach did.

4.1. BPPN Impact Angle Capacity: Full Utilization of Available Resources

As demonstrated in Chapter 3, shaping the trajectory is an expensive task as far as the required resources are considered. Independent of the guidance law utilized, the pursuer must have sufficient look angle and acceleration capacities so as to achieve a desired impact angle. The objective of this section is to reveal the relationship between the physical limits and the impact angle capacity of the BPPN guidance law stated as

$$\dot{\gamma} = N\dot{\lambda} + \beta v \tag{4.1}$$

This is the same law in Eq. (2.10) expressed in a slightly different from via Eq. (2.17).

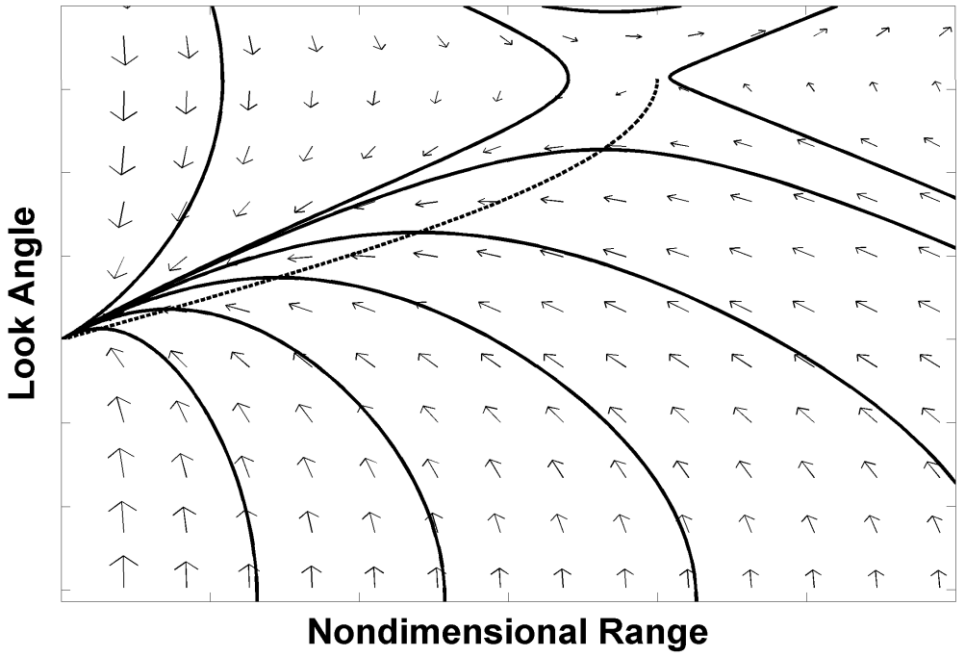

Figure 4.1 General picture of the BPPN state plane with the locus of maximum look angles superimposed

Since the look angle is the sole variable on which the analytical foundations in Section 2.1 settle, the treatment of the constraint associated with it turns out to be relatively easy. Retaining the general picture of the state plane trajectories presented in Section 2.1.1, Figure 4.1 shows the behavior of the look angle with respect to the nondimensional range for a general navigation gain value. It is seen that each of the convergent trajectories in the lower part of the figure has a maximum located to the left of the equilibrium point. The main idea in dealing with the look angle constraint is to make the pursuer travel on a trajectory whose maximum look angle is not higher than the constraint value. The dashed curve superimposed on the trajectories belongs to the locus of maximum look angle values. To determine the locus, the slope information is required. It follows from Eq. (2.23) that

$$\frac{\mathrm{d}}{\mathrm{d}\rho}\sin\varepsilon = c\left(N-1\right)\rho^{N-2} + \frac{1}{N-2} \tag{4.2}$$

Setting the slope to zero, the integration constant can be found as

$$c = -\frac{1}{\left(N-1\right)\left(N-2\right)\left(\rho^{*}\right)^{N-2}} \tag{4.3}$$

where ρ^{*} is the range at which the maximum look angle ε^{*} occurs. Using Eq. (4.3) back in Eq. (2.23) produces the equation of the locus as

$$\rho^{*} = \left(N-1\right)\sin\varepsilon^{*} \tag{4.4}$$

so that Eq. (4.3) can be written as

$$c = -\frac{1}{\left(N-1\right)^{N-1}\left(N-2\right)\left(\sin\varepsilon^{*}\right)^{N-2}} \tag{4.5}$$

This equation establishes the relationship of the integration constant with the look angle constraint. Now, Eq. (2.23) evaluated at the initial instant turns out

$$c\rho_{\mathrm{i}}^{N-1}+\frac{\rho_{\mathrm{i}}}{N-2}-\sin\varepsilon_{\mathrm{i}}=0 \tag{4.6}$$

which, with the help of Eq. (2.15), can further be manipulated into

$$cr_{\mathrm{i}}^{N-1}\beta^{N-1}+\frac{r_{\mathrm{i}}}{N-2}\beta-\sin\varepsilon_{\mathrm{i}}=0 \tag{4.7}$$

As for the acceleration limit; Eq. (2.29) indicates that the BPPN law produces a monotonously decreasing nondimensional path angle rate trend. This implies that the extreme value of the acceleration has to be encountered either at the beginning or at the end of the engagement. The results of Section 2.2 suggest that the trajectory gets bent more efficiently when more control effort is applied later during the engagement. This is why the designer would want to assign the extreme acceleration to the final instant. The expressions for the initial and final values of the nondimensional path angle rate may be examined in the light of this. The initial value can be written from Eq. (2.28) as

$$\gamma_{\mathrm{i}}'=-N\frac{\sin\varepsilon_{\mathrm{i}}}{\rho_{\mathrm{i}}}+1 \tag{4.8}$$

The final value, on the other hand, can be found from Eq. (2.29) knowing that the target will be captured at the end:

$$\gamma_{\mathrm{f}}'=-\frac{2}{N-2} \tag{4.9}$$

For reasonable (it was demonstrated in Section 2.2 that the use of a high navigation gain requires a high look angle limit and leads to a high initial acceleration value)

values of the navigation gain, it can be inferred that the magnitude of the final value will *most probably* be higher than the magnitude of the initial value. For example; if $\varepsilon_{\mathrm{i}} = 0$, it follows that $\gamma'_{\mathrm{i}} = 1$ and it is possible to have $\left|\gamma'_{\mathrm{i}}\right| > \left|\gamma'_{\mathrm{f}}\right|$ only if $N > 4$. Furthermore, a nonzero initial look angle will push this limiting value of the navigation gain to even higher values. Nevertheless, the designer should check the accelerations after the guidance parameters have been calculated as a precaution against the unwanted case of having the initial value higher than the final one. So, focusing on the final acceleration, Eq. (4.9) can be transformed into

$$a_{\mathrm{f}} = -\frac{2}{N-2}\beta v_{\mathrm{f}}^2 \tag{4.10}$$

using Eq. (2.11), Eq. (2.16) and Eq. (2.17). If this final value is to be equal to the acceleration constraint a^*, which is by definition a positive quantity, the following would be true:

$$a^* = \frac{2}{N-2}\beta v_{\mathrm{f}}^2 \tag{4.11}$$

As seen, the acceleration depends on the final value of the speed, which is not known beforehand. The first solution to this problem that comes to mind would probably be assuming a constant speed. However, this trivial solution is far from being realistic. In reality, the speed of the pursuer will change under the action of actors such as thrust, drag and gravity. To establish the foundation of a realistic solution, the acceleration of a vehicle moving through the air may be considered. Typically, the aerodynamic lift force on such a vehicle can be represented as follows:

$$F_{\mathrm{L}} = \frac{1}{2} d_{\mathrm{a}} v^2 S_{\mathrm{r}} C_{\mathrm{L}} \tag{4.12}$$

where d_{a} is the air density, S_{r} is the reference area and C_{L} is the lift coefficient. Then, the acceleration of the vehicle can be written as

$$a = \kappa v^2 \tag{4.13}$$

In this definition, κ acts as a proportionality agent between the acceleration and the speed squared. *m* being the mass, κ assumes the form below:

$$\kappa = \frac{d_a S_r C_L}{2m} \tag{4.14}$$

Returning to the problem associated with Eq. (4.11); the concept of *constant maximum lift coefficient* [43] would be useful as an alternative to the trivial solution. It is the case with the aerodynamically controlled vehicles that they can sustain a maximum level of lift force which determines their acceleration capability. This maximum value typically occurs at a certain maximum angle of attack, beyond which the vehicle stalls due to the dramatically dropping lift capacity. The maximum sustainable lift force is characterized by the peak value of the lift coefficient C_L^*. In certain applications, the maximum lift coefficient may be considered sufficiently constant over the operational speed interval. Examples to such behavior over the subsonic region can be observed in [48] (see for example Figs. 4 and 58). If, in addition to assuming the lift coefficient constant, the air density and the mass are considered unchanging, the following can be written due to Eq. (4.13):

$$a^* = \kappa^* v^2 \tag{4.15}$$

where κ^* is the proportionality *constant* associated with the acceleration constraint. It is true that the reference area in Eq. (4.14) is constant; however, the assumptions of constant air density and constant mass made to obtain Eq. (4.15) need to be justified. The first assumption is likely to hold for a ground launched pursuer attacking a ground target because it is unlikely to experience high altitude differences during the engagement. As for the second assumption, the mass is naturally constant when there is no exhaust; so, if the guidance process starts after the burnout, the assumption will hold.

So, with the help of the maximum constant lift coefficient concept, Eq. (4.11) can be converted into

$$\kappa^* = \frac{2}{N-2}\beta \tag{4.16}$$

If this expression is used in Eq. (4.7), the following is obtained:

$$cr_{\mathrm{i}}\left\{(N-2)\frac{r_{\mathrm{i}}\kappa^*}{2}\right\}^{N-1} + \frac{r_{\mathrm{i}}\kappa^*}{2} - \sin\varepsilon_{\mathrm{i}} = 0 \tag{4.17}$$

which, replacing the integration constant from Eq. (4.5), can at last be manipulated into

$$\left\{\frac{r_{\mathrm{i}}\kappa^*}{2(N-1)}\right\}^{N-1}\left(\frac{N-2}{\sin\varepsilon^*}\right)^{N-2} - \frac{r_{\mathrm{i}}\kappa^*}{2} + \sin\varepsilon_{\mathrm{i}} = 0 \tag{4.18}$$

The nonlinear equation above is not difficult to solve for N using a simple iteration routine. For example, starting from an initial guess, the navigation gain value can be updated according to

$$\tilde{N}_{\mathrm{new}} = \tilde{N}_{\mathrm{old}} + k_N \left| e_N \right| \tag{4.19}$$

where k_N is a gain that drives the numerical process and e_N is the left hand side of Eq. (4.18) evaluated with $\tilde{N}_{\mathrm{old}}$. It is advisable to set the initial guess to some value close to 2, which is the lowest possible value as mentioned in Section 2.1. This way, the navigation gain is forced to be higher with each iteration until the error becomes negligibly small. After the iteration has converged, the β value may be obtained through Eq. (4.16).

Having so decided the guidance parameters N and β that fully utilize the available resources, the designer would want to calculate the impact angle that is to be obtained. Setting the upper integral limit to zero in Eq. (2.32), the impact angle happens to be

$$\gamma_{\mathrm{f}} = \gamma_{\mathrm{i}} + \int_{\rho_{\mathrm{i}}}^{0} \frac{cN\theta^{N-2} + \dfrac{2}{N-2}}{\sqrt{1-\left(c\theta^{N-1} + \dfrac{\theta}{N-2}\right)^2}} \mathrm{d}\theta \tag{4.20}$$

where the integration constant follows from Eq. (2.23) along with Eq. (2.15) as

$$c = \left(\sin\varepsilon_{\mathrm{i}} - \frac{\beta r_{\mathrm{i}}}{N-2}\right) \frac{1}{\left(\beta r_{\mathrm{i}}\right)^{N-1}} \tag{4.21}$$

The procedure explained above is applied to the reference engagement geometry described in Section 2.2. The selected range of ε^* values is between 20° and 60°. Assuming a constant speed and thereby eliminating the need for κ^*, the selected range of a^* values is 20 m/s^2 and 60 m/s^2. The achievable impact angle contours are presented in Figure 4.2. The contourless region belongs to those cases in which, with the corresponding look angle constraint, the initial acceleration value exceeds the corresponding acceleration constraint. For example with $\varepsilon^* = 50°$ and $a^* = 30$ m/s^2, it turns out that $N = 7.78$, which, as mentioned above, may be considered to be too high for practical purposes. Although in this case, the final acceleration is the intended value of 30 m/s^2, the initial acceleration turns out to be much higher. The main idea of the plot is this: A pursuer with its look angle and acceleration limits belonging to a contour cannot reach the impact angles corresponding to the contours situated *above* that contour. Likewise, a pursuer with the said limits belonging to a contour can reach all the impact angles corresponding to the contours situated *below* that contour. The coordinates of the *lowermost* point of the vertical impact contour are approximately 51° and 41 m/s^2, which are very close to the extreme values produced by the optimal scenario as shown in Table 3.1. This resemblance is not

surprising at all since BPPN itself has been proved on various occasions in this dissertation, such as in Section 2.3.2.3, to be an efficient guidance law.

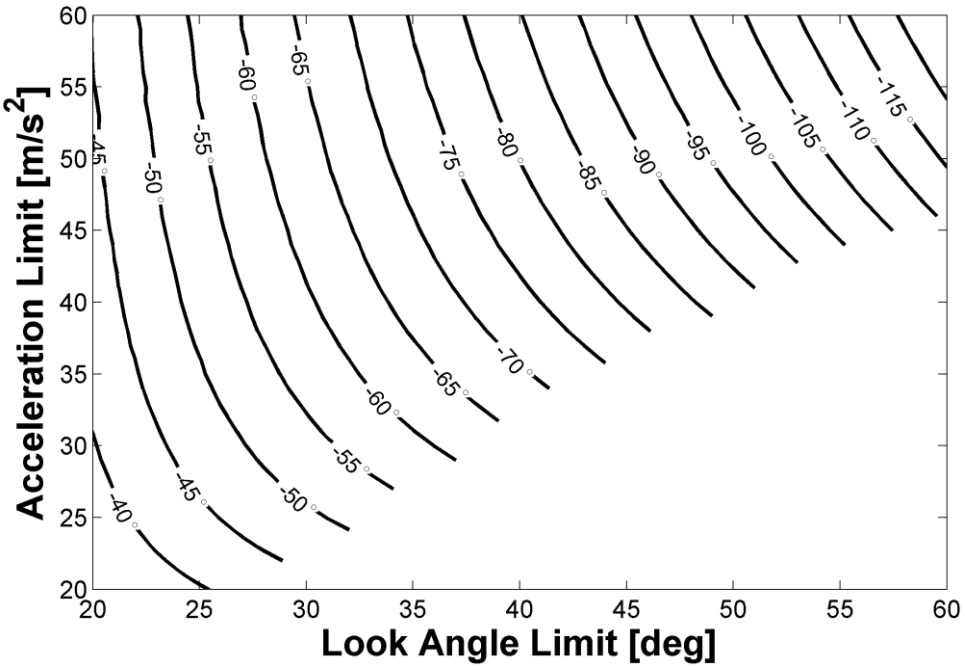

Figure 4.2 Contours of achievable impact angle under physical limitations

If the point representing the physical limits of the system happens to be located *below* a desired impact angle contour, this means that the resources are insufficient to reach that impact angle. This statement should not be misinterpreted. If there is an insufficiency indicated by the current analysis, it belongs to the BPPN law; that is, it is most likely not a global one. There might be other guidance laws to satisfy the desired impact angle under the same look angle and acceleration constraints. However, it is very important to perceive that the impact angle achievable by BPPN should not be very far from the impact angle achievable by the *most efficient* guidance law, whatever that guidance law is. This is because, as mentioned above, the BPPN guidance law is an efficient method for trajectory shaping.

One last remark needs to be made now: Although it is true that the procedure outlined in this section yields as by-products the navigation gain and bias values required to achieve a specific impact angle value, it should not be utilized for this purpose in order to guide the pursuer. This is because such a practice of beforehand calculation of the parameters would result in an open loop type of guidance, which might lead to the violation of constraints. A closed loop implementation involving the online application of the described numerical routine would not be very convenient either, especially when there is a better alternative as will be introduced in Section 4.3.

4.2. Formulation for Look Angle and Acceleration Constrained Impact Angle Control

The switching condition seen in Eq. (3.10) is time-dependent. Replacing that condition with an equivalent one which involves the nondimensional range and making use of Eq. (2.17), the following guidance law can be written:

$$\dot{\gamma} = \begin{cases} N\dot{\lambda} + \beta v & \text{if } \rho \le \rho_s \\ N\dot{\lambda} & \text{otherwise} \end{cases} \tag{4.22}$$

where subscript s denotes the switching instant, which is so defined that it belongs to the midcourse phase. When Eq. (4.22) is examined, it can be seen that there are three parameters to be specified by the user: N, β and ρ_s. The user cannot assign these parameters freely; there is at least the objective of capturing the target with a desired impact angle $\gamma_{f,d}$. For realistic pursuers, this user-specified constraint is likely to be accompanied by two additional constraints as mentioned in the previous section: ε^*, the look angle constraint and a^*, the acceleration constraint. In short; this constrained guidance problem involves three given parameters, which are $\gamma_{f,d}$, ε^* and a^*, to solve for three unknown parameters that are N, β and ρ_s.

The equation associated with the look angle constraints is the one derived in Section 4.1. For convenience, Eq. (4.7) is repeated below:

$$cr_{\mathrm{i}}^{N-1}\beta^{N-1}+\frac{r_{\mathrm{i}}}{N-2}\beta-\sin\varepsilon_{\mathrm{i}}=0 \tag{4.7}$$

Next, if the final path angle constraint, i.e. the desired impact angle, is to be obtained, Eq. (3.5) evaluated at the switching instant must be written as

$$\gamma_{\mathrm{f,d}}=\gamma_{\mathrm{s}}-\frac{N}{N-1}\varepsilon_{\mathrm{s}} \tag{4.23}$$

where the switching value of the look angle from Eq. (2.23) is

$$\varepsilon_{\mathrm{s}}=\sin^{-1}\left(c\rho_{\mathrm{s}}^{N-1}+\frac{\rho_{\mathrm{s}}}{N-2}\right) \tag{4.24}$$

and the switching value of the path angle from Eq. (2.32) is

$$\gamma_{\mathrm{s}}=\gamma_{\mathrm{i}}+\int_{\rho_{\mathrm{i}}}^{\rho_{\mathrm{s}}}\frac{cN\theta^{N-2}+\dfrac{2}{N-2}}{\sqrt{1-\left(c\theta^{N-1}+\dfrac{\theta}{N-2}\right)^{2}}}\mathrm{d}\theta \tag{4.25}$$

So, Eq. (4.23) can be combined with Eq. (4.24) and Eq. (4.25) to obtain

$$\gamma_{\mathrm{f,d}}=\gamma_{\mathrm{i}}+\int_{\rho_{\mathrm{i}}}^{\rho_{\mathrm{s}}}\frac{cN\theta^{N-2}+\dfrac{2}{N-2}}{\sqrt{1-\left(c\theta^{N-1}+\dfrac{\theta}{N-2}\right)^{2}}}\mathrm{d}\theta-\frac{N}{N-1}\sin^{-1}\left(c\rho_{\mathrm{s}}^{N-1}+\frac{\rho_{\mathrm{s}}}{N-2}\right) \tag{4.26}$$

Lastly, the acceleration constraint needs to be attended. From Eq. (2.28), the initial and switching values of the nondimensional path angle rate are

$$\gamma_{\mathrm{i}}' = -N\frac{\sin\varepsilon_{\mathrm{i}}}{\rho_{\mathrm{i}}} + 1 \tag{4.27}$$

$$\gamma_{\mathrm{s}}' = -N\frac{\sin\varepsilon_{\mathrm{s}}}{\rho_{\mathrm{s}}} + 1 \tag{4.28}$$

It is true that the inequality $\rho_{\mathrm{i}} > \rho_{\mathrm{s}}$ holds and as demonstrated in Figure 3.4, the inequality $\sin\varepsilon_{\mathrm{i}} < \sin\varepsilon_{\mathrm{s}}$ is very likely to hold for a ground-to-ground scenario. Then, it can be said that the absolute value of the switching rate will *probably* be higher than that of the initial rate. As the adverb "probably" implies, the opposite might also be true under certain circumstances. However, this is of little importance since the focus is not on the switching instant itself but the one immediately after it. At this instant, the bias ceases to exist; so, the acceleration jumps to a certain negative value that is expected to have the maximum magnitude encountered within the entire duration of the engagement. Such jumps can be witnessed in Figure 3.3. The author thinks that a realistic scenario in which the maximum acceleration magnitude does not belong to this instant would be an extreme rarity. Hence, continuing with Eq. (2.29) evaluated at the switching instant rather than the initial instant, the following may be obtained:

$$\gamma_{\mathrm{s}}' = -cN\rho_{\mathrm{s}}^{N-2} - \frac{2}{N-2} \tag{4.29}$$

Then, Eq. (2.25) yields

$$\lambda_{\mathrm{s}}' = \frac{\gamma_{\mathrm{s}}' - 1}{N} \tag{4.30}$$

which is converted to its dimensional form with the help of Eq. (2.16) and Eq. (2.17) as

$$\dot{\lambda}_{\mathrm{s}} = \frac{\gamma'_{\mathrm{s}} - 1}{N} \beta v_{\mathrm{s}} \tag{4.31}$$

From Eq. (4.22), the path angle rate just after the switching instant is

$$\dot{\gamma}\big|_{t=t_{\mathrm{s}}^{+}} = \left(\gamma'_{\mathrm{s}} - 1\right) \beta v_{\mathrm{s}} \tag{4.32}$$

and Eq. (2.11) finally dictates that

$$a\big|_{t=t_{\mathrm{s}}^{+}} = \left(\gamma'_{\mathrm{s}} - 1\right) \beta v_{\mathrm{s}}^{2} \tag{4.33}$$

or

$$a^{*} = -\left(\gamma'_{\mathrm{s}} - 1\right) \beta v_{\mathrm{s}}^{2} \tag{4.34}$$

The minus sign is due to the fact that $a^{*} > 0$ and $\sigma = 1$. As seen in Eq. (4.34), the acceleration depends on the switching value of the speed, which is not known beforehand. The solution is again to resort to the concept of constant maximum lift coefficient as represented by Eq. (4.15). As a result, Eq. (4.34) can be written as

$$\kappa^{*} = -\left(\gamma'_{\mathrm{s}} - 1\right) \beta \tag{4.35}$$

This equation can be combined with Eq. (2.29) to have

$$\kappa^{*} = \left(cN \rho_{\mathrm{s}}^{N-2} + \frac{N}{N-2} \right) \beta \tag{4.36}$$

Now the general picture of the constrained guidance problem is this:

Given: $\varepsilon^*, \kappa^*, \gamma_{\mathrm{f,d}}$

Find: $N, \beta, \rho_{\mathrm{s}}$

The relationships to be used in the solution are

$$cr_{\mathrm{i}}^{N-1}\beta^{N-1} + \frac{r_{\mathrm{i}}}{N-2}\beta - \sin\varepsilon_{\mathrm{i}} = 0 \tag{4.7}$$

$$\gamma_{\mathrm{f,d}} = \gamma_{\mathrm{i}} + \int_{\rho_{\mathrm{i}}}^{\rho_{\mathrm{s}}} \frac{cN\theta^{N-2} + \dfrac{2}{N-2}}{\sqrt{1-\left(c\theta^{N-1} + \dfrac{\theta}{N-2}\right)^2}}\,\mathrm{d}\theta - \frac{N}{N-1}\sin^{-1}\left(c\rho_{\mathrm{s}}^{N-1} + \frac{\rho_{\mathrm{s}}}{N-2}\right) \tag{4.26}$$

$$\kappa^* = \left(cN\rho_{\mathrm{s}}^{N-2} + \frac{N}{N-2}\right)\beta \tag{4.36}$$

where

$$c = -\frac{1}{(N-1)^{N-1}(N-2)(\sin\varepsilon^*)^{N-2}} \tag{4.5}$$

As seen, there are three equations that can be used to solve for the three guidance parameters. It is obvious that this highly nonlinear equation set could be solved with some numerical method, possibly with brute force. However, the aim here is to devise a sufficiently simple solution so that it could pass for practical a guidance method implementable in a guidance computer. Unlike in [43], the author fails to come up with a smart numerical algorithm. This is why an alternative solution based on almost the same structure will be proposed in the next section.

4.3. Look Angle Constrained Impact Angle Control with Acceleration Check

Since the equation set obtained at the end of the previous section is not easily solvable, an alternative approach with predetermined navigation gains will be presented here. The guidance law of choice is the discontinuous structure given in Eq. (3.12). Utilizing Eq. (2.17) and taking the switching condition from Eq. (3.5) rather than from Eq. (3.4), the guidance law is:

$$\dot{\gamma} = \begin{cases} N_{\mathrm{M}}\dot{\lambda} + \beta v & \text{if } \gamma - \dfrac{N_{\mathrm{T}}}{N_{\mathrm{T}} - 1}\varepsilon > \gamma_{\mathrm{f,d}} \\ N_{\mathrm{T}}\dot{\lambda} & \text{otherwise} \end{cases} \tag{4.37}$$

Then, Eq. (4.5) and Eq. (4.6) are combined using N_{M} instead of N to yield

$$\frac{\rho_{\mathrm{i}}^{N_{\mathrm{M}}-1}}{\left(N_{\mathrm{M}}-1\right)^{N_{\mathrm{M}}-1}\left(N_{\mathrm{M}}-2\right)\left(\sin\varepsilon^{*}\right)^{N_{\mathrm{M}}-2}} - \frac{\rho_{\mathrm{i}}}{N_{\mathrm{M}}-2} + \sin\varepsilon_{\mathrm{i}} = 0 \tag{4.38}$$

When the midcourse navigation gain is an integer, this happens to be a polynomial in ρ_{i}. In the case of multiple positive roots, the solution sought is most likely to be the greatest one since smaller ones might place the pursuer to the left side of the extreme point of the trajectory such that ε^{*} may never be reached. The simplest case happens with $N_{\mathrm{M}} = 3$, which has been shown to constitute a favorable midcourse guidance solution in Section 3.2.1. In this case, the initial nondimensional range can be obtained as

$$\rho_{\mathrm{i}} = 2\sin\varepsilon^{*}\left(1 + \sqrt{1 - \frac{\sin\varepsilon_{\mathrm{i}}}{\sin\varepsilon^{*}}}\right) \tag{4.39}$$

After solving for the nondimensional range, the β value to keep the pursuer on the preferred trajectory can be obtained by utilizing Eq. (2.15) as

$$\beta = \frac{\rho_{\mathrm{i}}}{r_{\mathrm{i}}} \tag{4.40}$$

As seen, the initial range to the target is required in addition to the initial speed (the procedure described in Section 4.1 also requires the initial range, which is a fact not highlighted there so as not to add another complicating factor to the already complicated situation). The pursuer might under- or overshoot the intended maximum look angle depending on the accuracy of the range information. If the designer thinks that the initial range value supplied to the pursuer is not reliable, a range observer may be employed before initializing the midcourse guidance.

Before proceeding further, the reader should notice that what follows is not a direct part of the proposed guidance methodology but merely a way of verifying, before the engagement starts, that the selected bias value will create such a proper trajectory that the pursuer will not have to exert too much effort after the switching instant, which happens to be the critical point of the discontinuous bias application approach.

The rate of the LOS angle at the switching instant is needed to obtain the initial value of the terminal acceleration. To this end, the switching value of the path angle can be calculated *numerically* from Eq. (2.32). What complicates the procedure is that the switching range is not known in advance; the switching is executed when the guidance algorithm decides that the bias integral has reached the desired level. As might be predicted, the solution to this seeming paradox is an *iterative* routine. Starting from an initial guess for ρ_{s}, Eq. (4.24) and Eq. (4.25) are used to write the following:

$$\varepsilon_{\mathrm{s}} = \sin^{-1}\left(c\rho_{\mathrm{s}}^{N_{\mathrm{M}}-1} + \frac{\rho_{\mathrm{s}}}{N_{\mathrm{M}}-2} \right) \tag{4.41}$$

$$\gamma_{\mathrm{s}} = \gamma_{\mathrm{i}} + \int_{\rho_{\mathrm{i}}}^{\rho_{\mathrm{s}}} \frac{cN_{\mathrm{M}}\theta^{N_{\mathrm{M}}-2} + \dfrac{2}{N_{\mathrm{M}}-2}}{\sqrt{1-\left(c\theta^{N_{\mathrm{M}}-1} + \dfrac{\theta}{N_{\mathrm{M}}-2} \right)^2}} \mathrm{d}\theta \tag{4.42}$$

Now, invoking the potential impact angle function from Eq. (4.23), the following is written:

$$\gamma_{\mathrm{f,d}} - \left(\gamma_{\mathrm{s}} - \frac{N_{\mathrm{T}} \varepsilon_{\mathrm{s}}}{N_{\mathrm{T}} - 1} \right) = 0 \tag{4.43}$$

If the relationship above is satisfied within a certain error tolerance; that is, the potential value calculated using the iterated switching values of the flight path and look angles becomes nearly the same as the desired impact angle, the iteration stops. If not, the routine goes back to Eq. (4.41) with an updated nondimensional range value. The update logic may be based on the fact that the impact angle will be more and more negative as the switching instant is delayed such as

$$\tilde{\rho}_{\mathrm{s,new}} = \tilde{\rho}_{\mathrm{s,old}} + k_{\gamma} e_{\gamma}$$

where k_{γ} is a gain that drives the numerical process and e_{γ} is the left hand side of Eq. (4.43) evaluated with $\tilde{\gamma}_{\mathrm{s,old}}$ and $\tilde{\varepsilon}_{\mathrm{s,old}}$. After the iteration has converged, Eq. (4.31) can be used to write

$$\dot{\lambda}_{\mathrm{s}} = \frac{\gamma_{\mathrm{s}}' - 1}{N_{\mathrm{M}}} \beta v_{\mathrm{s}} \tag{4.44}$$

It should be noted that β is the one that has been obtained above in Eq. (4.40). So, Eq. (4.33) may be modified into the following form:

$$a\big|_{t=t_{\mathrm{s}}^{+}} = \frac{N_{\mathrm{T}}}{N_{\mathrm{M}}} \left(\gamma_{\mathrm{s}}' - 1 \right) \beta v_{\mathrm{s}}^2 \tag{4.45}$$

after which Eq. (4.13) can be used to arrive finally at

$$\kappa_{\mathrm{s}} = -\frac{N_{\mathrm{T}}}{N_{\mathrm{M}}} \left(\gamma_{\mathrm{s}}' - 1 \right) \beta \tag{4.46}$$

If the κ^* value seen in Eq. (4.15), which represents the aerodynamic capacity of the pursuer, turns out to be at least equal to the value obtained above, i.e. if $\kappa_s \leq \kappa^*$, this means that the pursuer will be able to sustain the acceleration commanded by the guidance law. However, if the designer finds out that the capacity will be insufficient to carry out the mission objectives, some form of compromise should be reached such as changing the navigation gains, lowering the impact angle expectancy or changing the initial conditions etc.

It is now time to present some examples of the constrained guidance process. The reference engagement geometry introduced in Section 2.2 is considered once more. One of the points in the vicinity of the vertical impact contour in Figure 4.2 is the one with a look angle limit of 49° and an acceleration limit of 44 m/s^2, which corresponds to a κ limit of 0.000704 m $^{-1}$ as per Eq. (4.15). These values are selected as the constraint values. Along with the practical method based on Eq. (4.37) to be used as outlined in this section, the solution based on Eq. (4.1) is also utilized to demonstrate the continuous bias application approach even it is deemed impractical. The former method is represented by letter D and the latter one is represented by letter C. With the constraint values above, the navigation gain value to be used in C happens to be 4.126 whereas the corresponding β value is 0.000748 m $^{-1}$. For D, the midcourse and terminal navigation gain values are selected as 3 and 2, respectively. The β value is calculated from Eq. (4.40) as 0.000547 m $^{-1}$. The pursuer starts with a speed of 250 m/s and decelerates according to $\dot{v} = -0.00007v^2$. There is no gravity. If there was, it would assist the pursuer during the descent and the situation would accordingly be less challenging for the guidance algorithm. Besides the simulations with no command following dynamics, additional simulations are performed with $\tau_a = 0.4$ s as in Eq. (3.32) as a disturbing factor. As practiced in the previous chapter, the last guidance command is held when the range is less than 30 m. The simulation results are summarized in Table 3.1. The columns are self-explanatory owing to the tables presented previously throughout Chapter 3.

Table 4.1 Summary of the constrained guidance simulation results

Scn.	**Dyn.**	N	β [m^{-1}]	κ_{ext} [m^{-1}]	ε_{max} [deg]	E [m^2/s^3]	γ_f [deg]
C_1	Off	4.126	0.000748	−0.000705	49	8651	−90.0
C_2	On	4.126	0.000748	−0.000701	50.2	8778	−91.5
D_1	Off	$3 \rightarrow 2$	0.000547	−0.000668	49	8228	−90.0
D_2	On	$3 \rightarrow 2$	0.000547	−0.000673	50.2	8631	−90.5

In Figure 4.3, the look angle variations are displayed. It is seen that the limit is slightly violated when the pursuer dynamics is on. The simple remedy would be to assume a slightly lower value than the actual limit. Here, the spatial trajectory and the path angle plots are not included because quite a number of similar plots have already been presented. It can be expressed that the impact angle values exhibited in Table 4.1 confirm that in each case, the guidance objective is met with sufficient accuracy. Figure 4.4 shows the κ histories. It is observed that the overall behavior is not affected much by the lagged response. Table 4.1 indicates that the κ limit is only violated by C_1. This negligible amount of violation results from not updating the command at the last moments. The most important implication of this figure is the fact that D, unlike C, does not utilize the full control effort when closing in on the target. The reflection of this advantage is also clear in the cost function values in the table. Finally, the author should remind the reader that it is D which is acknowledged as the truly feasible guidance law.

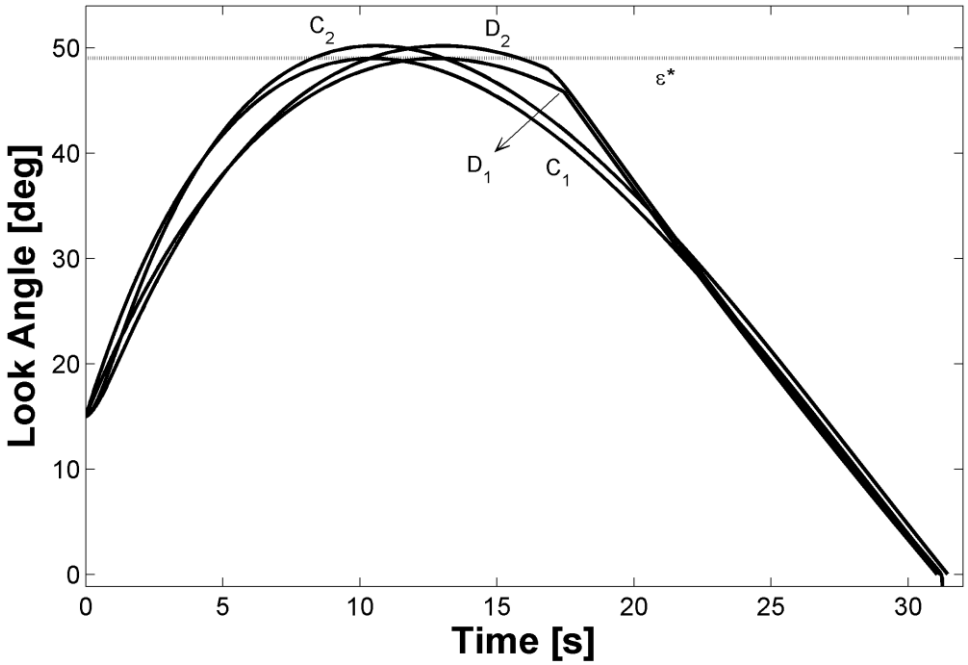

Figure 4.3 Look angle variations during constrained guidance produced by the continuous and discontinuous bias application strategies (see Table 4.1 for details)

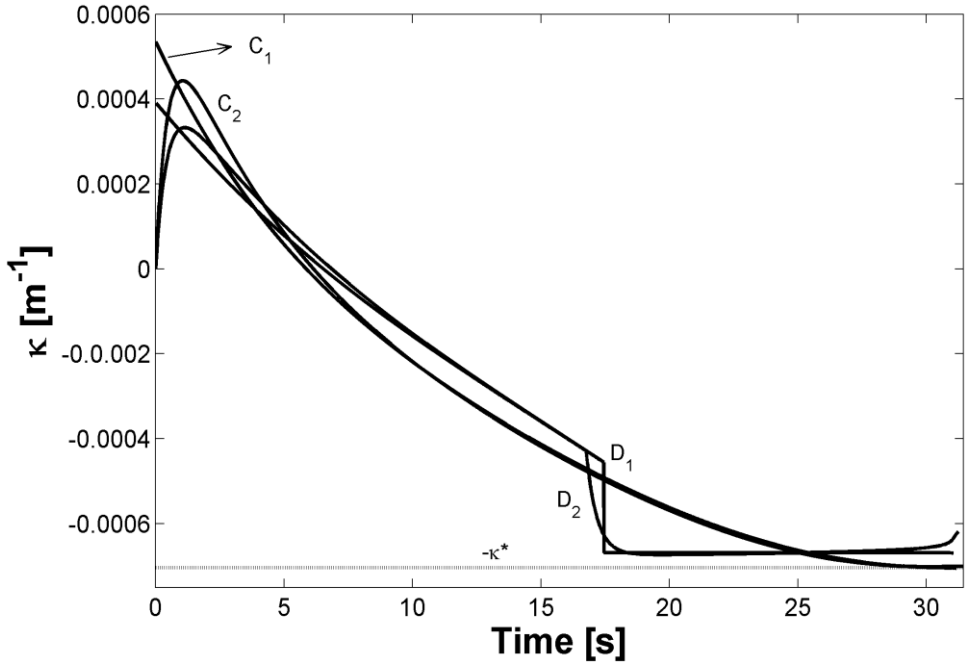

Figure 4.4 κ histories during constrained guidance produced by the continuous and discontinuous bias application strategies (see Table 4.1 for details)

CHAPTER 5

RANGE OBSERVER

As is the case with optimal control solutions, the time-to-go information would be valuable to any trajectory-shaping guidance law. The general problem with this variable is that it is almost never available directly since the shape of the trajectory is not available beforehand. Hence, it has to be estimated. One convenient way to estimate the time to go is to use the following approximation [2]:

$$t_{\text{go}} \approx \tilde{t}_{\text{go}} = -\frac{r}{\dot{r}} \tag{5.1}$$

Against a stationary target, the term in the denominator may promptly be replaced from Eq. (2.7) so that the approximation appears as

$$\tilde{t}_{\text{go}} = \frac{r}{v\cos\varepsilon} \tag{5.2}$$

It should be noted that the term in the nominator is not available. One can argue that Eq. (2.7) can be integrated to obtain the range; however, this would imply the availability of the initial range value, which is unlikely to be known in practice. One might still attempt to obtain the range through Eq. (2.8); yet, this, too, would most likely be unfruitful as the LOS angle rate, which is typically to be provided by an onboard seeker, is never noise-free. The look angle, on the other hand, is more likely to be reliable because it may be obtained as a combination of the Euler angle of the missile body and the angular deviation of the seeker axis with respect to the body. The former of these variables is typically supplied by the INS whereas the latter is

expected to be measured by a reliable displacement sensor such as an encoder. As a result, the range needs to be estimated via some proper means.

In the literature, the so-called “passive ranging” problem is typically solved for moving targets through the use of Kalman filters as in [49] and [50], where pursuer trajectory is often modified to enhance observability. The same approach would naturally be applicable for stationary targets as well; however, the direction followed in this paper deviates from that classical path for the sake of simplicity. The proposed single- and constant-gain range observer, which is based on the state observer methodology [46], is structured on the nonlinear kinematics and addresses the observability issue through a simple switching action that stops the pseudo range measurement from being fed back to the system when required. It should be kept in mind that this method is only meant for stationary targets.

5.1. Observer Structure

To build the observer, a system model and a measurement model are required. These can simply be obtained by rewriting Eq. (2.7) and Eq. (2.8) as [43]

$$\dot{r} = \iota = -v\cos\varepsilon \tag{5.3}$$

$$r = \mu = -\frac{v\sin\varepsilon}{\dot{\lambda}} \tag{5.4}$$

where ι is the input and μ is the measurement. In fact, naming μ as the pseudo measurement would be more appropriate because the range is not measured directly; an approximation is obtained by combining the outputs from the INS and the seeker. The block diagram of the proposed range observer is presented in Figure 5.1, where $\tilde{r}$ is the range estimate and *K* is the observer gain.

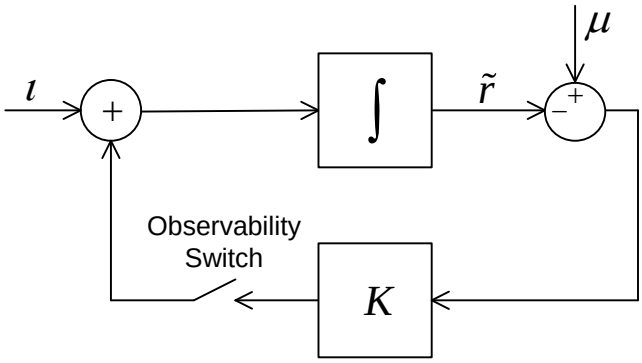

Figure 5.1 Range observer structure to estimate the range to a stationary target

It is well known that the range becomes unobservable on the collision course as mentioned in [49] and [50]. In this proposed structure, the unobservability manifests itself in the pseudo-measurement equation when the LOS angle rate is zero. The observability switch in the figure aims to address this potential problem. In reality, due to the noisy signal provided by the seeker, this phenomenon would show itself not when the LOS angle rate becomes identically zero but when its absolute value drops below a certain threshold, which depends on the system being studied. So; if this happens, one may simply switch off the error feedback, making the system flow through the open-loop route. If the observability switch goes off after the range estimation has converged, even the system model by itself without the erroneous measurement might still yield acceptable estimates.

The transfer function relating the output to the inputs can be written as

$$\tilde{R}(s) = \frac{1}{s+K}\mathrm{I}(s) + \frac{K}{s+K}\mathrm{M}(s) \tag{5.5}$$

which indicates that the observer essentially acts as a low-pass filter for both the input and the measurement, which is helpful to suppress the noise content in the seeker and the INS outputs.

The proposed range estimator is conveniently straightforward to implement with only two user defined parameters: The gain to adjust the bandwidth and the threshold to prevent the estimation process from collapsing. Since it operates independent of the guidance law, it may be used in conjunction with any law that would benefit from range information.

Even though the derivation above gives the impression that it is applicable only in the plane, the proposed range estimation method is a 3-D algorithm by nature. This should become apparent once the following is written

$$\dot{r} = -v\left(\vec{u}_v \bullet \vec{u}_r\right) \tag{5.6}$$

$$r = \frac{v}{\omega}\left\|\vec{u}_v \times \vec{u}_r\right\| \tag{5.7}$$

where $\vec{u}_v$ and $\vec{u}_r$ are the unit vectors parallel to the velocity vector and the LOS, respectively. ω denotes the magnitude of the angular velocity vector associated with the LOS. As seen, employing the definitions of dot and cross product operations renders such a smooth transition from the plane to the 3-D space possible. The range is a positive quantity; so, all the terms on the right hand side of the second equation may safely be kept positive.

The next subsection aims to present various aspects of the range observer in relation with filter parameters and practical implementation considerations. The performance of the observer in real flight tests is included in Appendix D.

5.2. Effects of Various Parameters on the Estimation Performance

Applied to the benchmark scenario presented in Section 2.2, the performance of the proposed range observer under the action of various actors is illustrated here. The initial guess is zero. Firstly, Figure 5.2 shows the performance as a function of the observer gain. As expected, the performance improves with increasing gain. In

practice, the selection of the gain value should be based upon a compromise between the desired transient performance and the noise content of the measurements. $K = 1\ \mathrm{s}^{-1}$, which provides an intermediate performance, will be used in the remaining part of this subsection.

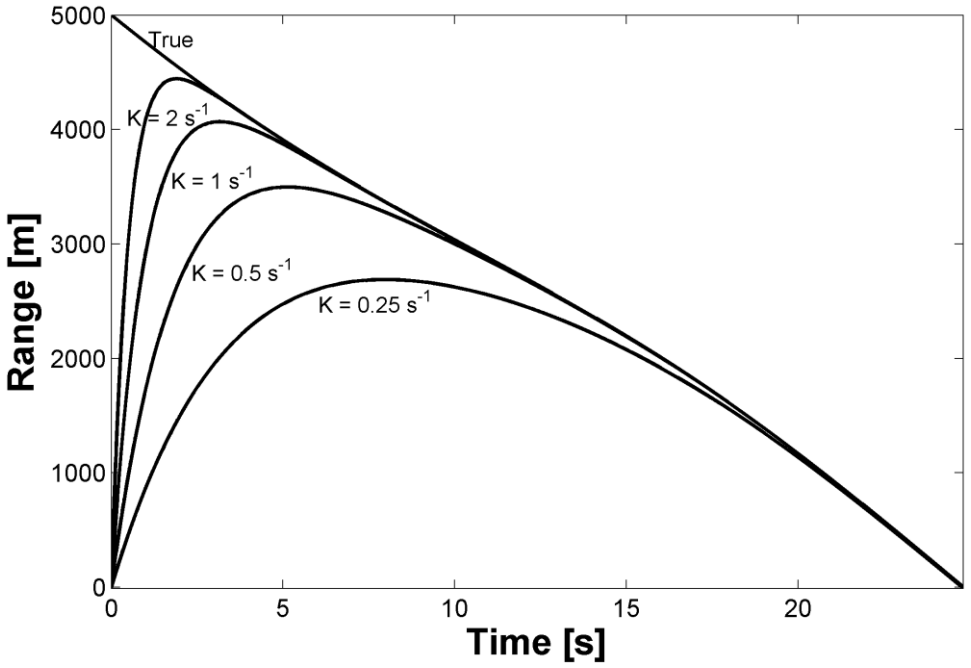

Figure 5.2 Effect of the observer gain on the range estimation performance

Figure 5.3 presents the results of simulation runs where the observability threshold value is varied in an exaggerated manner. As seen, the estimates remain somewhat parallel to the true range during the unobservable intervals. Then, the observers successfully recover once the LOS angle rate magnitude exceeds the threshold. In practice, this value should be adjusted by considering how much the trajectory followed is observable in conjunction with the quality level of the signals supplied by the sensors. In this specific example, the trajectory is highly observable as can be judged by the look angle variation seen in Figure 2.12.

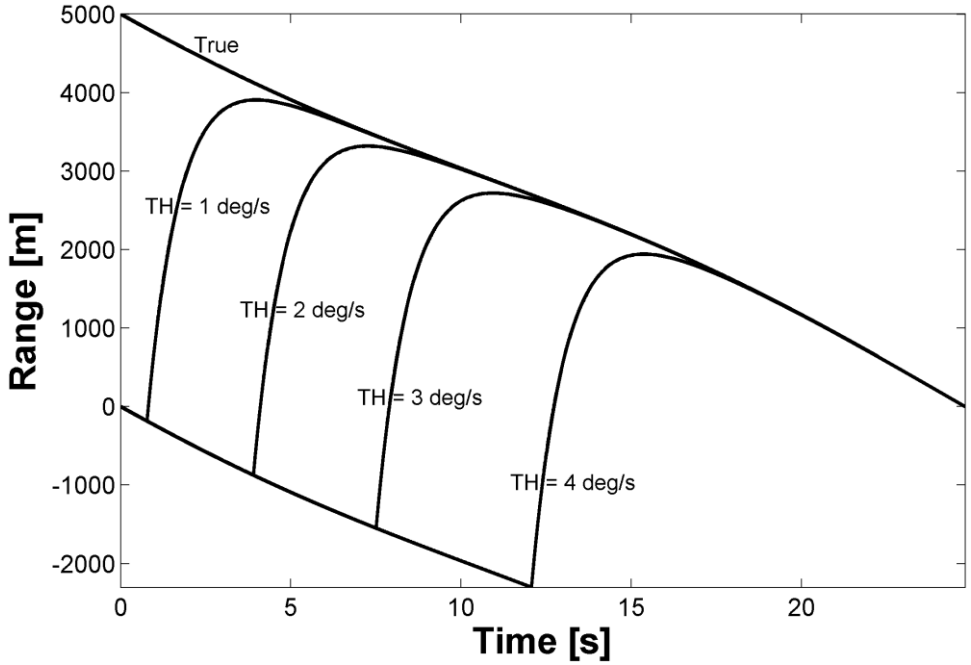

Figure 5.3 Effect of the observer threshold on the range estimation performance

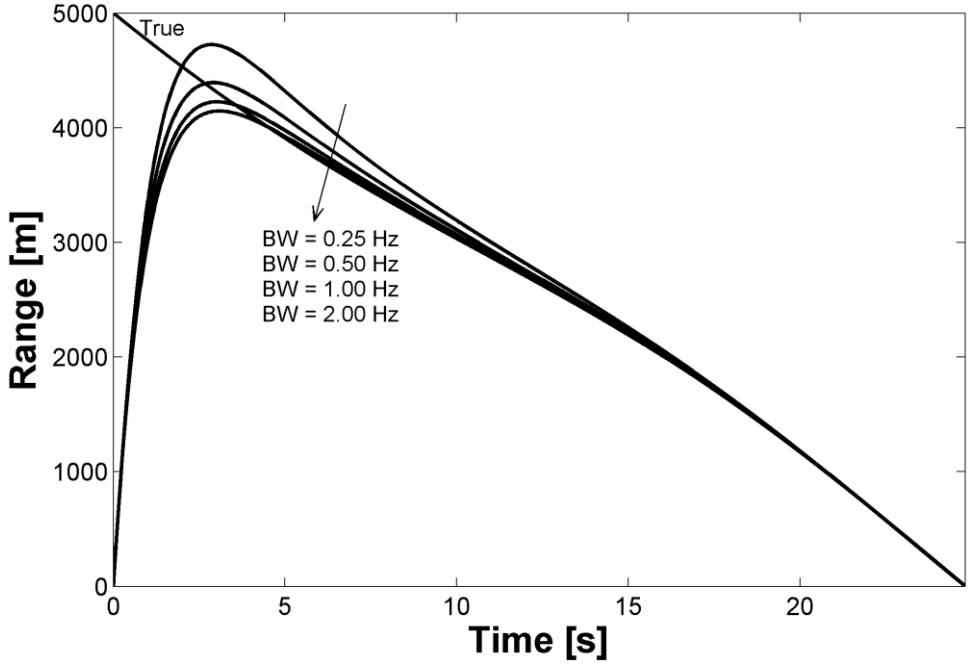

Figure 5.4 Effect of the seeker tracking bandwidth on the range estimation performance

In an idealized setting, the tracking loop of a gimballed seeker may be thought of as a first-order filter operating on the LOS angle rate. Figure 5.4 shows the effect of the tracking bandwidth on the estimation performance. It is observed that low bandwidth shows itself as lagged response, especially during the initial part of the trajectory where the LOS angle rate is relatively low.

The range observer is formulated in the continuous time domain; however, it has to be implemented in the discrete time domain for practical reasons such as the sampling time associated with the seeker. Figure 5.5 can be consulted for a brief assessment of the impact of such a factor. The sampling rates indicated on the figure indicate the frequencies at which the integrator seen in Figure 5.1 operates. Judging by the trends, it may be concluded that the range estimates would be acceptable as long as the sampling rate is not too low. It is seen that a sampling rate of 5 Hz produces a realistically smooth result. Modern seekers are likely to operate even at higher rates.

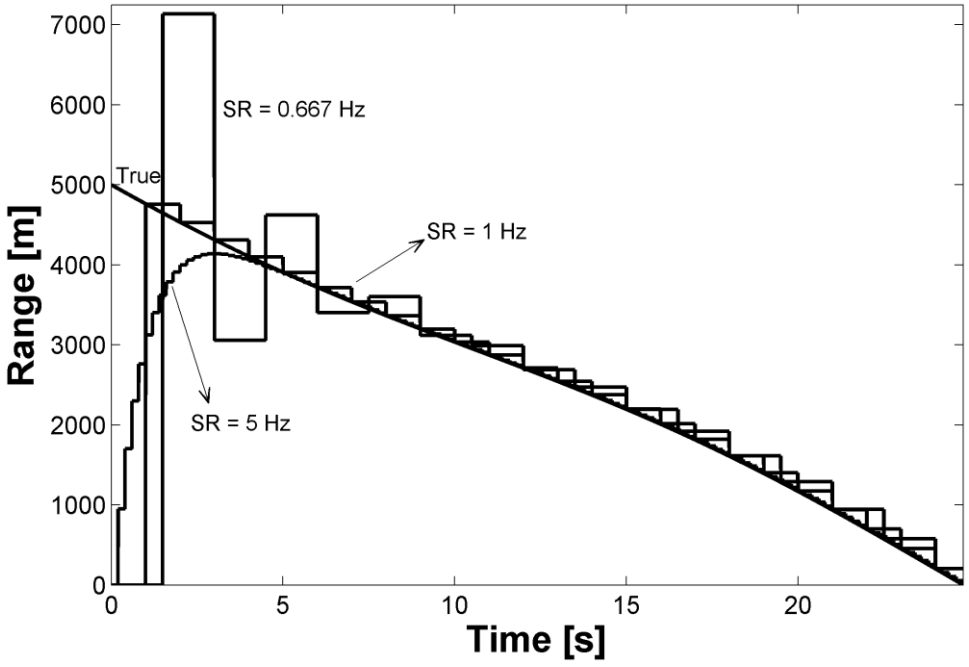

Figure 5.5 Effect of the sampling rate on the range estimation performance

Another important actor is the noise embedded in the LOS angle rate outputs provided by the seeker. Since the measurment noise is a discrete phenomenon, the observer is operated at 5 Hz to produce the results in Figure 5.6. The same noise set acts with three different standard derivations indicated on the figure. Considering the fact that the true LOS angle rate magnitude remains relatively low during the first few seconds, a severly contaminated LOS angle rate input would almost always result in huge estimation errors. Two of the curves shown in the figure exemplify such cases whereas the one contaminated the least is able to perform fairly well.

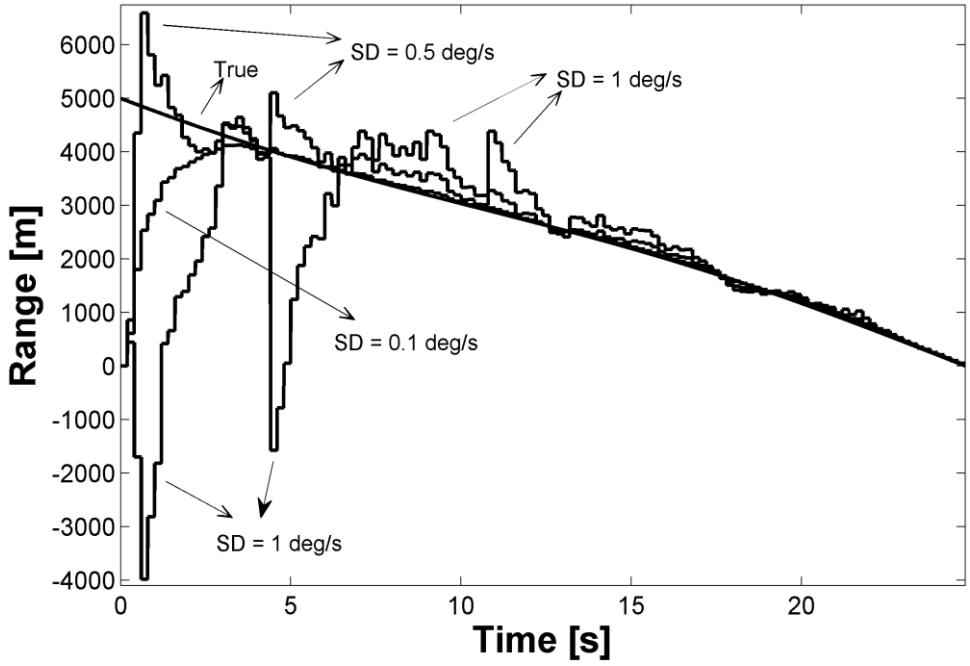

Figure 5.6 Effect of the noise in LOS angle rate on the range estimation performance

Lastly, the results of a hundred-run Monte Carlo analysis is presented in Figure 5.7. The only random variable is the LOS angle rate noise with a fixed standard deviation. The parameters are selected based on the observations from Figure 5.2 – Figure 5.6. The standard deviation of the noise is 0.3 °/s. The gain of the observer is 1 s^{-1} as before and its threshold is not activated. The tracking bandwidth is 1 Hz and the update frequency is 10 Hz. The curves seen in the figure represent upper and

lower estimation envelopes obtained by picking the extreme values of all the observer outputs at each time step. The envelopes are seen to narrow down to more or less reasonable levels in about three seconds. Also, it is observed that for higher range values, the lower estimation envelope is closer to the true range than the upper one. This is brought about by the seeker tracking delay.

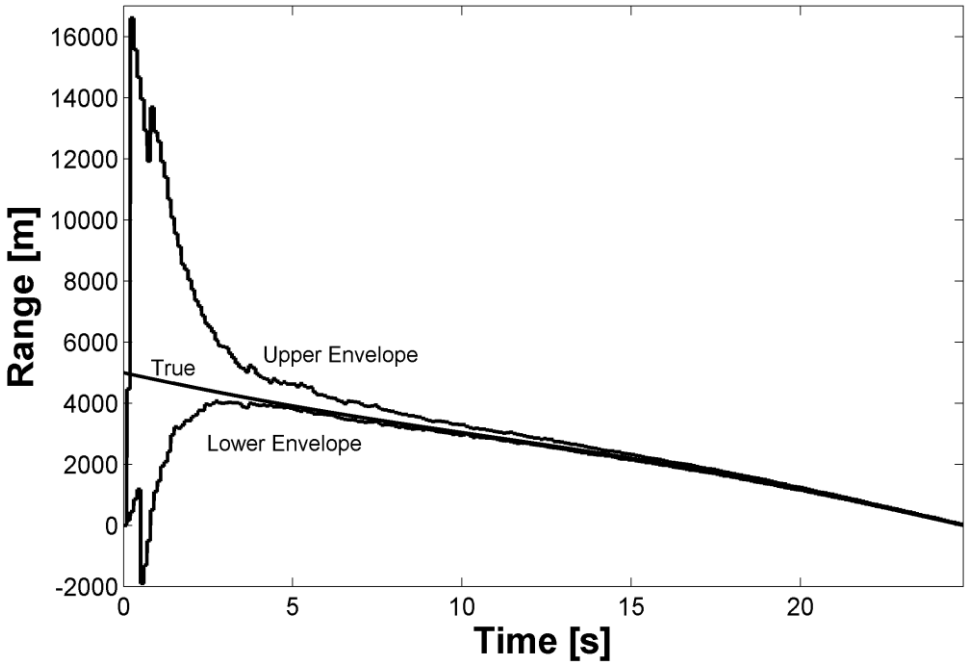

Figure 5.7 Range estimation error envelopes for a specific parameter set

CHAPTER 6

THE CASE OF MOVING TARGETS

So far, the target to be captured with a desired impact angle has been stationary. This chapter extends the focus to include moving targets. This is made possible by the use of the *collision triangle* concept, which is employed commonly in the literature as in [30] and [33]. To be able to construct the collision triangle, one needs to have prior knowledge of the *final* values of the pursuer and target velocities. The final values are, of course, not available until the last moment because in a real engagement, the speed of the pursuer will probably be varying under the action of external actors and the target might any time decide to change its speed and/or direction. The obvious solution is to assume that the velocities will not change after the triangle has been constructed. Such an assumption is unlikely to hold unless the time between the calculation and the impact is very short. The remedy could be doing the calculation repeatedly; yet, this implies a persistent flow of information about the target states to the guidance algorithm. In addition to external sources that would supply the required information, this difficulty could be overcome with an estimator such as the range observer presented earlier. This time, however, the estimator structure would presumably be more complex and the derivation and/or utilization of such an instrument is beyond the scope of this text. On the other hand, it might be argued that feeding the target information to the pursuer once before it takes off could be more feasible under certain practical circumstances. The uncertainty in this piece of information would then show itself in the final results. Therefore, the path to be followed in this chapter is to solve the problem for the case of specified speeds and then to evaluate the performance under disturbing factors.

6.1. Preliminaries

The general engagement geometry between a pursuer and a moving target is presented in Figure 6.1.

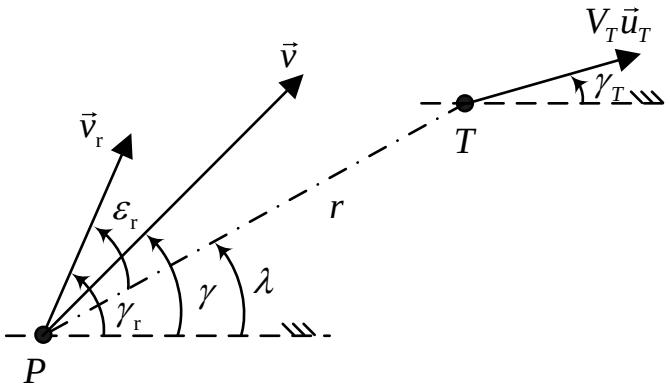

Figure 6.1 Planar engagement between the pursuer and its moving target

In addition to the previously defined quantities; V_T is the constant pursuer speed with its direction $\vec{u}_T$ and its path angle γ_T, and $\vec{v}_r$ is the relative velocity vector with its path angle γ_r and its look angle ε_r.

Based on Figure 6.1, the differential equations governing the engagement can be written as

$$\dot{r} = -v\cos(\gamma - \lambda) + V_T \cos(\lambda - \gamma_T) \tag{6.1}$$

$$r\dot{\lambda} = -v\sin(\gamma - \lambda) - V_T \sin(\lambda - \gamma_T) \tag{6.2}$$

These can be compared with Eq. (2.7) and Eq. (2.8) to see the influence of having a moving target.

The collision triangle is presented in Figure 6.2. Because the triangle corresponds to the steady-state part of the engagement, this picture might either belong to the final instant or some duration before it; hence *l*, a dummy scaling parameter with units of time. $\vec{u}$ is the velocity direction of the pursuer. It should be noted that the relative velocity vector must lie on the LOS for a successful capture as seen here.

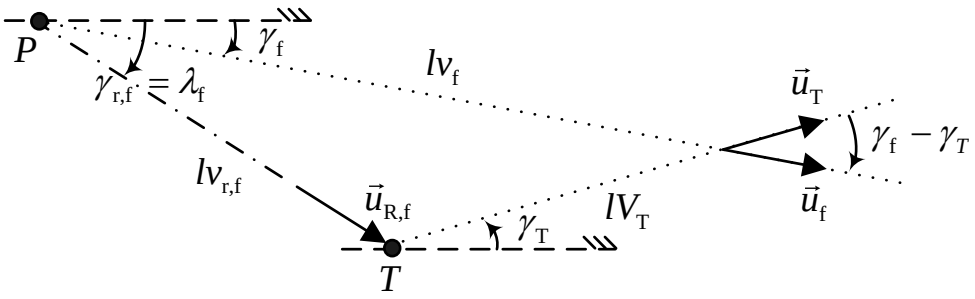

Figure 6.2 Collision triangle depicting the steady state of the engagement

Noting that the angles are negative in the clockwise direction, the sine theorem can be utilized to obtain the following:

$$\frac{\sin\left(\gamma_T - \lambda_{\mathrm{f}}\right)}{v_{\mathrm{f}}} = \frac{\sin\left(\gamma_{\mathrm{f}} - \lambda_{\mathrm{f}}\right)}{V_T} = \frac{\sin\left(\gamma_T - \gamma_{\mathrm{f}}\right)}{v_{\mathrm{r,f}}} \tag{6.3}$$

The collision triangle may be simplified by rotating it through an angle of $-\gamma_T$ such that the entire geometry is referenced with respect to a rotated frame of axes. Whereas this necessitates some modifications in the guidance code for a general engagement geometry, it is directly applicable when the target is constrained to move on the ground, which is the case being studied in this dissertation. The simplified version of the triangle is shown in Figure 6.3.

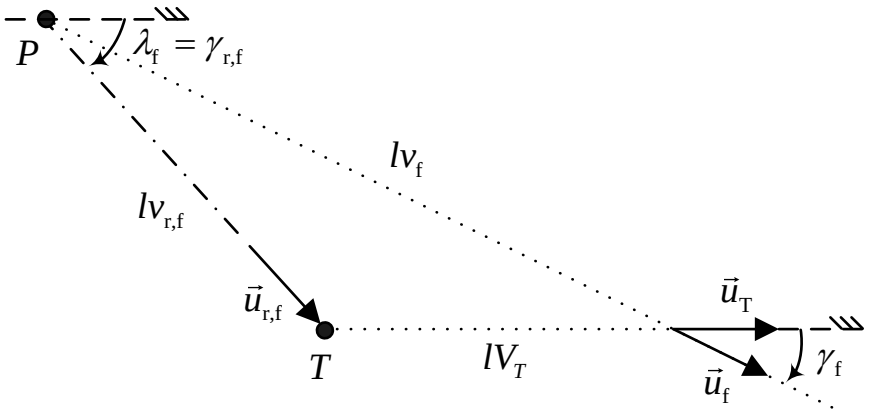

Figure 6.3 Simplified collision triangle against a ground target

With $\gamma_T = 0$, Eq. (6.3) can be used to obtain

$$\lambda_f = \gamma_f + \sin^{-1}\left(\frac{V_T}{v_{r,f}}\sin\gamma_f\right) \tag{6.4}$$

which, due to the cosine theorem, may be written as

$$\lambda_f = \gamma_f + \sin^{-1}\left(\frac{\sin\gamma_f}{\sqrt{\upsilon_f^2 - 2\upsilon_f\cos\gamma_f + 1}}\right) \tag{6.5}$$

where

$$\upsilon = \frac{v}{V_T} > 1 \tag{6.6}$$

In what follows, it is assumed that the information regarding the target velocity vector is available to the pursuer only before the launch. Therefore, the impact angle control tactic has to be open loop.

6.2. PPN-Based Implementation

As the first alternative to deal with moving targets, the guidance law to be applied is Eq. (3.10). Different navigation gains could have been assigned to the midcourse and terminal phases as in Eq. (3.12); yet, such an additional complexity is avoided here for the sake of simplicity. Before moving on, it must be underlined that there is no guarantee that the midcourse guidance phase will be stable with BPPN against a moving target. Fortunately, BPPN will eventually leave the stage to PPN, for which a *sufficient* condition to have a decreasing LOS angle rate magnitude is given as [5]

$$N > 2\frac{\upsilon+1}{\upsilon} \tag{6.7}$$

It would be wise to obey this inequality in order not to face harsh acceleration demands near the target.

As described in Section 3.2.1, the bias interval in Eq. (3.10) needs to be sufficiently less than the total engagement time. Assuming a nonincreasing pursuer speed and a receding target, a safe value would be

$$\Delta t = \frac{r_{\mathrm{i}}}{v_{\mathrm{i}} - V_T} \tag{6.8}$$

which is similar to (3.13).

The desired value of the bias integral can be written from Eq. (3.1) as

$$B_{\mathrm{d}} = \gamma_{\mathrm{f,d}} - \gamma_{\mathrm{i}} - N\left(\lambda_{\mathrm{f}} - \lambda_{\mathrm{i}}\right) \tag{6.9}$$

This time, however, the final LOS angle is not equal to the final look angle due to the target movement. Instead, Eq. (6.5) can be used in Eq. (6.9) to obtain

$$B_{\mathrm{d}} = -\left(N-1\right)\gamma_{\mathrm{f,d}} - \gamma_{\mathrm{i}} + N\left\{\lambda_{\mathrm{i}} - \sin^{-1}\left(\frac{\sin\gamma_{\mathrm{f,d}}}{\sqrt{\upsilon_{\mathrm{f}}^2 - 2\upsilon_{\mathrm{f}}\cos\gamma_{\mathrm{f,d}} + 1}}\right)\right\} \tag{6.10}$$

As seen, the right hand side of the equation is entirely composed of known parameters. The combination of Eq. (6.10) with Eq. (6.8) gives the bias as

$$b = \frac{-\left(N-1\right)\gamma_{\mathrm{f,d}} - \gamma_{\mathrm{i}} + N\left\{\lambda_{\mathrm{i}} - \sin^{-1}\left(\frac{\sin\gamma_{\mathrm{f,d}}}{\sqrt{\upsilon_{\mathrm{f}}^2 - 2\upsilon_{\mathrm{f}}\cos\gamma_{\mathrm{f,d}} + 1}}\right)\right\}}{r_{\mathrm{i}}/\left(v_{\mathrm{i}} - V_T\right)} \tag{6.11}$$

This form should be compared with Eq. (3.14) to appreciate the influence of the target movement.

It should be noted that the final speed of the pursuer, in addition to the known target speed, must be available to calculate the bias value. The trivial solution is to assume a constant speed. This, in general, cannot be assumed but the situation is far from hopeless. It would be fair to surmise that the guidance designer will always be capable of designating the speed interval to which the to-be-realized final speed will belong. The nontrivial solution is to use a value from this interval to construct the collision triangle.

Furthermore, it would be wise to update the bias value according to Eq. (3.16) if the pursuer speed is not constant. However, there is a slight problem here. For example in a scenario where the speed continuously decreases, the integral will not have reached the desired value yet if the bias is removed as soon as t becomes higher than Δt. This issue can be handled by modifying the switching condition to include the bias integral. This modified form of Eq. (3.10) can be written as follows:

$$\dot{\gamma} = \begin{cases} N\dot{\lambda} + b & \text{if } B < B_{\mathrm{d}} \\ N\dot{\lambda} & \text{otherwise} \end{cases} \tag{6.12}$$

6.3. IPN-Based Implementation

As the second alternative to deal with moving targets, the following development is considered:

The relative velocity vector is

$$\vec{v}_{\mathrm{r}} = \vec{v} - V_T \vec{u}_{\mathrm{T}} \tag{6.13}$$

Referring to Figure 6.1, the scalar form of this equation can be written as

$$v_{\mathrm{r}} \cos\gamma_{\mathrm{r}} = v\cos\gamma - V_{\mathrm{T}} \cos\gamma_{\mathrm{T}} \tag{6.14}$$

$$v_{\mathrm{r}} \sin\gamma_{\mathrm{r}} = v\sin\gamma - V_{\mathrm{T}} \sin\gamma_{\mathrm{T}} \tag{6.15}$$

With the help of the complementary relationship

$$\varepsilon_{\mathrm{r}} = \gamma_{\mathrm{r}} - \lambda \tag{6.16}$$

and by utilizing Eq. (6.14) and Eq. (6.15), it can be shown that it is possible to convert Eq. (6.1) and Eq. (6.2) into

$$\dot{r} = -v_{\mathrm{r}} \cos\varepsilon_{\mathrm{r}} \tag{6.17}$$

$$r\dot{\lambda} = -v_{\mathrm{r}} \sin\varepsilon_{\mathrm{r}} \tag{6.18}$$

As seen, these equations are essentially the same as Eq. (2.7) and Eq. (2.8). Now, the following question arises: If the impact angle against a stationary can be controlled via the BPPN law as expressed in Eq. (2.10), can a similar control law be contrived to control the impact angle against a moving target? The answer is simply *yes*.

The formulation to make the moving target *seem stationary* to the guidance loop can be written as

$$\dot{\gamma}_{\mathrm{r}} = N\dot{\lambda} + b \tag{6.19}$$

This is the BIPN guidance rule [36]. If this rule can somehow be implemented, the resulting characteristics will be the *same* as those derived in Chapter 2.

The reason for terming this equation a rule rather than a law is because its implementation is unclear. In order for a relation to be considered a guidance law, it should issue commands that are meaningful to an autopilot. As might be appreciated by the reader, the rate of the relative path angle is not meaningful in that respect. To have a proper solution Eq. (6.14) and Eq. (6.15) can be exploited. Knowing that the velocity vector of the target is constant, differentiation and subsequent trigonometric manipulation yield the following:

$$v_{\mathrm{r}}\dot{\gamma}_{\mathrm{r}} = \cos\left(\gamma_{\mathrm{r}} - \gamma\right)v\dot{\gamma} - \sin\left(\gamma_{\mathrm{r}} - \gamma\right)\dot{v} \tag{6.20}$$

Making use of Eq. (6.19), this produces

$$\dot{\gamma} = \frac{\left(N\dot{\lambda} + b\right)v_{\mathrm{r}} + \sin\left(\gamma_{\mathrm{r}} - \gamma\right)\dot{v}}{\cos\left(\gamma_{\mathrm{r}} - \gamma\right)v} \tag{6.21}$$

This is the PPN-like guidance law that implements the BIPN guidance rule without requiring speed change. No singularity will occur here since the angle $\gamma_{\mathrm{r}} - \gamma$ remains acute because $\upsilon > 1$. The rate of change of speed, which is required for implementation, may be supplied by the INS in practice.

So, the impact angle control law, which is similar to Eq. (6.12) in logic, can now be written as

$$\dot{\gamma} = \begin{cases} \dfrac{\left(N\dot{\lambda} + b\right)v_{\mathrm{r}} + \sin\left(\gamma_{\mathrm{r}} - \gamma\right)\dot{v}}{\cos\left(\gamma_{\mathrm{r}} - \gamma\right)v} & \text{if } B < B_{\mathrm{d}} \\ \dfrac{Nv_{\mathrm{r}}\dot{\lambda} + \sin\left(\gamma_{\mathrm{r}} - \gamma\right)\dot{v}}{\cos\left(\gamma_{\mathrm{r}} - \gamma\right)v} & \text{otherwise} \end{cases} \tag{6.22}$$

The desired value of the bias integral can be obtained by integrating Eq. (6.19):

$$B_{\mathrm{d}} = \gamma_{\mathrm{r,f}} - \gamma_{\mathrm{r,i}} - N\left(\lambda_{\mathrm{f}} - \lambda_{\mathrm{i}}\right) \tag{6.23}$$

Noting from Figure 6.2 that $\gamma_{\mathrm{r,f}} = \lambda_{\mathrm{f}}$ and utilizing Eq. (6.5), Eq. (6.23) can be written as

$$B_{\mathrm{d}} = N\lambda_{\mathrm{i}} - \gamma_{\mathrm{r,i}} - \left(N-1\right)\left\{\gamma_{\mathrm{f,d}} + \sin^{-1}\left(\frac{\sin\gamma_{\mathrm{f,d}}}{\sqrt{\upsilon_{\mathrm{f}}^2 - 2\upsilon_{\mathrm{f}}\cos\gamma_{\mathrm{f,d}} + 1}}\right)\right\} \tag{6.24}$$

As expected, this equation is not the same as Eq. (6.10). Again, the right hand side of the equation is entirely composed of known parameters. As in Eq. (6.8), a safe value for the bias duration would be

$$\Delta t = \frac{r_{\mathrm{i}}}{v_{\mathrm{r,i}}} \tag{6.25}$$

which may be used in Eq. (6.24) to obtain the following expression for the bias term:

$$b_{\mathrm{i}} = \frac{N\lambda_{\mathrm{i}} - \gamma_{\mathrm{r,i}} - \left(N-1\right)\left\{\gamma_{\mathrm{f,d}} + \sin^{-1}\left(\dfrac{\sin\gamma_{\mathrm{f,d}}}{\sqrt{\upsilon_{\mathrm{f}}^2 - 2\upsilon_{\mathrm{f}}\cos\gamma_{\mathrm{f,d}} + 1}}\right)\right\}}{r_{\mathrm{i}}/v_{\mathrm{r,i}}} \tag{6.26}$$

Here, it is important to indicate that this equation gives the *initial* bias. Unlike the PPN-based implementation presented in the previous section, the relative speed is

bound to change under the action of Eq. (6.21) even if the pursuer speed remains unchanging. As a result, the speed weighting in Eq. (3.16) needs to be performed as

$$b = b_{\mathrm{i}} \frac{v_{\mathrm{r}}}{v_{\mathrm{r,i}}} \tag{6.27}$$

6.4. Examples

The reference engagement geometry is modified such that the target, which is initially 3 km away from the origin, moves away with a constant speed of 50 m/s. Four scenarios with different configurations are considered. The first and third scenarios use the guidance law in Eq. (6.12) whereas the second and fourth scenarios are undergone with the one in Eq. (6.22). Unlike the first two scenarios that run in ideal conditions, the last two scenarios are disturbed by pursuer dynamics, gravity, and drag. The first item is modeled as in Eq. (3.32) with $\tau_{\mathrm{a}} = 0.35$ s. The modeling of the second item is as shown in Eq. (3.35). The last item is modeled via $\dot{v} = -0.00007v^2$ as done in Section 4.3. As before, the guidance command is not updated during the last 30 m when there is disturbance. The last detail is about the construction of the approximate collision triangles: For the last two scenarios, the final speed would be equal to the initial speed as required by the conservation of energy if there was no drag as is the case with the first two scenarios. To account for the effect of drag, the triangles are formed with a final pursuer speed of 200 m/s whereas the actual values happen to be about 190 m/s. This speed difference is another disturbing element for the already disturbed scenarios.

The summary of the results is in Table 6.1. The first column indicates the scenario number whereas the second one indicates the implementation each scenario is based on. The third column shows whether there is disturbance or not. The total engagement durations are shown in the fourth column. The durations are given here because the time axes of the upcoming plots are normalized for the sake of a compact presentation. The remaining columns are the same as those in the previous tables

such as Table 3.3. It is to be noted that the E values of the last two scenarios are strikingly lower than those of the first to scenarios since they receive assistance from gravity and, more importantly, since their average speeds are lower due to gravity and drag.

Table 6.1 Summary of the simulation results against a moving target

Scn.	**Imp.**	**Dist.**	t_f [s]	a_{ext} [m/s^2]	ε_{max} [deg]	E [m^2/s^3]	γ_f [deg]
1	BPPN	Off	21.5	−95.3	64.5	29934	−90.0
2	BIPN	Off	20.5	−82.7	60.5	28916	−90.0
3	BPPN	On	43.9	+31.3	80.6	4901	−89.4
4	BIPN	On	34.2	−28.9	64.7	6826	−88.9

Figure 6.4 presents the spatial trajectories. The trajectory belonging to the target is also shown. As also seen in the fourth column of Table 6.1, it takes longer due to speed loss to reach the target when there is disturbance. It is observed that BPPN trajectories are higher than BIPN trajectories. The accelerations are plotted in Figure 6.5. When the speed is constant, it is seen that BPPN and BIPN perform comparably. The acceleration requirement of the former turns out to be a bit higher. However, the things change when the speed is not constant anymore. BIPN performs noticeably worse as also evidenced by the cost function values in the seventh column of Table 6.1. This is due to the form of the guidance law expressed in Eq. (6.22), where both velocities are varying. In Figure 6.6, the third scenario is seen to have a rather high look angle requirement. This may be attributed to the fact that unlike the BIPN-based implementation, the PPN-based implementation does not have a solution based on the look angle when the target is not stationary. As compared to the first scenario, a worse result is obtained with a varying pursuer speed. Next, Figure 6.7 shows that the desired impact angle can be said to be obtained successfully in each case. This is verified by the numerical figures in Table 6.1. As expected, the performances of the disturbed scenarios are not perfect. Lastly, the bias profiles that enable the vertical impact condition can be seen in Figure 6.8.

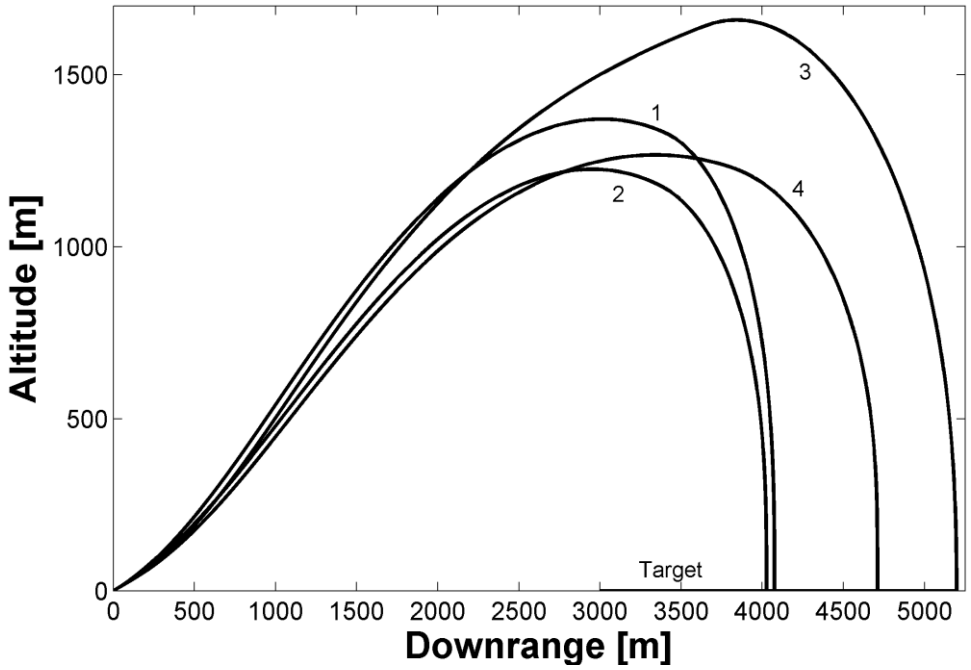

Figure 6.4 Spatial trajectories against a moving target produced by the PPN- and IPN-based guidance schemes (see Table 6.1 for details)

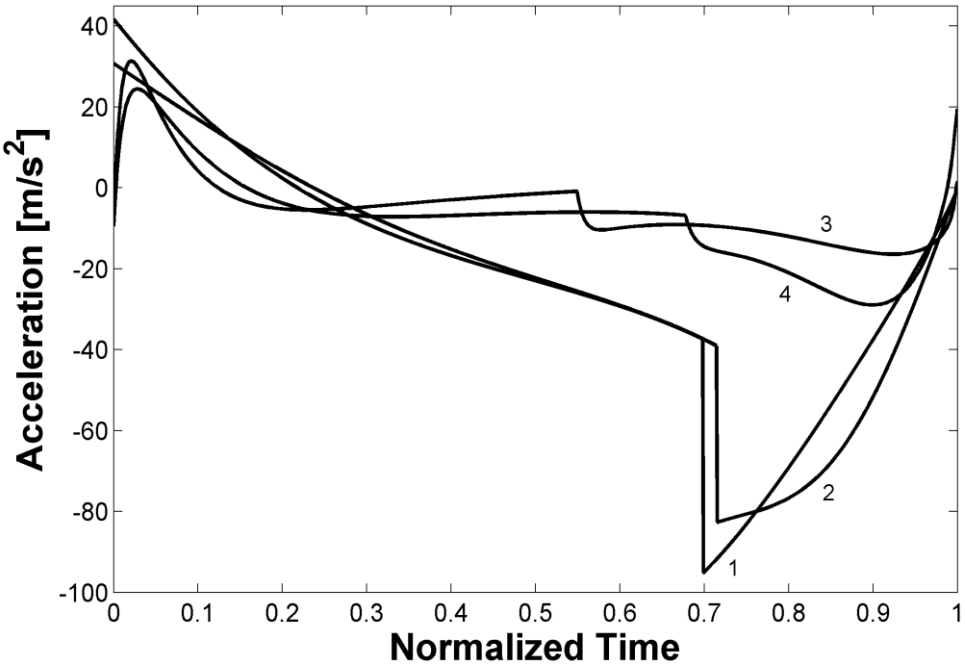

Figure 6.5 Acceleration histories against a moving target produced by the PPN- and IPN-based guidance schemes (see Table 6.1 for details)

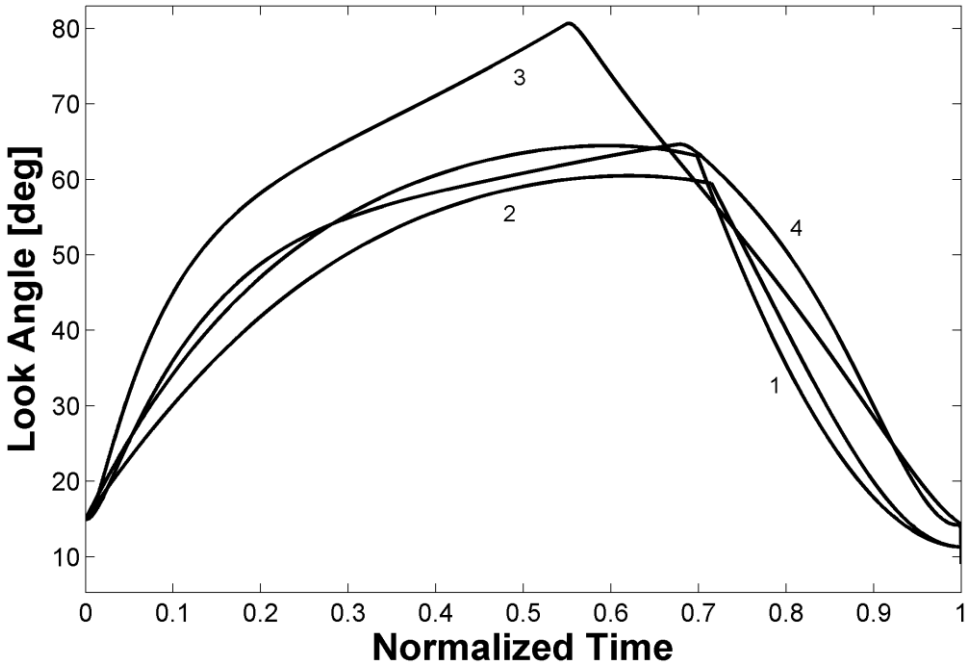

Figure 6.6 Look angle variations against a moving target produced by the PPN- and IPN-based guidance schemes (see Table 6.1 for details)

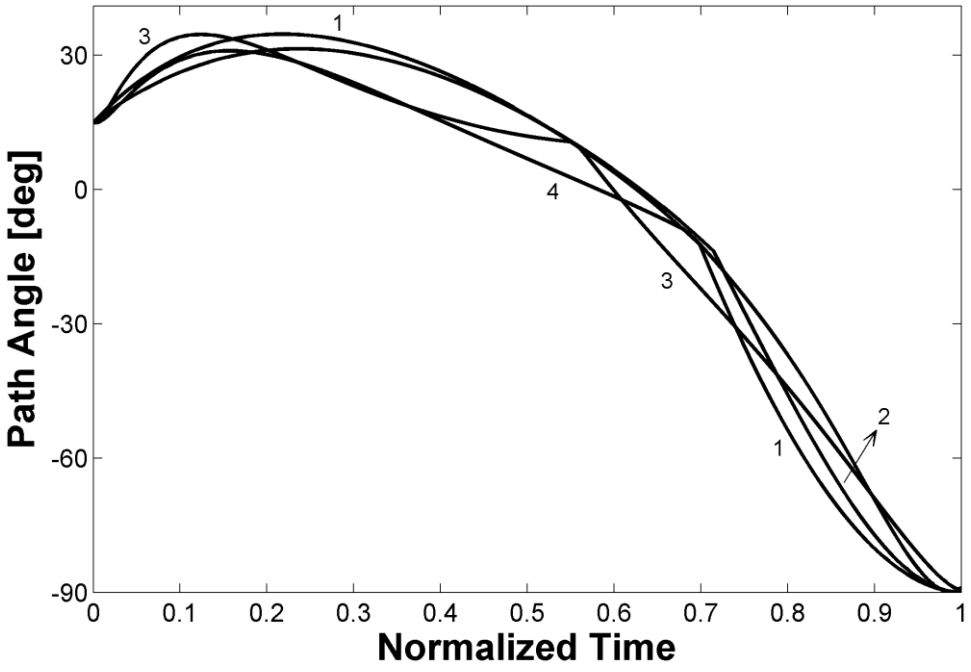

Figure 6.7 Path angle trends against a moving target produced by the PPN- and IPN-based guidance schemes (see Table 6.1 for details)

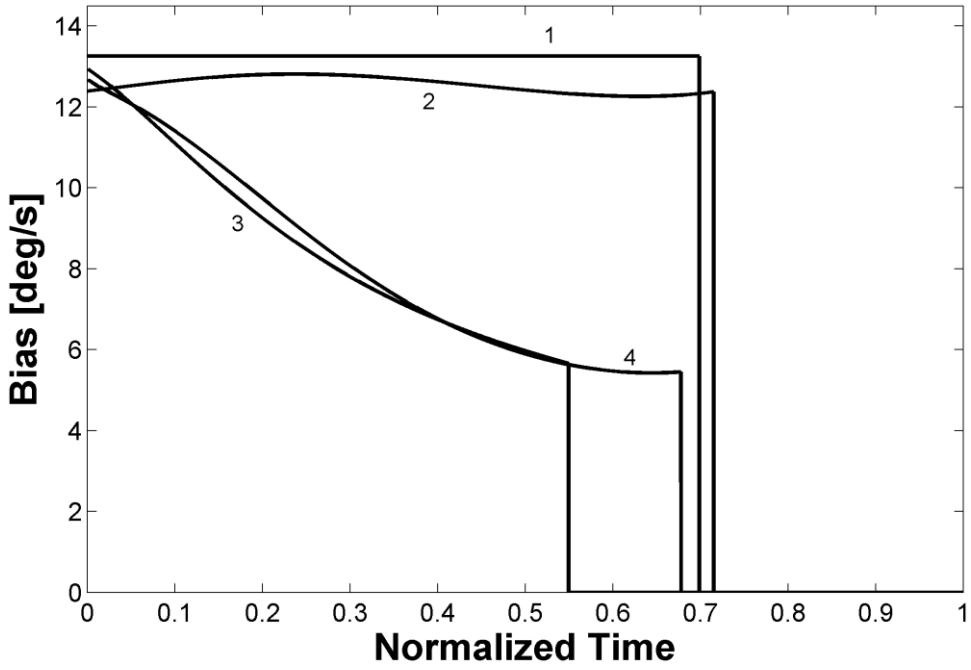

Figure 6.8 Bias profiles against a moving target produced by the PPN- and IPN-based guidance schemes (see Table 6.1 for details)

Figure 6.9 presents the sensitivity of the impact angle to the variation in target speed when there is no other disturbance. It is observed that the two different implementations behave very similarly. There is no error when the speed is 50 m/s, which is the value used by the guidance algorithms. The approximate slope of the lines is 20°, which is less than half of the value in Figure 3.25. This means that the guidance loop becomes less sensitive to the speed variation when the formulation takes the target movement into account.

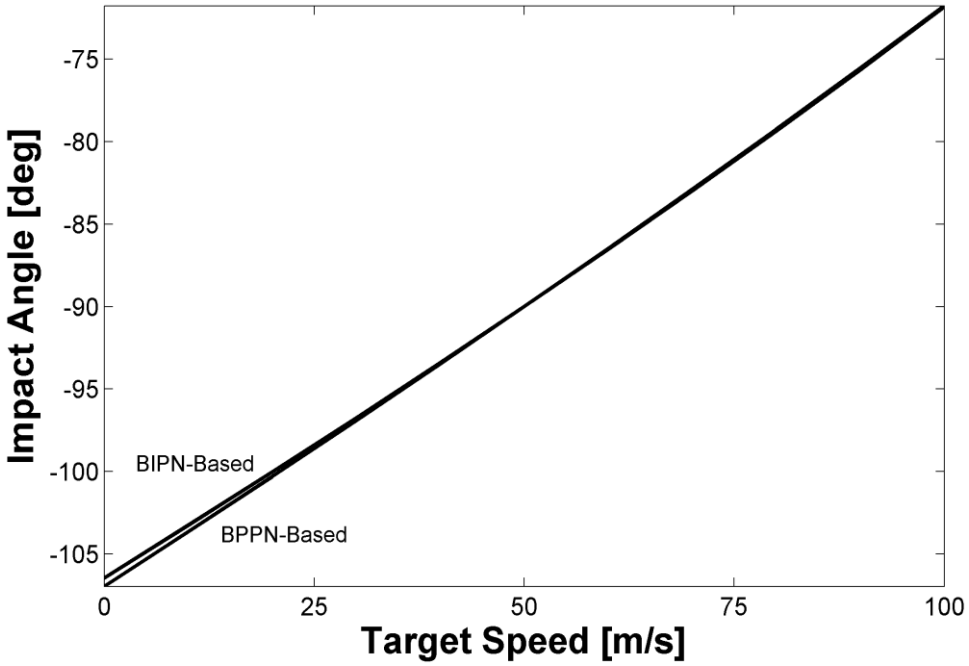

Figure 6.9 Impact angle sensitivities of the PPN- and IPN-based guidance schemes to target speed variation

CHAPTER 7

PLANE PURSUIT FOR EXTENSION TO THREE DIMENSIONS

The BPPN guidance law as investigated in this study has planar implementation logic. It is therefore required to bring the pursuer's velocity vector from an arbitrary initial orientation onto a preferred maneuver plane when the engagement is 3-D. This plane, on which the pursuer is to perform its BPPN action, should be so selected that it involves the final velocity direction from which the designer desires the target to be approached. With such a segmented structure, the philosophy of the suggested method becomes similar to the sliding mode control approach: There is an initial *reaching* phase named plane pursuit, in which the pursuer tries to catch the maneuver plane. Then, it *slides* on this plane, or surface, to eventually capture the target. Once converged, the pursuer will never leave the surface because the PPN guidance law will result in a planar engagement in the 3-D space if the target is stationary or if, initially, the velocity vector of the target is contained in the plane formed by the LOS and the velocity vector of the pursuer (see Appendix E for proofs).

7.1. Midcourse Guidance Against a Stationary Target

Figure 7.1 shows a snapshot during a general 3-D engagement against a stationary target. The unit vector $\vec{u}_{\mathrm{f,d}}$ ending at the target denotes the desired impact vector. There are an infinite number of planes involving this vector and the final maneuver plane must be one of these for the guidance objectives to be met.

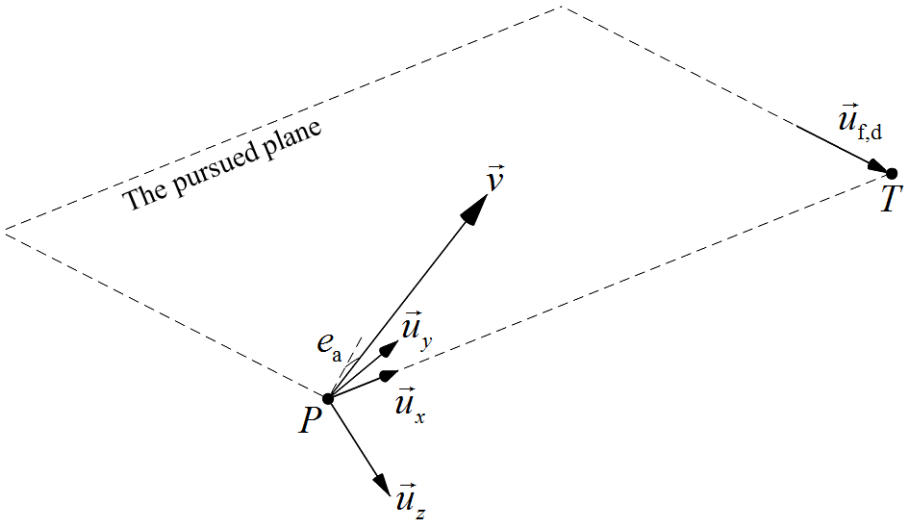

Figure 7.1 A snapshot from the plane-pursuit phase against a stationary target

It is proposed in this study that the plane to be pursued be constructed using the instantaneous LOS and the desired final direction. This greatly simplifies the plane-pursuit phase because if any other plane was selected, there would be a translational error as well in addition to the angular error e_{a} shown in the figure. On top of that, the knowledge of the target position would also be required. The aim during the plane-pursuit phase is to nullify e_{a}, which is defined as the smallest angle between the velocity vector and the pursued plane. It needs to be noted that the pursued plane continuously rotates about $\vec{u}_{\mathrm{f,d}}$ while the reaching is in progress. The plane ceases rotation and becomes the fixed maneuver plane once e_{a} is sufficiently small. One might argue that a disadvantage of the proposed method is that it does not provide the most convenient initial angular conditions for the BPPN phase since they happen to be set indirectly the moment the pursued plane is reached. Whereas it is true that more favorable initial conditions could be imposed by devising alternative strategies, such a potentially tedious path is not taken here as the proposed method is able to provide a satisfactory solution to the problem.

Now, making use of the reference frame attached to the pursued plane with $\vec{u}_x$ pointing along the LOS; $\vec{u}_y$, which is normal to the plane, can be obtained by the operation

$$\vec{u}_y = \vec{u}_{\mathrm{f,d}} \times \vec{u}_x \tag{7.1}$$

Then, the third unit vector $\vec{u}_z$ happens to lie on the plane. The fact that the error has positive correlation with the dot product of two vectors can be represented as

$$e_{\mathrm{a}} \sim \vec{u}_v \bullet \vec{u}_y \tag{7.2}$$

which means that the error increases as the unit vectors approach to each other and vice versa. Hence, the error may be driven to zero by using such an acceleration policy as follows:

$$\vec{a} = f\left(\vec{u}_v \bullet \vec{u}_y\right)\left(\vec{u}_v \times \frac{\vec{u}_v \times \vec{u}_y}{\left|\vec{u}_v \times \vec{u}_y\right|}\right) \tag{7.3}$$

The acceleration vector operates in a direction perpendicular to the velocity vector to reduce the error so that the speed is kept constant. It is seen that the magnitude is a function of the previously mentioned dot product. To see what kind of a function this could be, some help from the linear domain might be useful.

7.1.1. Guidance Controller

It may be appreciated that the velocity pursuit guidance [1] is similar to the plane pursuit methodology proposed against a stationary target. The difference between these two is that the plane-pursuit guidance aims to drive the angular error to zero so that the velocity vector lies on the pursued plane instead of driving the look angle ε, which is defined in Figure 1.1, to zero so that the velocity vector lies on the LOS. In

this respect, the angles e_a and ε become counterparts and it may therefore be expected that a controller able to nullify ε in a linear environment could also nullify e_a in a nonlinear environment.

Figure 7.2 shows the block diagram of the velocity pursuit guidance loop. The aim of the controller is to regulate ε to zero by rejecting the disturbance created by the initial velocity $\dot{y}_i$ acting as a step input. The initial displacement is zero since the LOS is always attached to the pursuer.

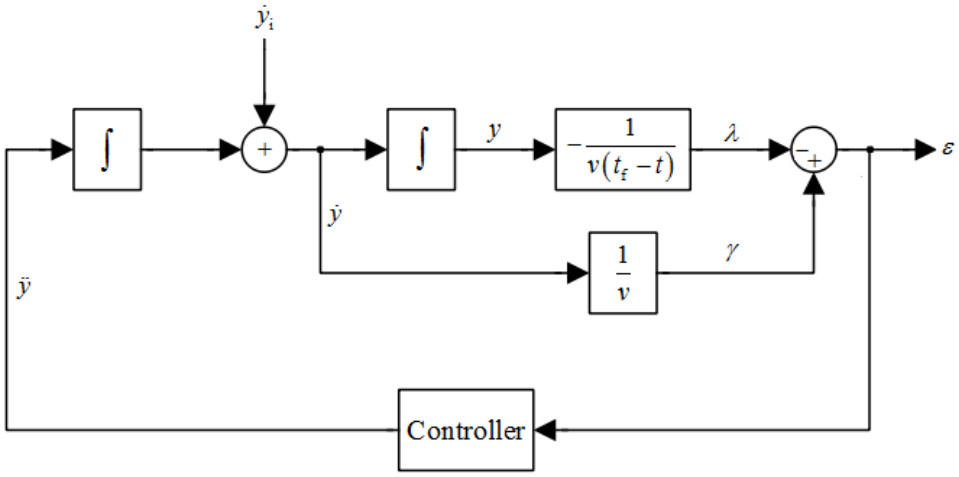

Figure 7.2 Block diagram of the velocity pursuit guidance loop

The linear system shown above is time-variant. It can be converted into a time-invariant form by assuming that $T_{go} = t_f - t$ is constant. The closed-loop transfer function, where the controller is represented by $C(s)$, then happens to be

$$\frac{\mathrm{E}(s)}{\dot{Y}_i(s)} = \frac{T_{go}s^2 + s}{vT_{go}s^2 - T_{go}C(s)s - C(s)} \tag{7.4}$$

which is

$$\frac{\mathrm{E}(s)}{\dot{Y}_{\mathrm{i}}(s)} = \frac{\dfrac{\mathrm{E}(s)}{\dot{Y}(s)}}{1 - \dfrac{\mathrm{E}(s)}{\dot{Y}(s)}\dfrac{C(s)}{s}} \tag{7.5}$$

where

$$\frac{\mathrm{E}(s)}{\dot{Y}(s)} = \frac{T_{\mathrm{go}}s + 1}{vT_{\mathrm{go}}s} \tag{7.6}$$

So, the characteristic equation of (7.5) becomes

$$-\frac{T_{\mathrm{go}}s + 1}{vT_{\mathrm{go}}s^2}C(s) = -1 \tag{7.7}$$

With proportional control, i.e. $C(s) = -k$, a generic root locus plot corresponding to Eq. (7.7) is shown in Figure 7.3. It can be shown for low gain values that the locus is circular with a radius of $1/T_{\mathrm{go}}$. This means that if an underdamped response is desired for large values of the time to go, the designer is stuck with a low-bandwidth system. The system can be sped up with high gain; however, the response would be a somewhat sluggish one due to its first-order nature. The remedy might be to use a controller with the following structure:

$$C(s) = -k\frac{s + a}{s + b} \tag{7.8}$$

If the condition $a > b$, i.e. lag compensation, is met, the pole of the controller could be used to suppress the dynamics of the open-loop zero and its zero would be useful in enhancing the dynamic capacity of the guidance loop. In fact, Figure 7.3 will still be applicable with Eq. (7.8) if the controller pole is utilized to cancel out the open-loop zero, yielding a circle with a radius of *a*.

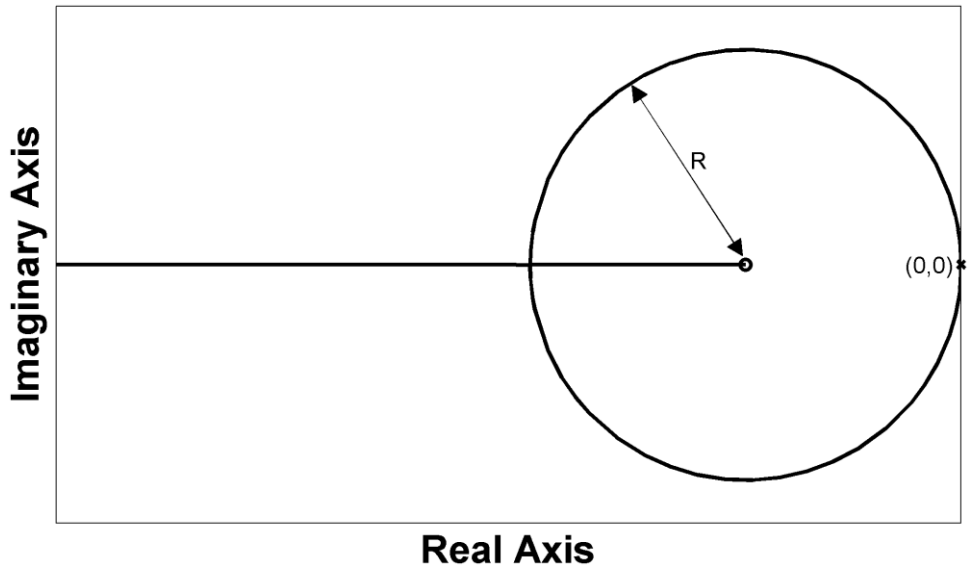

Figure 7.3 Root locus of the transfer function corresponding to velocity pursuit with proportional controller

7.1.2. Design Example

A pursuer with $v = 250$ m/s is considered. The range interval of interest is between 5000 m and 3000 m. Lower range values are not considered since the plane-pursuit guidance is a midcourse method; it should have already ended when the pursuer gets nearer to the target so that enough time would be left for terminal maneuvers. The root locus of the system corresponding to a range of 4000 m with the additions of a controller pole to −0.1 and a controller zero to −0.5 is presented in Figure 7.4. As seen, the open-loop zero is nicely suppressed by the closed-loop pole and the complex conjugate poles can be selected to have a satisfactory transient performance.

The dominant closed-loop poles can be made to have a damping ratio of, for example, 0.707 with the following controller:

$$C(s) = -229\frac{s+0.5}{s+0.1} \tag{7.9}$$

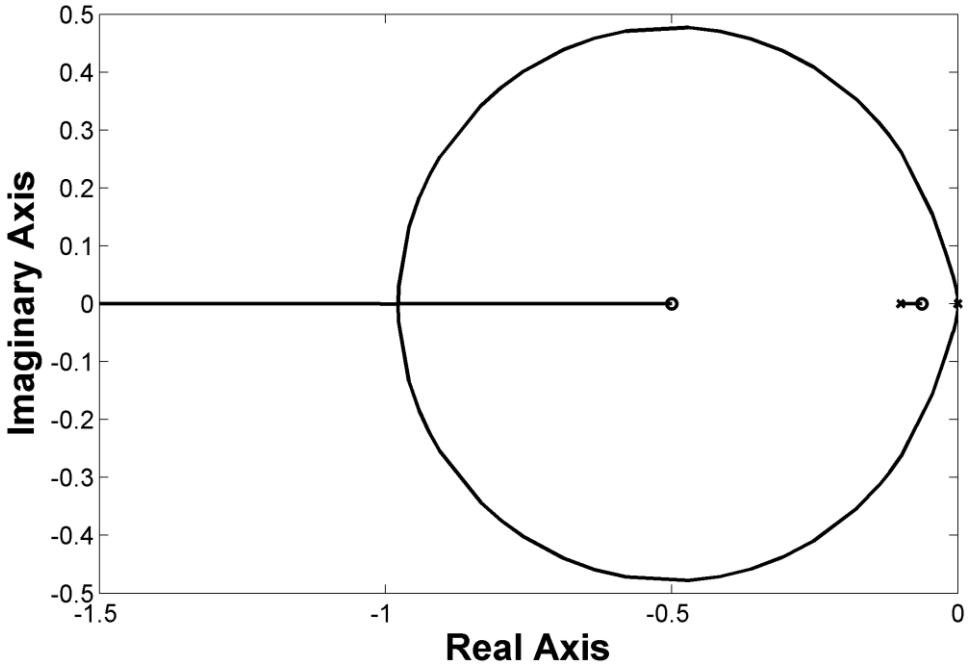

Figure 7.4 Root locus of the velocity-pursuit system with lag controller

With this selection, the closed-loop systems from Eq. (7.4) become

$$\left.\frac{\mathrm{E}(s)}{\dot{Y}_{\mathrm{i}}(s)}\right|_{r=5000\ \mathrm{m}} = \frac{(s+0.05)(s+0.1)s}{250(s+0.0503)(s^2+0.9657s+0.4552)} \tag{7.10}$$

$$\left.\frac{\mathrm{E}(s)}{\dot{Y}_{\mathrm{i}}(s)}\right|_{r=4000\ \mathrm{m}} = \frac{(s+0.0625)(s+0.1)s}{250(s+0.0629)(s^2+0.9531s+0.4553)} \tag{7.11}$$

$$\left.\frac{\mathrm{E}(s)}{\dot{Y}_{\mathrm{i}}(s)}\right|_{r=3000\ \mathrm{m}} = \frac{(s+0.0833)(s+0.1)s}{250(s+0.0836)(s^2+0.9324s+0.4564)} \tag{7.12}$$

So, it can be concluded that the same controller can be employed to obtain nearly the same response over a wide range interval. It is interesting here to note that the transient response will be under the influence of the controller pole acting as a closed-loop zero located at −0.1. The Bode diagrams of Eq. (7.11) are shown in Figure 7.5. The magnitude plot demonstrates that the closed-loop system behaves

well as a disturbance rejecter in the entire frequency domain, including the zero frequency at which the initial heading error operates.

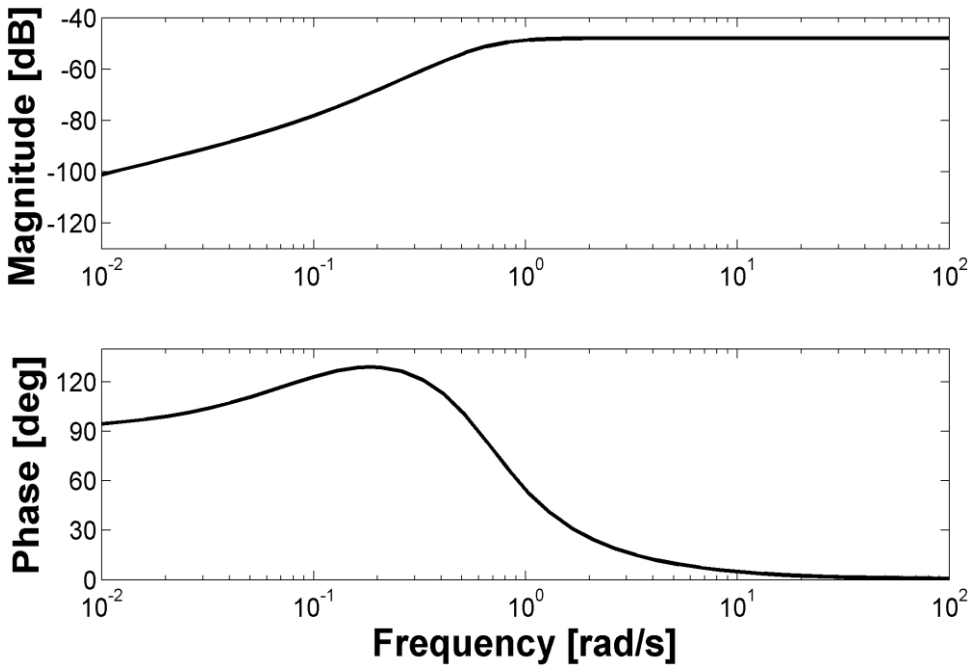

Figure 7.5 Bode diagrams of the closed-loop velocity-pursuit system

The following initial conditions are used for the example nonlinear engagement scenario: The constant-speed pursuer starts from the origin with an azimuth angle of 60° and an elevation angle of 25°. The target is located 5 km away along the *x*-axis. The azimuth and elevation vectors of the terminal velocity vector are respectively desired to be 45° and −60°. The midcourse phase of the engagement is simulated for a time interval of 12 s. The coordinate variations for unsaturated and saturated (with a maximum lateral acceleration of 100 m/s^2) pursuits are plotted in Figure 7.6 whereas the acceleration histories can be found in Figure 7.7. Figure 7.8 demonstrates how the error is nullified. The harmony between the linear system of Eq. (7.11) and the nonlinear one is encouraging. It is also seen that the price paid due to the saturated acceleration is merely a slower response, which can quite easily be tolerated since the target is still far away.

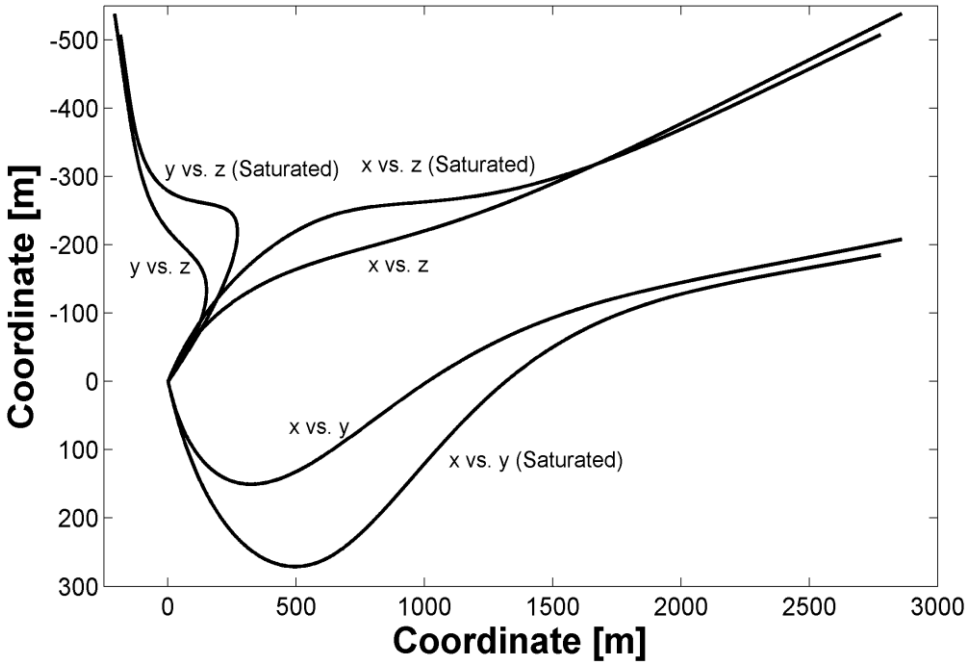

Figure 7.6 Coordinate variations produced by the plane-pursuit guidance against a stationary target

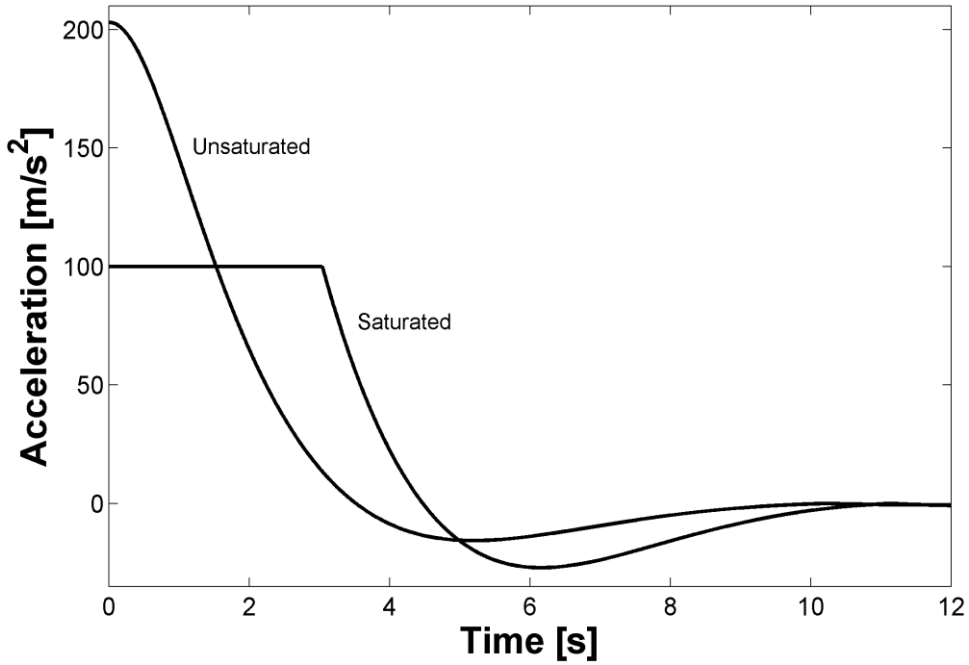

Figure 7.7 Acceleration histories produced by the plane-pursuit guidance against a stationary target

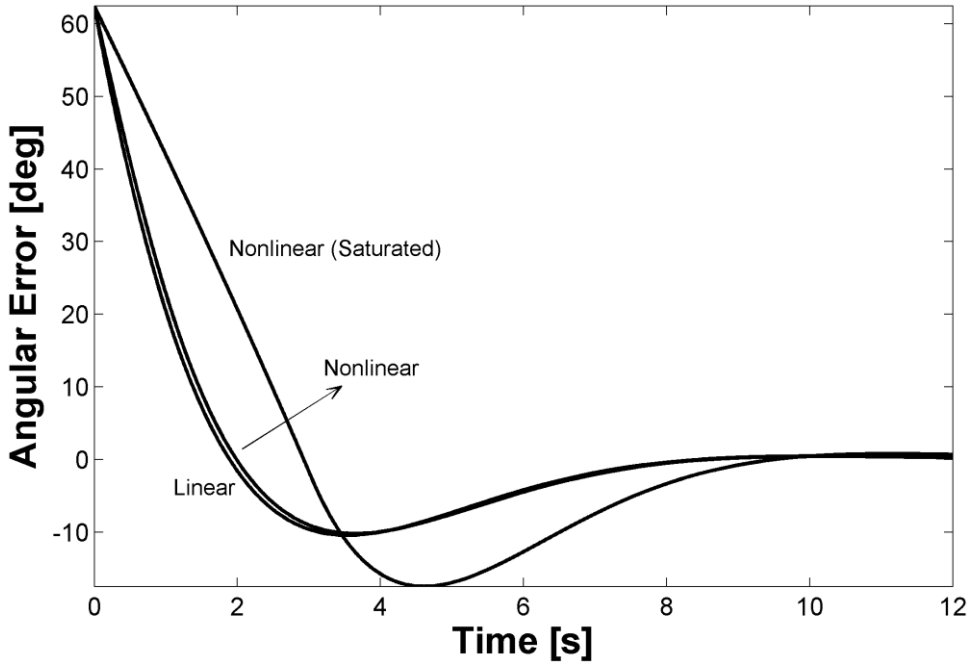

Figure 7.8 Rejection of the heading error as produced by the plane-pursuit guidance against a stationary target

7.1.3. Control of Impact Direction

Referring to Figure 7.1; if the velocity vector lies on the pursued plane, i.e. $e_{\mathrm{a}} = 0$, the path angle on this plane can be calculated as

$$\gamma = \operatorname{atan}_2\left[\underbrace{\left(\vec{u}_x \times \vec{u}_v\right)\bullet\vec{u}_y}_{\sin\gamma}, \underbrace{\vec{u}_x \bullet \vec{u}_v}_{\cos\gamma}\right] \tag{7.13}$$

Similarly, the desired impact angle is

$$\gamma_{\mathrm{f,d}} = \operatorname{atan}_2\left[\underbrace{\left(\vec{u}_x \times \vec{u}_{\mathrm{f,d}}\right)\bullet\vec{u}_y}_{\sin\gamma_{\mathrm{f,d}}}, \underbrace{\vec{u}_x \bullet \vec{u}_{\mathrm{f,d}}}_{\cos\gamma_{\mathrm{f,d}}}\right] \tag{7.14}$$

and the LOS angle is

$$\lambda = \text{atan}_2\left[\underbrace{\left(\vec{u}_x \times \vec{u}_r\right)\bullet\vec{u}_y}_{\sin\lambda}, \underbrace{\vec{u}_x \bullet \vec{u}_r}_{\cos\lambda}\right] \tag{7.15}$$

where $\vec{u}_r$ is the unit vector that inherits the duty of staying parallel to the LOS from $\vec{u}_x$, which remains constant during the second phase along with $\vec{u}_y$ and $\vec{u}_z$.

The BPPN guidance law to be used for the demonstration purpose is the one presented in Eq. (3.15). Noting that the LOS angle at the beginning of the biased guidance phase is always zero, the bias term given in Eq. (3.14) may be modified as

$$b = -\frac{\gamma_\text{i} + \left(N_\text{M} - 1\right)\gamma_\text{f,d}}{r_\text{i}/v_\text{i}} \tag{7.16}$$

The initial range value may be obtained by running the range observer introduced in Chapter 5 throughout the plane-pursuit phase in its 3-D mode by using Eq. (5.6) and Eq. (5.7) as the system and measurement models, respectively.

In 2-D domain, the BPPN guidance law in Eq. (2.10) may be claimed to be meaningful in such a way that it manages to convey the necessary sense of direction associated with the acceleration; the acceleration vector will point *up* if the path angle rate is positive and *down* if it is negative. In the 3-D domain, however, the need for a more direct manner of specifying the acceleration vector may be appreciated. Therefore, based on the vector form of PPN [1], Eq. (2.10) can be expressed as

$$\vec{a} = N\vec{\omega}\times\vec{v} + bv\left(\vec{u}_y \times \vec{u}_v\right) \tag{7.17}$$

where $\vec{\omega}$ is the angular velocity vector of the LOS. The cross product determines the bias direction. In what follows, Eq. (3.15) will be implemented this way.

Now, 3-D impact angle control will be demonstrated with an example. The pursuer starts from the origin with a constant speed of 250 m/s to capture the stationary target located 5 km away along the *x*-axis. The initial azimuth and elevation angles of the pursuer are 40° and 25°, respectively whereas the desired azimuth and elevation angles at the instant of impact are 50° and −60°, respectively. The plane-pursuit phase controller is the one given in Eq. (7.9), but with its gain divided by five. The need for such a modification may be understood if the transient response in Figure 7.8 is examined. As seen there, the error is fully rejected around $t = 10\ \mathrm{s}$; yet, its value becomes momentarily zero around $t = 2\ \mathrm{s}$. There is no reason for the pursuer to wait for the steady state to switch to BPPN; it can do so as soon as the angular error becomes zero. However, it would be overkill in terms of acceleration effort to switch too early. Accordingly, the plane-pursuit performance is intentionally hindered by lowering the controller gain. As for the guidance gains to be used in Eq. (3.15), they are selected as $N_{\mathrm{M}} = 3$ and $N_{\mathrm{T}} = 2$.

Figure 7.9 and Figure 7.10 show the spatial trajectories of the pursuer, where the end of the plane-pursuit phase is indicated. The history of the acceleration magnitude is presented in Figure 7.11. The three different phases of the engagement are clearly seen. It can be shown that the most expensive phase according to Eq. (2.38) is the PPN phase whereas the least expensive on is the BPPN phase. Lastly, Figure 7.12 verify that the desired impact angles are obtained as intended.

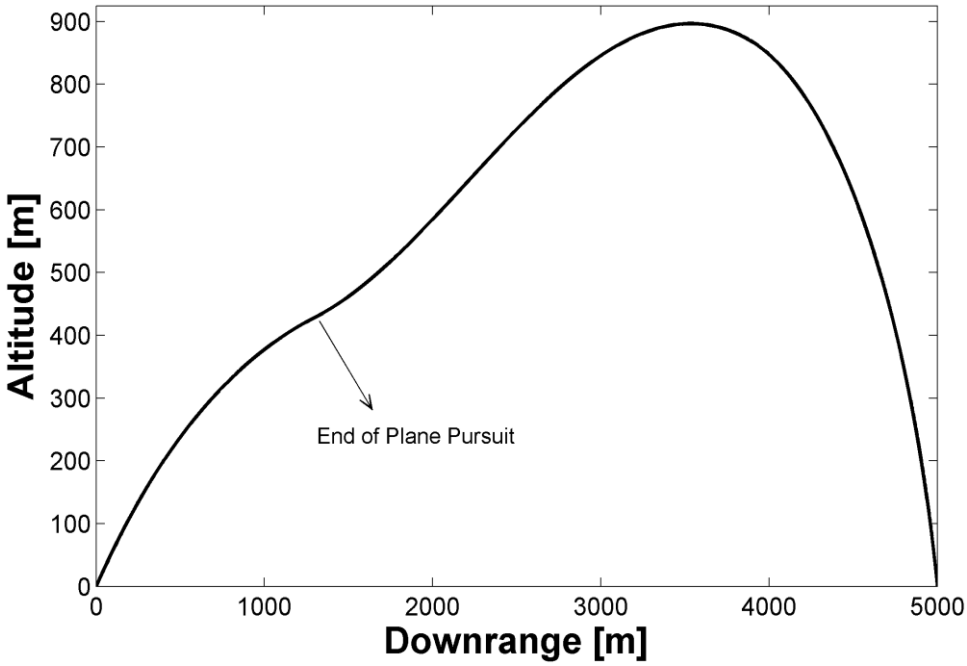

Figure 7.9 Side view of the 3-D trajectory produced by the plane-pursuit guidance followed by the discontinuous bias application strategy

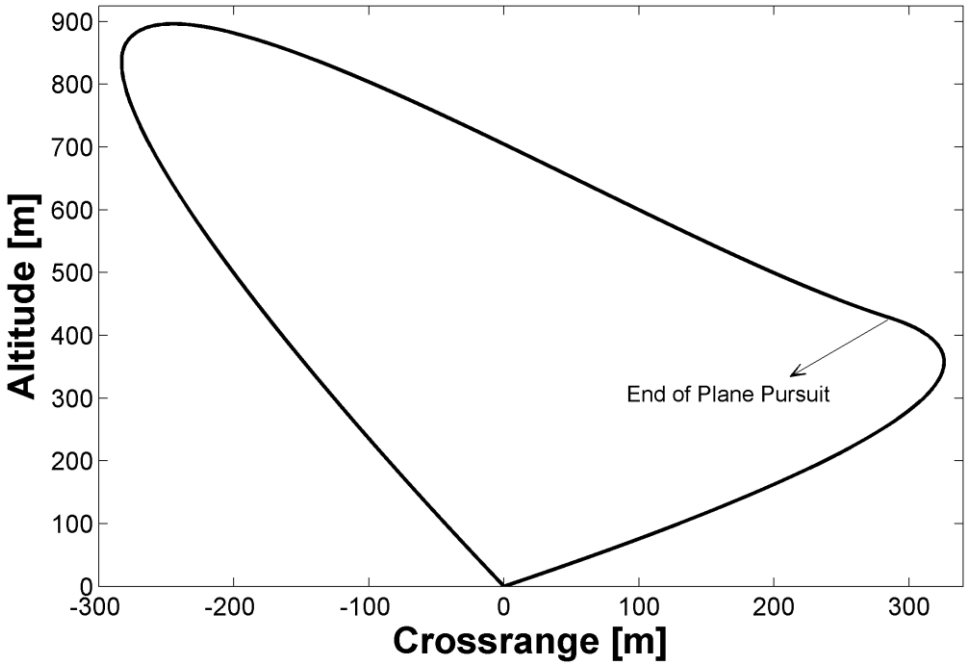

Figure 7.10 Rear view of the 3-D trajectory produced by the plane-pursuit guidance followed by the discontinuous bias application strategy

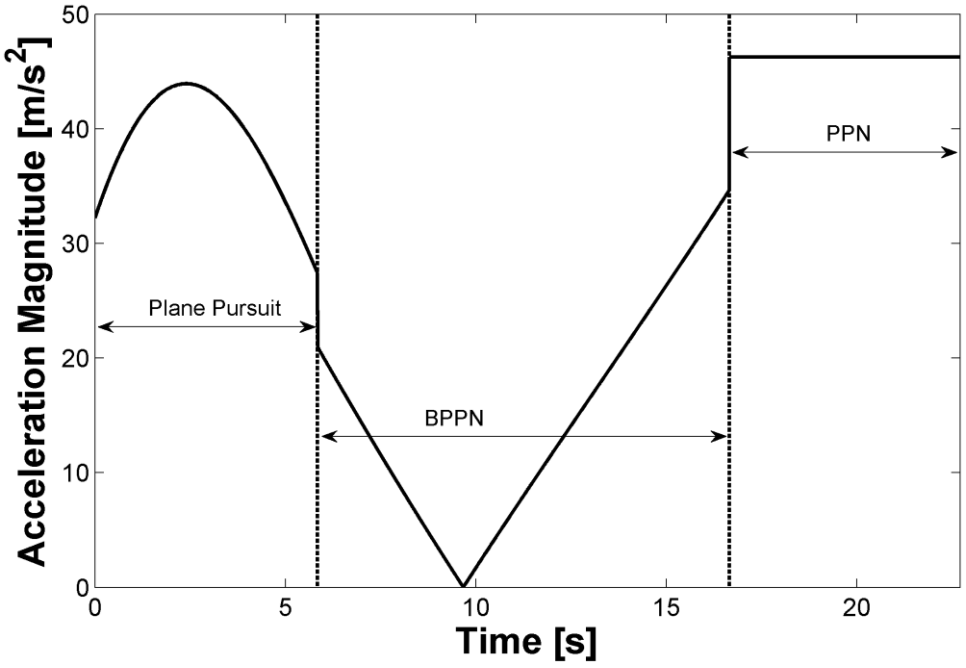

Figure 7.11 Acceleration magnitude history produced by the plane-pursuit guidance followed by the discontinuous bias application strategy

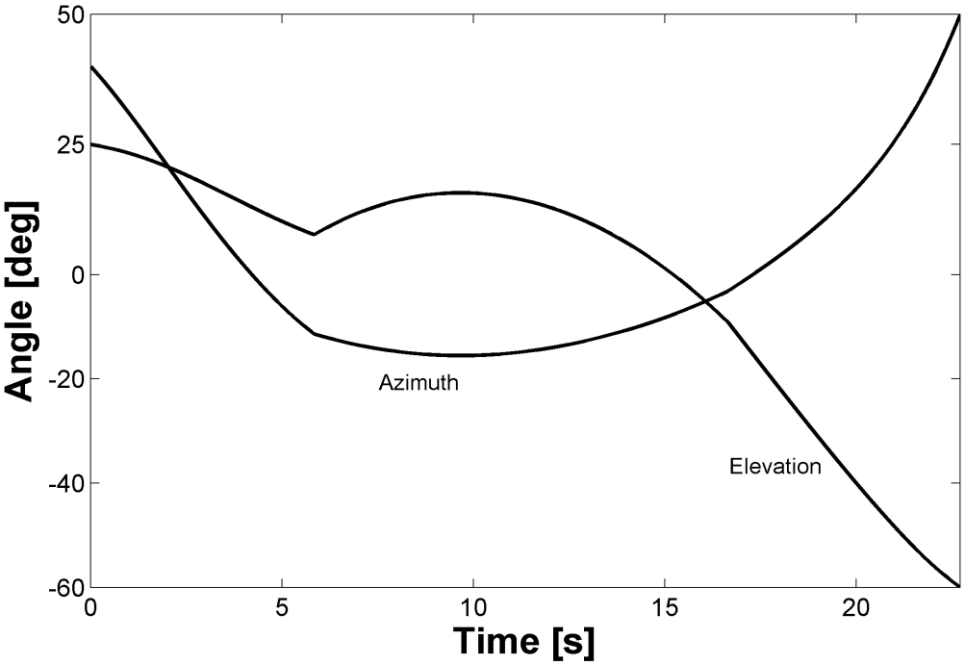

Figure 7.12 Azimuth and elevation angle trends produced by the plane-pursuit guidance followed by the discontinuous bias application strategy

7.2. Midcourse Guidance Against a Moving Target

Figure 7.13 shows a snapshot during a general 3-D engagement against a moving target. The unit vector $\vec{u}_{\mathrm{f}}$ ending at the target denotes the desired final velocity direction and $\vec{v}_T$ is the velocity vector of the target. The maneuver plane must simply be the one defined by these vectors; there is no other choice since $\vec{u}_{\mathrm{f,d}}$, $\vec{v}_T$ and $\vec{v}$ must be coplanar for the BPPN guidance as presented in this dissertation can work. The aim during the plane-pursuit phase is to nullify the translational error e_{t} shown in the figure, which is defined as the smallest distance between the pursuer position and the pursued plane. There is no need to concentrate on the angular error e_{a} since it will automatically be nullified once the plane is reached. This has to be so because of the physics of the problem. It should be noted that the pursued plane remains inertially fixed unless the target maneuvers.

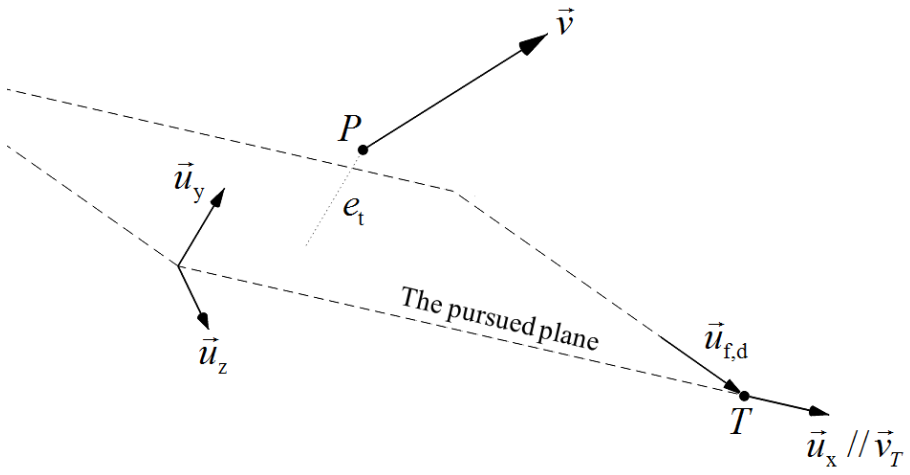

Figure 7.13 A snapshot from the plane-pursuit phase against a moving target

Making use of the reference frame attached to the pursued plane with $\vec{u}_x$ parallel to $\vec{v}_T$; $\vec{u}_y$, which is normal to the plane, can be obtained by the operation

$$\vec{u}_y = \vec{u}_{\mathrm{f,d}} \times \vec{u}_x \tag{7.18}$$

There is a right triangle in Figure 7.13 formed by points *P*, *T* and the point on the pursued plane that is the closest to point *P*. This information can be used to calculate the translational error as

$$e_t = (\vec{p} - \vec{p}_T) \bullet \vec{u}_y \tag{7.19}$$

where $\vec{p}$ and $\vec{p}_T$ are the position vectors of the pursuer and the target, respectively. To be able to calculate this error, at least one point on the target trajectory such as the initial target position needs to be available to the pursuer. Intuitively, the translational error may be driven to zero by using the following acceleration policy:

$$\vec{a} = -f(e_t)\vec{u}_y \tag{7.20}$$

However, such a policy requires change in the magnitude of the velocity vector. Therefore, Eq. (7.20) is slightly changed into

$$\vec{a} = -f(e_t)\frac{\vec{u}_y - (\vec{u}_y \bullet \vec{u}_v)\vec{u}_v}{\left|\vec{u}_y - (\vec{u}_y \bullet \vec{u}_v)\vec{u}_v\right|} \tag{7.21}$$

so that the acceleration vector remains perpendicular to the velocity vector. As practiced in the previous subsection, some help from the linear domain might be useful to see what kind of function could be used to produce the acceleration magnitude.

7.2.1. Guidance Controller

It may be appreciated that the plane-pursuit methodology proposed against a moving target is similar to the altitude-hold control loop [51]. The difference lies in the fact that the plane-pursuit guidance aims to drive the translational error to zero so that the velocity vector lies on the pursued plane instead of maintaining the path angle zero at

the desired altitude. In this respect, it may therefore be expected that a controller able to hold the altitude in a linear environment could also nullify e_t in a nonlinear environment.

Figure 7.14 shows the block diagram of the altitude-hold control loop. The aim of the controller is to drive the error to zero under the action of initial velocity as a disturbance. The initial displacement may or may not be zero; the control loop is not affected by this quantity in terms of disturbance rejection.

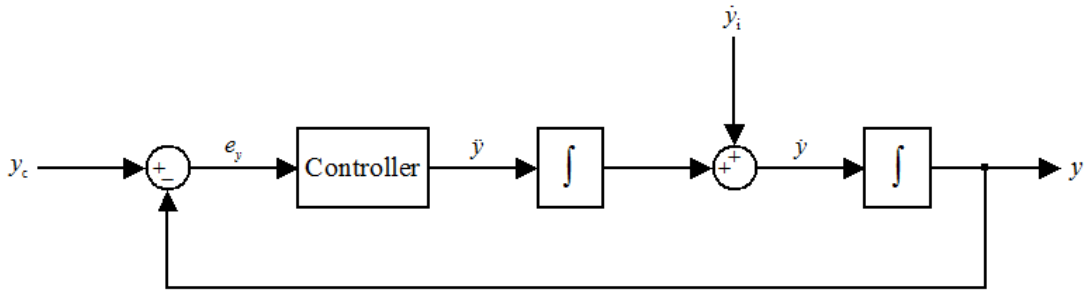

Figure 7.14 Block diagram of altitude-hold control loop

The transfer function of the open-loop system, which is independent of the time to go, can readily be written as

$$\frac{Y(s)}{E_y(s)} = \frac{C(s)}{s^2} \tag{7.22}$$

whereas the closed-loop command-following system is

$$\frac{Y(s)}{Y_c(s)} = \frac{C(s)}{s^2 + C(s)} \tag{7.23}$$

and the closed-loop disturbance-rejection system is

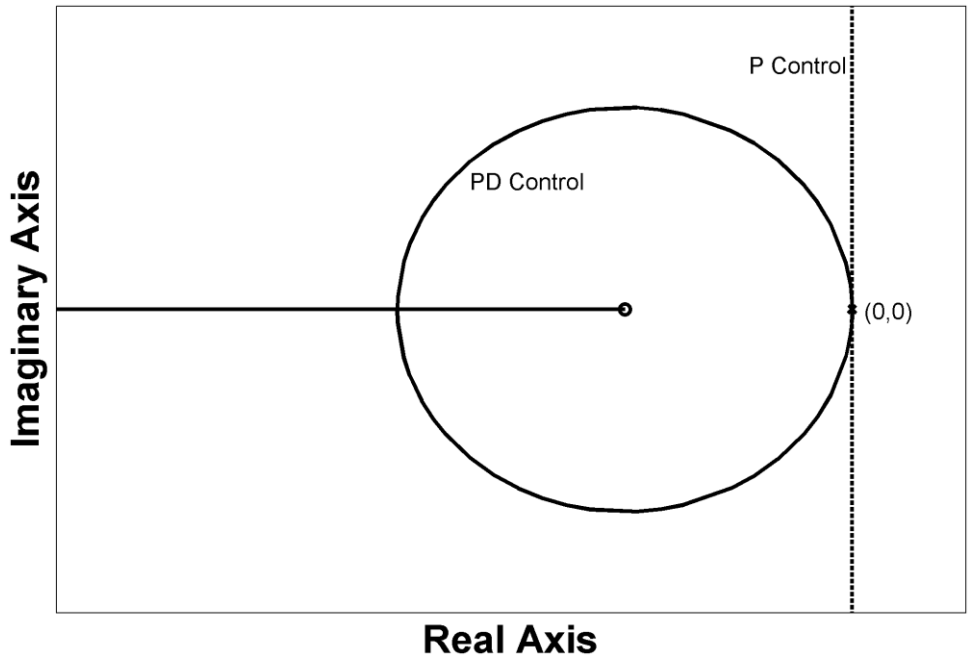

Figure 7.15 Root locus of the transfer function corresponding to altitude hold with two different controllers

$$\frac{Y(s)}{\dot{Y}_{\mathrm{i}}(s)} = \frac{s}{s^2 + C(s)} \tag{7.24}$$

The root locus of Eq. (7.22) with proportional control, i.e. $C(s) = k$, is shown in Figure 7.15 in dashed lines. It is obvious that the closed-loop system is on the verge of instability; therefore, another control strategy must be devised. It is easy to see that the system may be forced to yield a proper response with the addition of a controller zero, corresponding to proportional-derivative type of control. The root locus with $C(s) = s + a$ is also presented in the same figure, the radius of the circle being equal to *a*. Since a proportional-derivative controller is not physically realizable, it can be implemented as follows:

$$C(s) = k\frac{s + a}{s + b} \tag{7.25}$$

which is in the same form as Eq. (7.8) except that $b \gg a$, implying lead compensation. With such a controller, the command-following transfer function from Eq. (7.23) becomes

$$\frac{Y(s)}{Y_c(s)} = \frac{ks + ka}{s^3 + bs^2 + ks + ka} \tag{7.26}$$

which can follow step- and ramp-type inputs with no steady-state error. It might be tempting to have $a = 0$ so that the displacement commands are tracked as if the system was a second-order filter. However with Eq. (7.25) as the controller, Eq. (7.24) becomes

$$\frac{Y(s)}{\dot{Y}_i(s)} = \frac{(s+b)s}{s^3 + bs^2 + ks + ka} \tag{7.27}$$

It is seen that the *s* term in the nominator is allowed to stay as long as $a \neq 0$. If $a = 0$, the disturbance created by the initial velocity cannot be completely rejected in the steady state. So, *a* should be kept nonzero.

7.2.2. Design Example

Unlike the previous case of velocity pursuit, the altitude-hold control system does not vary with time. As a result, a controller to yield the desired response characteristics may be designed without knowing the engagement details. Placing the controller zero to −0.5 as in Eq. (7.9), a reasonable midcourse guidance response may be achieved. Selecting the location of the controller pole ten times as far as the zero location, the root locus plot seen in Figure 7.16 is obtained. A dominant couple of complex conjugate poles with a damping ratio of, for example, 0.707 can be obtained using the following controller:

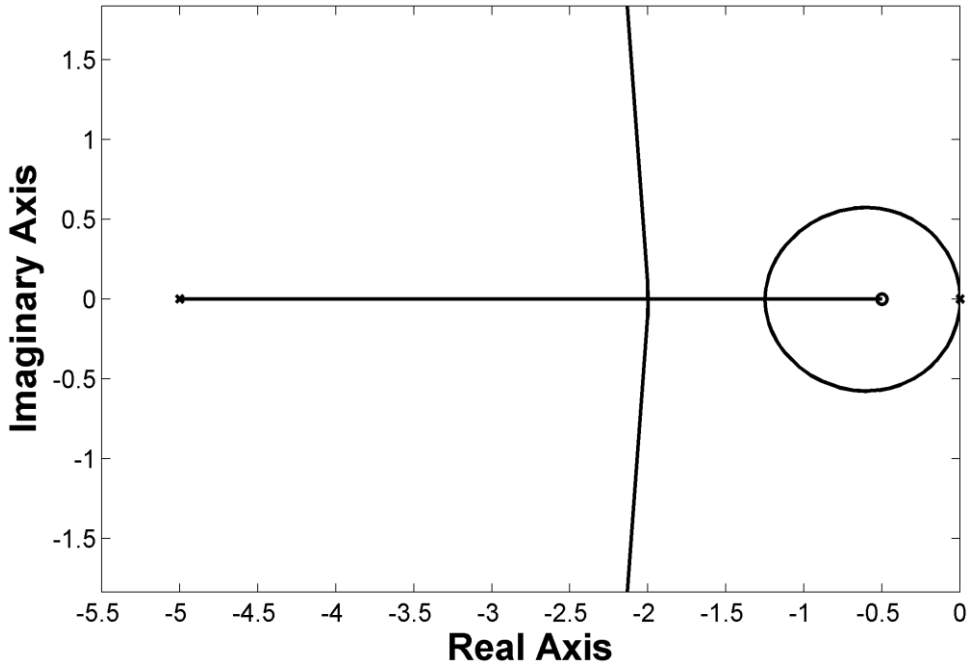

Figure 7.16 Root locus of the altitude-hold system with the lead controller

$$C(s) = 5.1\frac{s+0.5}{s+5} \tag{7.28}$$

The command-following system from Eq. (7.26) then happens to be

$$\frac{Y(s)}{Y_{\mathrm{c}}(s)} = \frac{5.1(s+0.5)}{(s+0.384)\left(s^2+1.154s+0.6629\right)} \tag{7.29}$$

The Bode diagrams of the system above are presented in Figure 7.17. The closed-loop bandwidth is 1.73 rad/s.

On the other hand, the disturbance-rejection system from Eq. (7.27) appears as

$$\frac{Y(s)}{\dot{Y}_{\mathrm{i}}(s)} = \frac{(s+5)s}{(s+0.384)\left(s^2+1.154s+0.6629\right)} \tag{7.30}$$

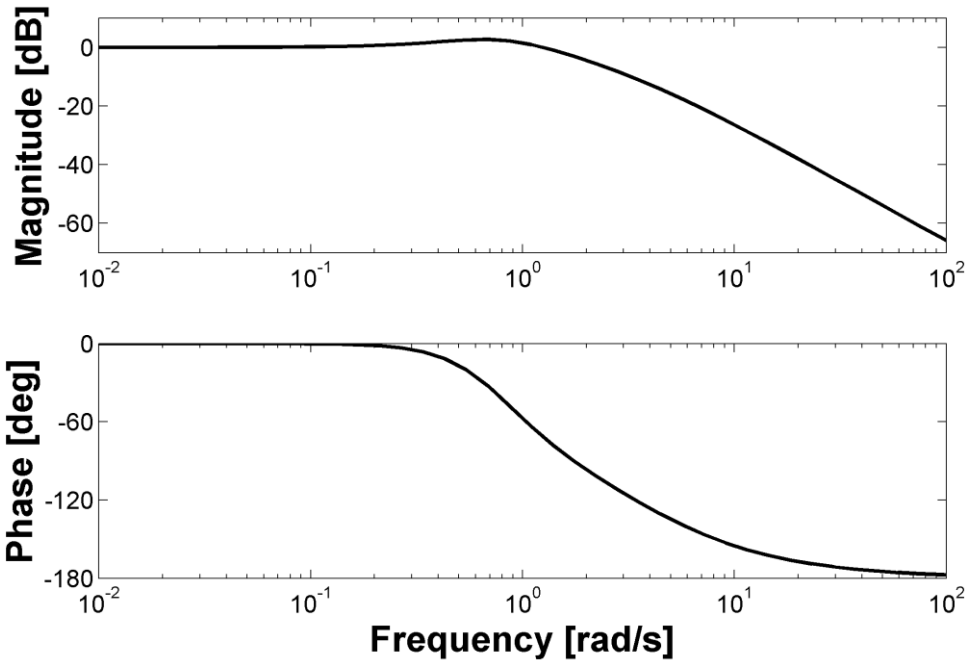

Figure 7.17 Bode diagrams displaying the command-following characteristics of the closed-loop altitude-hold system

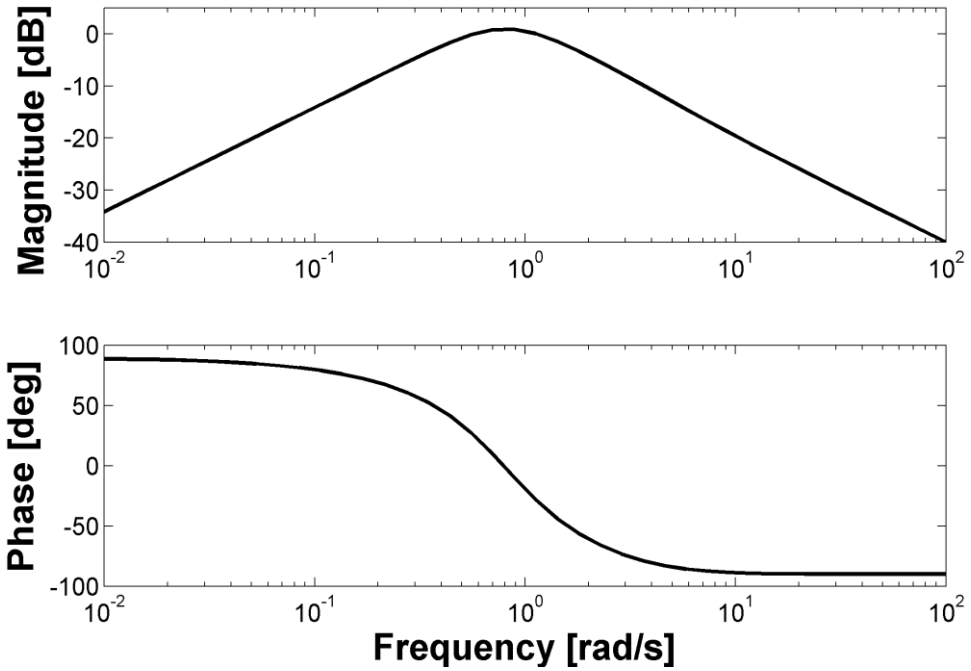

Figure 7.18 Bode diagrams displaying the disturbance-rejection characteristics of the closed-loop altitude-hold system

The Bode diagrams of Eq. (7.30) are shown in Figure 7.18. The magnitude plot reveals that the rejection fails in the neighborhood of 1 rad/s. Nonetheless, as the frequency approaches to zero, which is the value at which the initial heading error operates, the system exhibits the desired attenuation characteristic.

As for the nonlinear engagement example, the conditions are almost the same as before: The pursuer starting from the origin with a constant speed of 250 m/s tries to reach a planar engagement condition against a nonaccelerating target moving along the *x*-axis with a speed of 50 m/s. The initial azimuth and elevation angles of the pursuer are 60° and 25°, respectively. The initial range is 5 km. The terminal velocity vector of the pursuer is desired to have an azimuth angle of 45° and an elevation angle of −60°. The midcourse phase of the engagement is simulated for a time interval of 12 s. For unsaturated and saturated (with a saturation level of 100 m/s^2) cases, the coordinate variations are plotted in Figure 7.19. It is seen that both pursuers eventually converge to the same plane, as expected. The corresponding acceleration histories are presented in Figure 7.20. Figure 7.21 demonstrates how the angular errors are nullified. Lastly, Figure 7.22 presents how the translational errors are regulated. Besides the unsaturated and saturated responses, there is a third curve presented for comparison purposes. It is not unexpected to see that Eq. (7.20) performs better than Eq. (7.21). The interesting detail here is the fact that the nonlinear response produced by Eq. (7.20) and the linear response from Eq. (7.30) are virtually indistinguishable. This phenomenon can be appreciated by realizing that the translational error dynamics within the nonlinear simulation environment is not nonlinear provided that the applied acceleration is maintained parallel to the normal vector of the pursued plane, which is fixed in inertial coordinates. Finally, a comparison of Figure 7.6 – Figure 7.8 and Figure 7.19 – Figure 7.21 reveals that the controllers represented by Eq. (7.9) and Eq. (7.28) perform in harmony.

The chapter is concluded at this point. Unlike the practice in the previous section, a complete example of impact direction control is not presented for moving targets since doing so would be little more than a rehash of what has been presented for stationary targets.

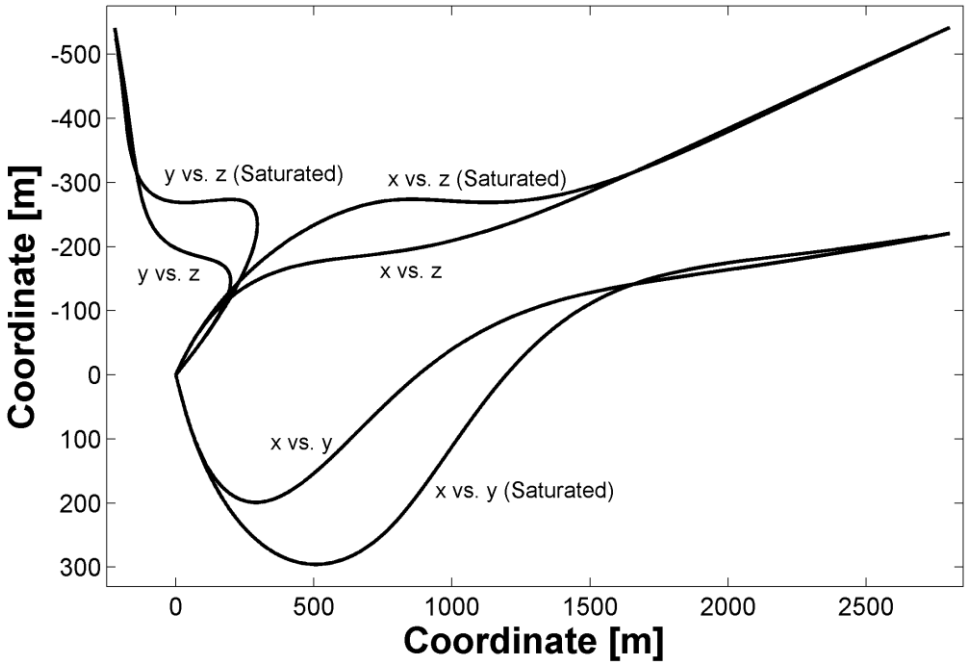

Figure 7.19 Coordinate variations produced by the plane-pursuit guidance against a moving target

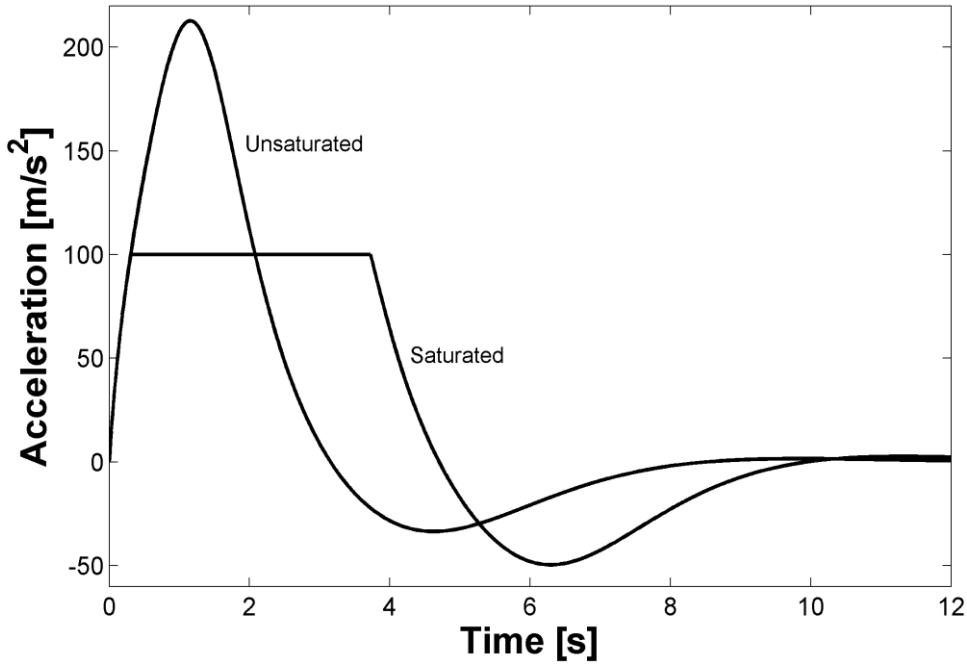

Figure 7.20 Acceleration histories produced by the plane-pursuit guidance against a moving target

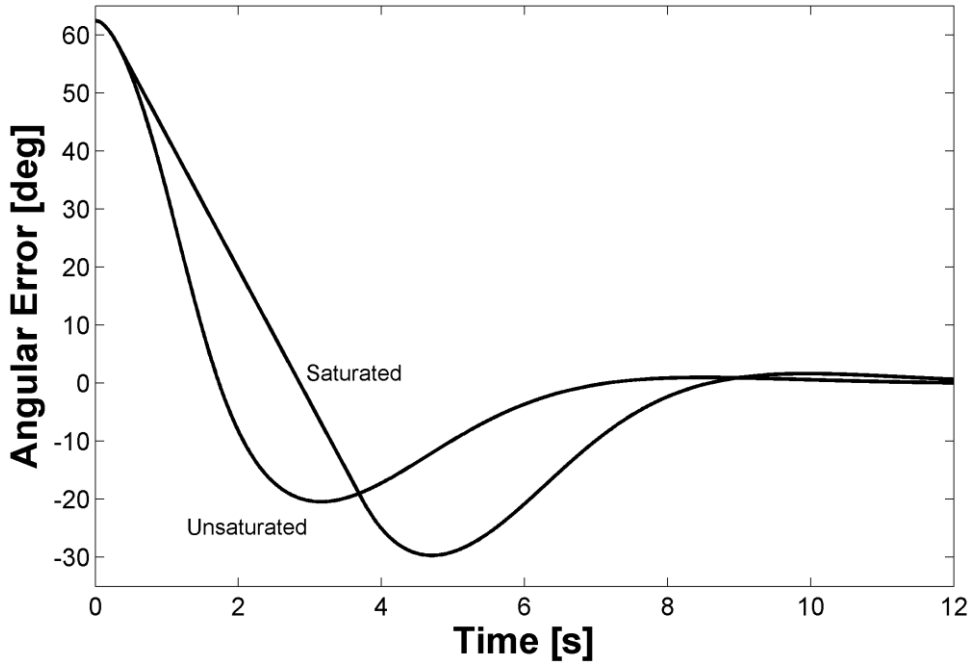

Figure 7.21 Angular error responses produced by the plane-pursuit guidance against a moving target

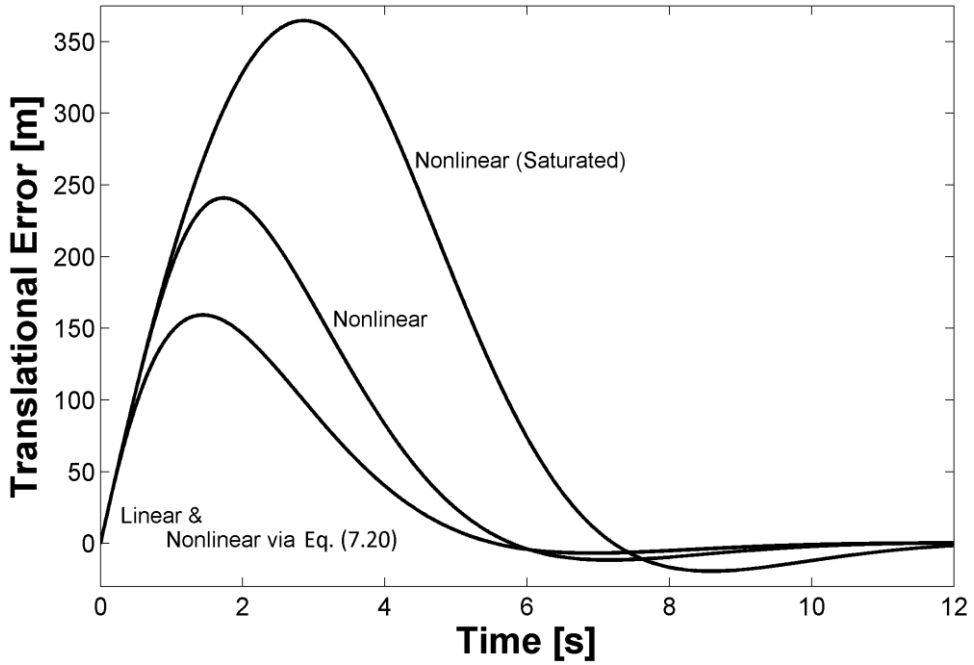

Figure 7.22 Translational error behaviors produced by the plane-pursuit guidance against a moving target

CHAPTER 8

CONCLUSIONS

Independent of the subject, it can usually be argued that there are more ways than one to accomplish an objective. In an area relevant to the discipline of engineering, one of the basic duties of the engineer is to evaluate the relative costs of the alternative solutions before deciding which path to follow. This practice is necessary so that the available resources are not wasted.

The study of impact angle guidance is a good example in that respect. In the literature, there are many different methods with the same ultimate objective: capturing the target with a desired impact angle. Given infinite resources, it would be reasonable to expect that all these methods will be able to fulfill this objective. In practice, however, there are almost always a number of details that must be considered first. The availability of the information required by a guidance law is one concern. For example, the range- and time-to-go signals, which frequently appear in impact angle control routines, generally require some sort of estimation. Since even the simplest estimation process will introduce additional complications, a guidance law that does not require such inputs to do the same job would be advantageous. Another concern is associated with the control effort. For example in exoatmospheric applications, the control authority is sustained with thrust obtained by expending fuel, which can only be stored in limited quantities. In endoatmospheric applications, on the other hand, the control authority is realized by creating angle of attack, which when high, induces severe drag leading to speed loss. As a result, a guidance law that does the same job with less total control effort would be a natural choice. Yet another concern is the physical constraints. One constraint common to all vehicles is the acceleration limit whereas the look angle limit is applicable to pursuers with target seekers. If a control scheme threatens to violate these constraints, it might lose its status as a guidance law candidate. The author hopes that all of these concerns have

been addressed in this dissertation in a way that is justified within the field of guidance engineering.

The primary outcomes of the study are the three BPPN guidance laws based on the discontinuous, range-driven and error-based bias application tactics. With these nonlinear formulations, it is possible to capture a stationary target with a desired impact angle without using the time-to-go information. Firstly, the discontinuous method involves applying the bias, which is constant when the speed is constant, to shape the trajectory until the potential impact angle value equals the desired one. After the bias is removed, the pursuer finds the target using the classical PPN guidance law, which implies that this phase is open loop in terms of impact angle control. Secondly, the range-driven method is inspired by the unfeasible approach of continuous bias application. The implementation is realized by approximating the unavailable time-to-go term in the BPPN impact angle expression by an expression involving the range to go, where the range signal may be provided by the single-gain observer that is presented as a supplementary tool. This range observer can easily be constructed if the vehicle is readily equipped with a passive seeker able to measure the rate of the LOS angle. Lastly, the error-driven method is formulated by rewriting the potential impact angle function as an error term. Since the resulting dynamics is first order, the corresponding guidance gain needs to be sufficiently high in order for the impact angle error to be negligible. Through a number of simulation runs, some of which are ideal and the rest of which are disturbed by various realistic factors, these BPPN guidance laws are verified to perform as intended. It turns out that results closest to the optimal solution, which minimizes the total control effort, can be obtained by resorting to the discontinuous bias application with specific values of the navigation gains. The appropriate gain values happen to be 3 and 2 for the midcourse and terminal phases, respectively. The former value is not unexpected because, as shown, it is the optimal value in a linear two-point boundary value problem. As for the latter value, which is the lowest possible gain for the PPN loop, it generates a uniform control effort not unlike the optimal solution tends to do towards the end of the engagement.

Another topic that is investigated is the problem of constrained impact angle control. Because the range-driven and error-based formulations do not comply with the analytical solutions, the investigation is based on the continuous and discontinuous biasing schemes. The outcomes are threefold: First, it is possible by simple numerical means to calculate the impact angle capacity as a function of the look angle and acceleration limits under the action of continuous bias. This information is valuable to the designer in that impact angle requests beyond the reach of the pursuer can be avoided. Also, it should be noted that since the BPPN guidance law is an efficient method for trajectory shaping, it is reasonable to expect that the calculated capacity would not be very different from those achievable by other efficient methods. Second, it is shown that the problem of constrained impact angle control using discontinuous biasing is theoretically solvable; however, a straightforward numerical solution does not seem to exist. This is why an alternative solution is proposed as the third item, where the look angle constrained guidance problem is solved utilizing the available analytical foundation without paying attention to the acceleration limit. Then, whether or not the acceleration limit will be violated can be tested numerically. It so happens that the aforementioned combination of 3 and 2 as the navigation gains provides a physically meaningful solution to the constrained guidance problem. Therefore, it can be suggested that a realistic pursuer guided by BPPN with these specific gain values is more likely than not to achieve its objectives under physical constraints provided that the constraints are not too restrictive to allow the attainment of the desired impact angle.

The proposed impact angle guidance approach is not restricted to stationary targets. An extension can be made to cover moving targets by means of the expected collision triangle, which is constructed by assuming that the target will not accelerate after the engagement commences. Two methods are formulated to implement the discontinuous biasing approach. These are the PPN-based and IPN-based implementations, where the guidance action is based on the rotation of the pursuer velocity vector and of the relative velocity vector, respectively. Because the target is not stationary, the first implementation does not conform to the BPPN analytical solutions derived for stationary targets and consequently, the biased phase is not guaranteed to be stable. This, fortunately, is not a significant shortcoming owing to

the fact that the bias will eventually be removed. The second implementation, on the other hand, does not suffer this at all since IPN makes the target seem stationary to the guidance loop to begin with. This implementation is realized through a PPN-like control action so that no change in pursuer speed is required. As stated above, the assumption of the unchanging collision triangle is vulnerable to changes in the target speed. Changes in the pursuer speed are also harmful; yet in this case, the designer is not as helpless because the terminal speed of the pursuer may probably be predicted with some accuracy. The results of simulations involving gravity and drag show that slight variations of the expected speed do not impede the impact angle performance.

The BPPN methods described in this text are planar. However, the midcourse guidance technique named plane pursuit, which aims to bring the pursuer velocity vector to a plane containing the desired impact direction, can be employed to facilitate the 3-D extension. It turns out that the midcourse phase is analogous to the velocity pursuit guidance when the target is stationary. Against a moving target, on the other hand, it is analogous to the altitude-hold control loop. The simulation results show that the classical controllers that are designed based on these analogies perform as planned.

This study tries to address various aspects of the impact angle guidance problem by adopting a practical point of view. It would not be an overstatement to say that every single method described here should be feasible under realistic circumstances. In this respect, the author feels that this thesis will be a fine addition to the literature. While this is so, it is also true that this work is far from being a complete treatment of the subject. For example, it might have been more convenient to define the impact angle with respect to the body of the pursuer instead of its velocity vector. Admitting this does not degrade the current approach; the body vector will lead the velocity vector by the angle of attack, which implies that the designer has an indirect authority on the final value of the body angle by being able to control the impact angle. Nonetheless, a body-referenced formulation could be considered as future work. Another subject for future research would be a range observer that does not require the target to be stationary. The knowledge that a ground target is constrained to move on the ground might somehow be incorporated into the formulation. Furthermore, the

case of moving targets is addressed only briefly in this text. This is an important and challenging topic that deserves overall attention. Therefore, this is another subject for future work, where the constrained guidance problem should also be studied.

REFERENCES

[1] Shneydor, N. A., *Missile Guidance and Pursuit*, Horwood, Chichester, West Sussex, 1998, p.70, p. 77, p. 101, pp. 102–103, p. 218.

[2] Zarchan, P., *Tactical and Strategic Missile Guidance*, 6th ed., AIAA, Reston, VA, 2012, p.13, pp. 24–25, pp. 569–601, pp. 777–789.

[3] Yang, C.-D., and Yang, C.-C., "A Unified Approach to Proportional Navigation", *IEEE Transactions on Aerospace and Electronic Systems*, Vol. 33, No. 2, 1997, pp. 557–567.

[4] Murtaugh, S. A., and Criel, H. E., "Fundamentals of Proportional Navigation", *IEEE Spectrum*, Vol. 3, No. 12, 1966, pp. 75–85.

[5] Guelman, M., "A Qualitative Study of Proportional Navigation", *IEEE Transactions on Aerospace and Electronic Systems*, Vol. AES-7, No. 4, 1971, pp. 637–643.

[6] Shukla, U. S., and Mahapatra, P. R., "The Proportional Navigation Dilemma—Pure or True?", *IEEE Transactions on Aerospace and Electronic Systems*, Vol. 26, No. 2, 1990, pp. 382–392.

[7] Becker, K., "Closed-Form Solution of Pure Proportional Navigation", *IEEE Transactions on Aerospace and Electronic Systems*, Vol. 26, No. 3, 1990, pp. 526–533.

[8] Yuan, P.-J., and Chern, J.-S., "Ideal Proportional Navigation", *Journal of Guidance, Control, and Dynamics*, Vol. 15, No. 5, 1992, pp. 1161–1165.

[9] Bryson, A. E., and Ho, Y.-C., *Applied Optimal Control*, Blaisdell, Waltham, MA, 1969, pp. 154–155.

[10] Kim, M., and Grider, K. V., "Terminal Guidance for Impact Attitude Angle Constrained Flight Trajectories", *IEEE Transactions on Aerospace and Electronic Systems*, Vol. AES-9, No. 6, 1973, pp. 852–859.

[11] Lin., C.-F., *Modern Navigation, Guidance, and Control Processing*, Prentice Hall, Englewood Cliffs, NJ, 1991, pp. 562–583.

[12] Idan, M., Golan, O. M., and Guelman, M., "Optimal Planar Interception with Terminal Constraints", *Journal of Guidance, Control, and Dynamics*, Vol. 18, No. 6, 1995, pp. 1273–1279.

[13] Song, T. L., and Shin, S. J., "Time-Optimal Impact Angle Control for Vertical Plane Engagements", *IEEE Transactions on Aerospace and Electronic Systems*, Vol. 35, No. 2, 1999, pp. 1439–1444.

[14] Song, T. L., Shin, S. J., and Cho, H., "Impact Angle Control for Planar Engagements", *IEEE Transactions on Aerospace and Electronic Systems*, Vol. 35, No. 4, 1999, pp. 738–742.

[15] Ryoo, C.-K., Cho, H., and Tahk, M.-J., "Optimal Guidance Laws with Terminal Impact Angle Constraint", *Journal of Guidance, Control, and Dynamics*, Vol. 28, No. 4, 2005, pp. 724–732.

[16] Ohlmeyer, E. J., and Phillips, C. A., "Generalized Vector Explicit Guidance", *Journal of Guidance, Control, and Dynamics*, Vol. 29, No. 2, 2006, pp. 261–268.

[17] Ryoo, C.-K., Cho, H., and Tahk, M.-J., "Time-to-Go Weighted Optimal Guidance with Impact Angle Constraints", *IEEE Transactions on Aerospace and Electronic Systems*, Vol. 14, No. 3, 2006, pp. 483–492.

[18] Lee, J.-I., Jeon, I.-S., and Tahk, M.-J., "Guidance Law to Control Impact Time and Angle", *IEEE Transaction on Aerospace and Electronic Systems*, Vol. 43, No. 1, 2007, pp. 301–310.

[19] Rusnak, I.,Weiss, H., Eliav, R., and Shima, T., "Missile Guidance with Constrained Terminal Body Angle", *26th Convention of Electrical and Electronics Engineers in Israel*, IEEE, Eliat, 2010, pp. 45–49.

[20] Ratnoo, A., and Ghose, D., "State-Dependent Riccati-Equation-Based Guidance Law for Impact-Angle-Constrained Trajectories", *Journal of Guidance, Control, and Dynamics*, Vol. 32, No. 1, 2009, pp. 320–325.

[21] Park, B.-G., Kim, T.-H., and Tahk, M.-J., "Optimal Impact Angle Control Guidance Law Considering the Seeker's Field-of-View Limits", *Proceedings of the Institution of Mechanical Engineers, Part G: Journal of Aerospace Engineering*, Vol. 227, No. 8, 2013, pp. 1347–1364.

[22] Taub, I., and Shima, T., "Intercept Angle Missile Guidance Under Time Varying Acceleration Bounds", *Journal of Guidance, Control, and Dynamics*, Vol. 36, No. 3, 2013, pp. 686–699.

[23] Arita, S., and Ueno, S., "Optimal Feedback Guidance for Nonlinear Missile Model with Impact Time and Angle Constraints", *AIAA Guidance, Navigation, and Control Conference*, Boston, 2013.

[24] Maity, A., Oza, H. B., and Padhi, R., "Generalized Model Predictive Static Programming and Angle-Constrained Guidance of Air-to-Ground Missiles", *Journal of Guidance, Control, and Dynamics*, Vol. 37, No. 6, 2014, pp. 1897–1913.

[25] Kim, B. S., Lee, J. G., and Han, H. S., "Biased PNG Law for Impact with Angular Constraint", *IEEE Transactions on Aerospace and Electronic Systems*, Vol. 34, No. 1, 1998, pp. 277–288.

[26] Lu, P., Doman, D. B., and Schierman, J. D., "Adaptive Terminal Guidance for Hypervelocity Impact in Specified Direction", *Journal of Guidance, Control, and Dynamics*, Vol. 29, No. 2, 2006, pp. 269–278.

[27] Manchester, I. R., and Savkin, A. V., "Circular-Navigation-Guidance Law for Precision Missile/Target Engagements", *Journal of Guidance, Control, and Dynamics*, Vol. 29, No. 2, 2006, pp. 314–320.

[28] Ratnoo, A., and Ghose, D., "Impact Angle Constrained Interception of Stationary Targets", *Journal of Guidance, Control, and Dynamics*, Vol. 31, No. 6, 2008, pp. 1817–1822.

[29] Erer, K. S., and Tekin, R., "Saf Oransal Yöngüdüm Çarpma Açısına Yönelik Arafaz Güdüm Yöntemi", *TOK Otomatik Kontrol Ulusal Toplantısı*, İstanbul, 2008.

[30] Ratnoo, A., and Ghose, D., "Impact Angle Constrained Guidance Against Nonstationary Nonmaneuvering Targets", *Journal of Guidance, Control, and Dynamics*, Vol. 33, No. 1, 2010, pp. 269–275.

[31] Erer, K. S., and Merttopçuoglu, O., "Indirect Control of Impact Angle Against Stationary Targets Using Biased PPN", *AIAA Guidance, Navigation, and Control Conference*, Toronto, 2010.

[32] Erer, K. S., and Merttopçuoglu, O., "Indirect Impact-Angle-Control Against Stationary Targets Using Biased Pure Proportional Navigation", *Journal of Guidance, Control, and Dynamics*, Vol. 35, No. 2, 2012, pp. 700–704.

[33] Kumar, S. R., Rao, S., and Ghose, D., "Sliding-Mode Guidance and Control for All-Aspect Interceptors with Terminal Angle Constraints", *Journal of Guidance, Control, and Dynamics*, Vol. 35, No. 4, 2012, pp. 1230–1246.

[34] Ratnoo, A., and Ghose, D., "Kill-Band-Based Lateral Impact Guidance Without Line-of-Sight Rate Information", *Journal of Guidance, Control, and Dynamics*, Vol. 35, No. 6, 2012, pp. 1740–1750.

[35] Lee, C.-H., Kim, T.-H., Tahk, and M.-J, Whang, I.-H., "Polynomial Guidance Laws Considering Terminal Impact Angle and Acceleration Constraints", *IEEE Transactions on Aerospace and Electronic Systems*, Vol. 34, No. 1, 2013, pp. 74–92.

[36] Erer, K. S., and Özgören, M. K., "Control of Impact Angle Using Biased Proportional Navigation", *AIAA Guidance, Navigation, and Control Conference*, Boston, 2013.

[37] Lee, C. -H., Kim, T.-H., and Tahk, M.-J., "Interception Angle Control Guidance Using Proportional Navigation with Error Feedback", *Journal of Guidance, Control, and Dynamics*, Vol. 36, No. 5, 2013, pp. 1556–1561.

[38] Kim, T.-H., Park, B.-G., and Tahk, M.-J., "Bias-Shaping Method for Biased Proportional Navigation with Terminal-Angle Constraint", *Journal of Guidance, Control, and Dynamics*, Vol. 36, No. 6, 2013, pp. 1810–1816.

[39] Indig, N., Ben-Asher, J. Z., Farber, N., "Near-Optimal Spatial Midcourse Guidance Law with an Angular Constraint", *Journal of Guidance, Control, and Dynamics*, Vol. 37, No. 1, 2014, pp. 214–223.

[40] Sun, M., Xu, Q., Du, S., Chen, Z., and Zhang, D., "Practical Solution to Impact Angle Control in Vertical Plane", *Journal of Guidance, Control, and Dynamics*, Vol. 37, No. 3, 2014, pp. 1022–1027.

[41] Zhang, Y.-A., Ma, G.-X., and Wu, H.-L., "A Biased Proportional Navigation Guidance Law with Large Impact Angle Constraint and the Time-to-Go Estimation", *Proceedings of the Institution of Mechanical Engineers, Part G: Journal of Aerospace Engineering*, Vol. 228, No. 10, 2014, pp. 1725–1734.

[42] Tsalik, R., and Shima, T., "Inscribed Angle Guidance", *Journal of Guidance, Control, and Dynamics*, Vol. 38, No. 1, 2015, pp. 30–40.

[43] Tekin, R., and Erer, K. S., "Switched-Gain Guidance for Impact Angle Control under Physical Constraints", *Journal of Guidance, Control, and Dynamics*, Vol. 38, No. 2, 2015, pp. 205–216.

[44] Erer, K. S., Tekin, R., and Özgören, M. K., "Look Angle Constrained Impact Angle Control Based on Proportional Navigation", *AIAA Guidance, Navigation, and Control Conference*, Kissimee, FL, 2015.

[45] Polking, J. C., "ODE Software for MATLAB: DFIELD and PPLANE", http://math.rice.edu/~dfield/index.html, 2002. [cited 2 March 2015]

[46] Ogata, K., *Modern Control Engineering*, 4th ed., Prentice–Hall, Upper Saddle River, NJ, 2002, pp. 221–224, pp. 855–881.

[47] Savage, P. G., "What Do Accelerometers Measure?" Technical Report, Strapdown Associates, Inc., 2005.

[48] Nichols, J. O., "Analysis and Compilation of Missile Aerodynamic Data, Volume 1: Data Presentation and Analysis", NASA CR-2835, 1977.

[49] Aidala, V. J., "Kalman Filter Behavior in Bearings-Only Tracking Applications", *IEEE Transactions on Aerospace and Electronic Systems*, Vol. AES-15, No. 1, 1979, pp. 29–39.

[50] Taur, D.-R., and Chem, J.-S., "Passive Ranging for Dog-Fight Air-to-Air IR Missiles", *AIAA Guidance, Navigation, and Control Conference*, Portland, 1999, pp. 1737–1751.

[51] Blakelock, J. H., *Automatic Control of Aircraft and Missiles*, 2nd ed., John Wiley & Sons, NY, 1991, p. 102.

[52] Kirk, D. E., *Optimal Control Theory: An Introduction*, Dover, Mineola, NY, 1998, pp. 184–209.

[53] Wang, X., "Solving Optimal Control Problems with MATLAB — Indirect Methods", Technical Report, ISE Dept., NCSU, 2009.

APPENDIX A

NONLINEAR OPTIMAL CONTROL SOLUTION

Starting from a set of initial conditions, the optimal control enabling the achievement of a set of specified final conditions in some planar engagement geometry can be obtained by following the guidelines outlined in [52]. The states of the optimal control problem are selected as

$$x_1 = r \tag{A.1}$$

$$x_2 = \varepsilon \tag{A.2}$$

$$x_3 = \gamma \tag{A.3}$$

Referring to Eq. (2.7) and Eq. (2.8), the state equations below can be written for constant speed with the help of Eq. (2.4):

$$\dot{x}_1 = -V \cos x_2 \tag{A.4}$$

$$\dot{x}_2 = V \frac{\sin x_2}{x_1} + u \tag{A.5}$$

$$\dot{x}_3 = u \tag{A.6}$$

where u is the control. The cost function of the boundary value problem is defined as

$$E = \frac{1}{2} \int_0^{t_f} u^2 \mathrm{d}t \tag{A.7}$$

which is the same as Eq. (2.38). With α denoting the costate, the Hamiltonian can be constructed as

$$H = -V\alpha_1 \cos x_2 + V\alpha_2 \frac{\sin x_2}{x_1} + (\alpha_2 + \alpha_3)u + \frac{1}{2}u^2 \tag{A.8}$$

Exploiting the facts that $\mathrm{d}\bar{x}/\mathrm{d}t = \partial H/\partial\bar{\alpha}$ and $\mathrm{d}\bar{\alpha}/\mathrm{d}t = -\partial H/\partial\bar{x}$ and using Eq. (A.4) – Eq. (A.6), the differential equation set corresponding to the optimal control problem can be derived as

$$\begin{bmatrix} \dot{x}_1 \\ \dot{x}_2 \\ \dot{x}_3 \\ \dot{\alpha}_1 \\ \dot{\alpha}_2 \\ \dot{\alpha}_3 \end{bmatrix} = \begin{bmatrix} -V\cos x_2 \\ V\dfrac{\sin x_2}{x_1} - \alpha_2 - \alpha_3 \\ -\alpha_2 - \alpha_3 \\ V\alpha_2 \dfrac{\sin x_2}{x_1^2} \\ -V\alpha_1 \sin x_2 - V\alpha_2 \dfrac{\cos x_2}{x_1} \\ 0 \end{bmatrix} \tag{A.9}$$

It should be noted that the third equation complies with the requirement that $\partial H/\partial u = 0$.

The boundary conditions are

$$\left[\bar{x}(0) \quad \bar{x}(t_\mathrm{f})\right]^\mathrm{T} = \left[r_\mathrm{i} \quad \varepsilon_\mathrm{i} \quad \gamma_\mathrm{i} \quad 0 \quad 0 \quad \gamma_\mathrm{f}\right]^\mathrm{T} \tag{A.10}$$

The fourth and fifth conditions are seen to be zero, which follows from the fact that the final values of the range and the look angle must be zero in order to capture a stationary target. For a given initial condition set, the last boundary condition, which is the user-specified impact angle, is in fact the sole control parameter that determines the shape of the trajectory. The boundary conditions given in Eq. (A.10) are not sufficient to initiate the solution process because the final time is unknown;

an additional condition is required. Since the final time is free and the Hamiltonian does not explicitly depend on time, the Hamiltonian must identically be zero at all times. Therefore, the missing boundary condition can be obtained as

$$-V\alpha_1(0)\cos x_2(0)+V\alpha_2(0)\frac{\sin x_2(0)}{x_1(0)}-\frac{1}{2}\left\{\alpha_2(0)+\alpha_3(0)\right\}^2=0 \tag{A.11}$$

where it should be noted that the Hamiltonian is evaluated at the start of the engagement rather than at the end of it so that the preferred numerical routine is able solve the problem.

As implied above, the analytical capabilities end here; the solution of Eq. (A.9) with Eq. (A.10) and Eq. (A.11) necessitates numerical techniques. One relatively easy way to overcome this problem is to utilize the MATLAB command "bvp4c" [53]. The following is the MATLAB code used to solve the problem:

```
function sol=boundary_value_problem

solinit=bvpinit(linspace(0,1),[1000;0;0;0;0;0],10);
sol=bvp4c(@odefun,@bcfun,solinit);

function dydx=odefun(x,y,tf)

V=250; % pursuer speed

% differential equations
dydx=tf*[-V*cos(y(2))
          V*sin(y(2))/y(1)-y(5)-y(6)
         -y(5)-y(6)
          V*y(5)*sin(y(2))/y(1).^2
         -V*y(4)*sin(y(2))-V*y(5)*cos(y(2))/y(1)
          0];

function res=bcfun(ya,yb,tf)
V=250; % pursuer speed

% boundary conditions
res=[ya(1)-5000 % initial range
     ya(2)-15*pi/180 % initial look angle
     ya(3)-15*pi/180 % initial path angle
     yb(1) % final range
     yb(2) % final look angle
     yb(3)+pi/2 % final path angle
    -V*ya(4)*cos(ya(2))+V*ya(5)*sin(ya(2))/ya(1)-
     0.5*(ya(5)+ya(6))^2];
```

The states and their derivatives can be extracted from the solution as follows:

```
tf=sol.parameters; % final time
h=0.001; % time step
% states and their derivatives
[sxint,spxint]=deval(sol,(0:h:tf)/tf);
spxint= spxint/tf;
```

APPENDIX B

LINEAR OPTIMAL CONTROL SOLUTION

Following the guidelines outlined in [52], the Hamiltonian that follows from Eq. (2.50), Eq. (2.53) and Eq. (2.54) is

$$H = \alpha_1 x_2 + \alpha_2 u + \frac{1}{2}u^2 \tag{B.1}$$

where α denotes the costates. The necessary condition for optimal control associated with the costates dictates: $\mathrm{d}\bar{\alpha}/\mathrm{d}t = -\partial H/\partial \bar{x}$. Then, the corresponding differential equations are

$$\dot{\alpha}_1 = -\frac{\partial H}{\partial x_1} = 0 \tag{B.2}$$

$$\dot{\alpha}_2 = -\frac{\partial H}{\partial x_2} = -\alpha_1 \tag{B.3}$$

whose solutions yield

$$\alpha_1 = c_1 \tag{B.4}$$

$$\alpha_2 = -c_1 t + c_2 \tag{B.5}$$

where $\bar{c}$ denote the constants of integration. Next, using the necessary condition for optimal control associated with the control, i.e. $\partial H/\partial u = 0$, the following can be written:

$$\frac{\partial H}{\partial u} = \alpha_2 + u = 0 \tag{B.6}$$

as a result of which the optimal control turns out to be

$$u = -\alpha_2 \tag{B.7}$$

Using the dynamic constraints of Eq. (2.53), the differential equations associated with the second state can now be written as

$$\dot{x}_2 = -\alpha_2 \tag{B.8}$$

Utilizing Eq. (B.5), this turns into

$$\dot{x}_2 = c_1 t - c_2 \tag{B.9}$$

which is also the optimal control as per Eq. (B.7):

$$u = c_1 t - c_2 \tag{B.10}$$

The integrated form of Eq. (B.9) is

$$x_2 = \frac{1}{2} c_1 t^2 - c_2 t + c_3 \tag{B.11}$$

Based on Eq. (2.53), the differential equation associated with the first state is

$$\dot{x}_1 = \frac{1}{2} c_1 t^2 - c_2 t + c_3 \tag{B.12}$$

so that

$$x_1 = \frac{1}{6}c_1 t^3 - \frac{1}{2}c_2 t^2 + c_3 t + c_4 \tag{B.13}$$

Having obtained the representations of the states as functions of time, the boundary conditions stated in Eq. (2.51) and Eq. (2.52) can now be applied:

$$x_1(0) = x_{1,\mathrm{i}} = c_4 \tag{B.14}$$

$$x_2(0) = x_{2,\mathrm{i}} = c_3 \tag{B.15}$$

$$x_1(t_\mathrm{f}) = x_{1,\mathrm{f}} = \frac{1}{6}c_1 t_\mathrm{f}^3 - \frac{1}{2}c_2 t_\mathrm{f}^2 + c_3 t_\mathrm{f} + c_4 \tag{B.16}$$

$$x_2(t_\mathrm{f}) = x_{2,\mathrm{f}} = \frac{1}{2}c_1 t_\mathrm{f}^2 - c_2 t_\mathrm{f} + c_3 \tag{B.17}$$

Accordingly, the first two integration constants can be shown to assume the following forms:

$$c_1 = \frac{12}{t_\mathrm{f}^3}\left(x_{1,\mathrm{i}} - x_{1,\mathrm{f}}\right) + \frac{6}{t_\mathrm{f}^2}\left(x_{2,\mathrm{i}} + x_{2,\mathrm{f}}\right) \tag{B.18}$$

$$c_2 = \frac{6}{t_\mathrm{f}^2}\left(x_{1,\mathrm{i}} - x_{1,\mathrm{f}}\right) + \frac{2}{t_\mathrm{f}}\left(2x_{2,\mathrm{i}} + x_{2,\mathrm{f}}\right) \tag{B.19}$$

Finally, following from Eq. (B.10), the solution for the open-loop optimal control can be obtained as in Eq. (2.55).

APPENDIX C

ANALYTICAL BEHAVIOR OF PURE PROPORTIONAL NAVIGATION

It is known that the PPN guidance law in Eq. (2.9) leads to the following analytical solutions [43]:

$$\varepsilon = \sin^{-1}\left\{\sin\varepsilon_{\mathrm{i}}\left(\frac{r}{r_{\mathrm{i}}}\right)^{N-1}\right\} \tag{C.1}$$

$$\dot{\gamma} = -\frac{Nv\sin\varepsilon_{\mathrm{i}}}{r_{\mathrm{i}}}\left(\frac{r}{r_{\mathrm{i}}}\right)^{N-2} \tag{C.2}$$

These functions are plotted in Figure C.1 and Figure C.2, where the curves start from their respective gain values. These figures are as they appear in [43].

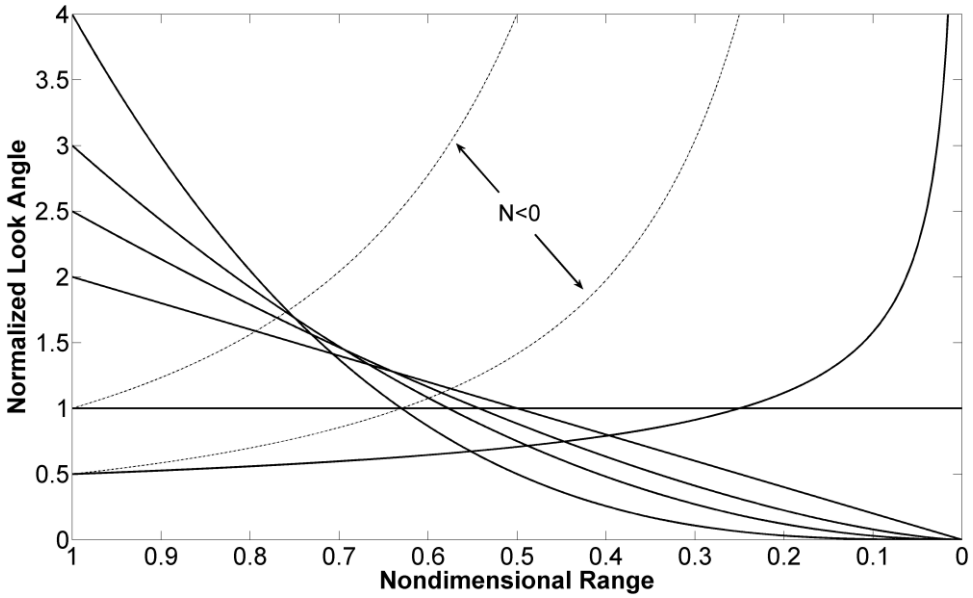

Figure C.1 Normalized look angle as a function of nondimesional range

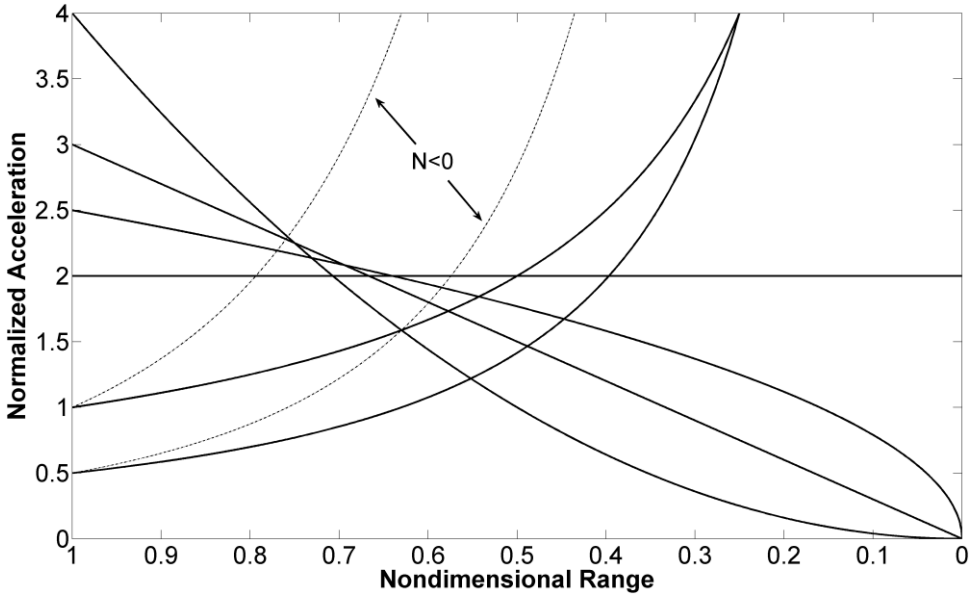

Figure C.2 Normalized acceleration as a function of nondimesional range

APPENDIX D

ACTUAL FLIGHT PERFORMANCE OF THE RANGE OBSERVER

Figure D.1 and Figure D.2, which appear here by courtesy of Roketsan, display two instances of the actual flight performance of the range observer detailed in Chapter 5. The smooth lines are those obtained by offline manipulation of the INS data and the others are the online products of the range observer. In each of the flights, the configuration of the vehicle is the same. The only difference that matters is the trajectories followed. The range histories in Figure D.1 belong to the trajectory that has low observability. As seen, the estimation performance is not satisfactory. On the other hand, the range histories of the trajectory with high observability are presented in Figure D.2, where the estimation is seen to be successful.

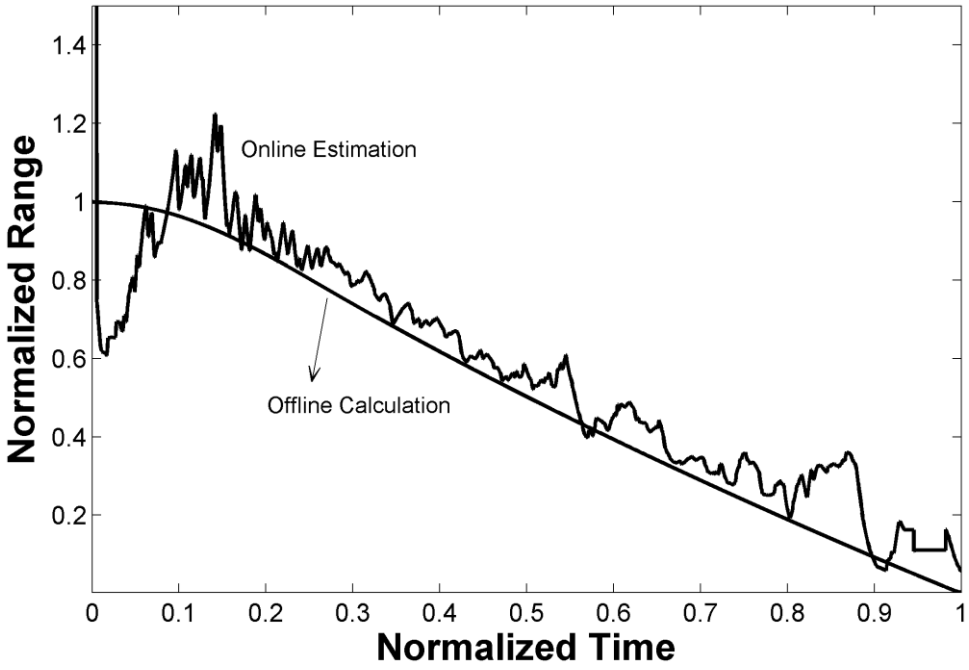

Figure D.1 Range estimation with low observability

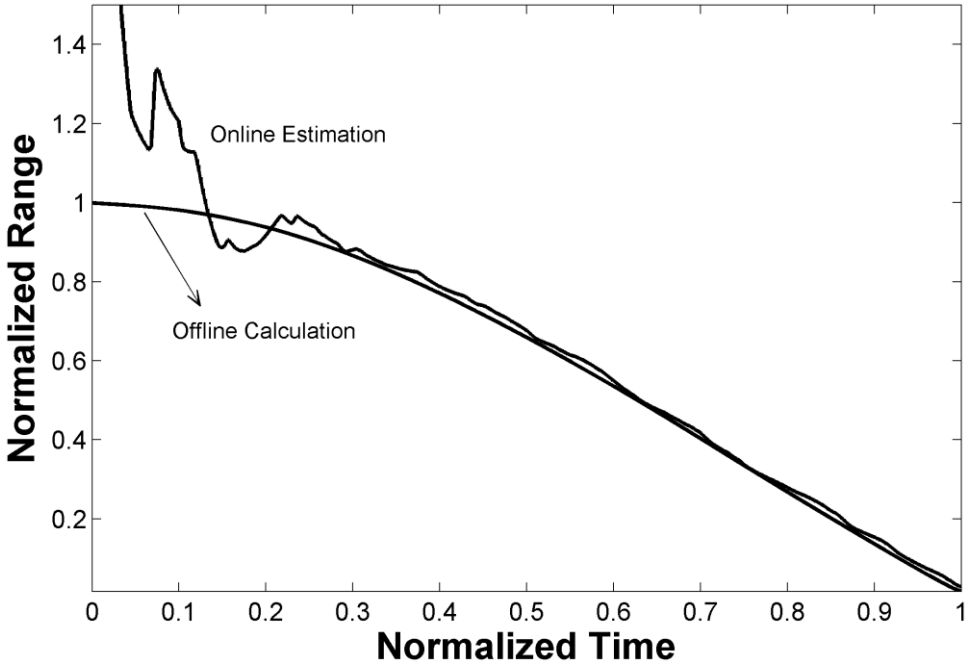

Figure D.2 Range estimation with high observability

APPENDIX E

PLANAR NATURE OF PURE PROPORTIONAL NAVIGATION

Claim: PPN will result in a planar engagement if, initially, the velocity vector of the target is contained in the plane formed by the LOS and the velocity vector of the pursuer. When the target is stationary, the engagement geometry is always planar.

Proof I: A 2-D PPN engagement is confined in, say, *xy* plane. If the viewing reference frame is changed to another one in the general 3-D space, the pursuer will still move in the same plane, except that the plane is not called *xy* plane anymore.

Proof II: PPN guidance law in vector form is expressed as [1]

$$\vec{a} = N\vec{\omega} \times \vec{v} \tag{E.1}$$

The angular velocity vector can be written as [1]

$$\vec{\omega} = \frac{\vec{r} \times \dot{\vec{r}}}{r^2} \tag{E.2}$$

Noting that $\vec{r} = \vec{p}_T - \vec{p}$, the preceding equation becomes

$$\vec{\omega} = \frac{\vec{r} \times \left(\vec{v}_T - \vec{v}\right)}{r^2} \tag{E.3}$$

So, the PPN law becomes

$$\vec{a} = \frac{N}{r^2}\left\{\vec{r} \times \left(\vec{v}_T - \vec{v}\right)\right\} \times \vec{v} \tag{E.4}$$

If $\vec{r}$, $\vec{v}$ and $\vec{v}_T$ are contained in the same plane, the cross product $\vec{r} \times \left(\vec{v}_T - \vec{v}\right)$ will result in a vector that is perpendicular to this plane. Application of the second cross product $\left\{\vec{r} \times \left(\vec{v}_T - \vec{v}\right)\right\} \times \vec{v}$ will bring the acceleration vector back to this plane. This result also covers the case with $\vec{v}_T = 0$.

CURRICULUM VITAE

Koray S. Erer
kserer@gmail.com

EDUCATION

2004 – 2008: Mechanical Engineering Department, METU

M.S.

Thesis Title: Verification and MATLAB Implementation of the Inverse Dynamics Model of the METU Gait Analysis System

1999 – 2004: Mechanical Engineering Department, METU

B.S.

EXPERIENCE

2006 – Present: Roketsan Missiles Inc.

Guidance & Control Engineer

2005 – 2006: Mechanical Engineering Department, METU

Teaching Assistant

PAPERS

Journal

1. K. S. Erer, "Adaptive Usage of the Butterworth Digital Filter", *Journal of Biomechanics*, 2007.
2. K. S. Erer and O. Merttopçuoğlu, "Indirect Impact-Angle-Control Against Stationary Targets Using Biased Pure Proportional Navigation", *Journal of Guidance, Control, and Dynamics*, 2012.
3. R. Tekin and K. S. Erer, "Switched-Gain Guidance for Impact Angle Control under Physical Constraints", *Journal of Guidance, Control, and Dynamics*, 2015.

International Conference

4. K. S. Erer and O. Merttopçuoğlu, "Indirect Control of Impact Angle Against Stationary Targets Using Biased PPN", *AIAA Guidance, Navigation, and Control Conference*, 2010.

5. K. S. Erer and M. K. Özgören, "Control of Impact Angle Using Biased Proportional Navigation", *AIAA Guidance, Navigation, and Control Conference*, 2013.

6. K. S. Erer, R. Tekin and M. K. Özgören, "Look Angle Constrained Impact Angle Control Based on Proportional Navigation", *AIAA Guidance, Navigation, and Control Conference*, 2015.

7. K. S. Erer and R. Tekin, "Considerations on Boost Phase Modeling and Guidance Command Generation", *AIAA Guidance, Navigation, and Control Conference*, 2015.

National Conference

8. K. S. Erer and R. Tekin, "Saf Oransal Yöngüdüm Çarpma Açısına Yönelik Arafaz Güdüm Yöntemi", *TOK Otomatik Kontrol Ulusal Toplantısı*, 2008.

9. K. S. Erer and R. Tekin, "Işına Binme Yöntemine Uygun Güdüm Döngüsü Tasarımı", *TOK Otomatik Kontrol Ulusal Toplantısı*, 2009.

10. K. S. Erer and R. Tekin, "İleri Hız Değişiminin Füze Yanal Dinamiğine Etkileri Üzerine Bir İnceleme", *TOK Otomatik Kontrol Ulusal Toplantısı*, 2010.

SKILLS AND KNOWLEDGE

Languages

Turkish (native), English (fluent), German (intermediate)

Computer

MATLAB (Simulink, xPC Target)